Quantitative and Systems Pathology for Therapeutic Response Prediction

Dana Faratian

MD Thesis

The University of Edinburgh

2009

Declaration

I, Dana Faratian, hereby certify that this thesis has been composed by myself, and that it is a record of my work and work conducted under my direct supervision, and that it has not been accepted in partial or complete fulfilment of any other degree or professional qualification.

Dana Faratian
University of Edinburgh
2009

Acknowledgements

Firstly, I would like to acknowledge and thank David Harrison for the opportunity to carry out this MD. Without his constant mentorship, supervision, and intellectual and financial support, none of this would be possible. I would also like to thank Simon Langdon for his additional support, advice and guidance during the course of this work.

Systems biology is, by its very nature, multidisciplinary. I would particularly like to thank Alexey Goltsov, Galina Lebedeva, and Igor Goryanin in Edinburgh. Without their input there would be no mathematical model, which is included in this thesis as an appendix. I would also like to thank Michael Idowu, Bob Clyde, and John Crawford at the University of Abertay, Dundee, who have developed the alternative S-systems approach and provided additional analysis in Chapter 2.

Without the following people this work would not have been completed:

Peter Mullen, who performed the timecourse experiments for input into the mathematical model, and additional inhibitor experiments for Sprouty and ovarian cancer model validation.

Charlene Kay, who performed cell culture, marked TMA cores for invasive tumour, and performed immunohistochemistry for ER and PR on TEAM trial slides.

InHwa Um, who has diligently performed immunofluorescence and AQUA analysis for pathway profiling.

John Bartlett for allowing me to conduct some of this work in his laboratory.

This work was also part-funded by a Breast Cancer Campaign pilot grant, a Cancer Research UK Clinical Bursary, and latterly Breakthrough Breast Cancer.

Abstract

The measurement of tissue biomarkers for therapeutic response prediction in cancer patients has become standard pathological practice, but only for a very limited number of targets. This is in spite of massive intellectual and financial investment in molecular pathology for translational cancer research. A re-evaluation of current approaches, and the testing of new ones, is required in order to meet the challenges of predicting responses to existing and novel therapeutics, and individualising therapy.

Herein I critique the current state of tissue biomarker analysis and quantification in cancer pathology and the reasons why so few novel biomarkers have entered the clinic. In particular, we examine the central role of signalling pathway biology in sensitivity and resistance to targeted therapy. I discuss how accurate quantification, and the ability to simulate biological responses over time and space, may lead to more accurate prediction of therapeutic response. I propose that different mathematical techniques used in the nascent field of systems biology (ordinary differential equation-based, S-systems, and Bayesian approaches) may provide promising new avenues to improve prediction in clinical and pathological practice. I also discuss the challenges and opportunities for quantification in pathological research and practice.

I have examined the role of cellular signalling pathways in therapeutic sensitivity and resistance in three different ways. Firstly, I have taken a hypothesis-driven and reductionist approach and shown that decreased Sprouty 2, a feedback inhibitor of MAPK and PI3K signalling, is associated with trastuzumab-resistance *in vitro* and in a cohort of breast cancer patients treated with trastuzumab. Secondly, I have characterised the activation state of ten growth and survival pathways across different histological subtypes of ovarian cancer using quantitative fluorescence microscopy. I have shown that unsupervised clustering of phosphoprotein expression profiles results in new subgroups with distinct biological properties (in terms of proliferation and apoptosis), and which predict therapeutic response to

chemotherapy. Thirdly, I have developed a new mathematical model of PI3K signalling, parameterised using quantitative phosphoprotein expression data from cancer cell lines using reverse-phase protein microarrays, and shown that quantitative PTEN protein expression is the key determinant of resistance to anti-HER2 therapy *in silico*. Furthermore, the quantitative measurement of PTEN is more predictive of response than other pathway components taken in isolation and when tested by multivariate analysis in a cohort of breast cancers treated with trastuzumab. For the first time, a systems biology approach has successfully been used to stratify patients for personalised therapy in cancer, and is further compelling evidence that PTEN, appropriately measured in the clinical setting, refines clinical decision-making in patients treated with anti-HER2 therapies.

Corrections to MD thesis

Dana Faratian

1.	P4	L-last line	**or** will report
2.	P7	L6	estimates **of** figures
3.	P7	L4	lapatinib
4.	P7	L-last-3	**nor a** clinical effect
5.	P8	Para 2 L2	deleted (**a**) single
6.	P9	L4	rarely **in** a systematic
7.	P9	L19	bee**n** tested ... **is** yet
8.	P12	L17	**to** some questions
9.	P17	L15	oncogene**s**
10.	P18	L23	meta**p**lastic ... **is** (not as)
11.	P26	L17	deleted **recent**
12.	P38	L22	an**d**
13.	P40	L20	(Her1-3) **abnormalities** are associated
14.	P42	L5	incubation with **anti-**ER or PR **antibodies**
15.	P45	Fig 3.2	Number of assessable cores, **number of cases (n)**
16.	P53	L8	deleted **to date**
17.	P63	L8	(Figure 4.**5**)
18.	P71	L11	transcript**s**
19.	P74	Table 5.2	concentration**s** and antigen retrieval conditions specified
20.	P93	L4	**(Thr202/Tyr204)** deleted
21.	P96	L21	pathologic**al**
22.	P100	L4	(Figures **in** Appendix D)
23.	P105	L25	deleted **to have**
24.	P6	1.3.2 L10	ma**r**ker

PCR – Polymerase Chain Reaction

PR – Progesterone Receptor

PRC – Pearson's Regression Coefficient

PI3K – Phosphoinositol-3-kinase

PTEN – Phosphatase and Tensin Homolog

RPPA – Reverse Phase Protein Array

RTK – Receptor Tyrosine Kinase

RT-PCR – Reverse Transcriptase Polymerase Chain Reaction

STAT – Signal Transducers and Activators of Transcription

TACT – Taxotere as Adjuvant Chemotherapy Trial

TANGO – Paclitaxel, Anthracycline, Gemcitabine & Cyclophosphamide

TEAM – Tamoxifen and Exemestane Adjuvant Multicentre

TIIα – Topoisomerase IIα

TMA – Tissue Microarray

VEGFR – Vascular Endothelial Growth Factor Receptor

WB – Western Blotting

Table of Contents

Index of figures and tables

Chapter 1: The current state of tissue biomarker quantification in pathology.

1.1 Background

The published literature is awash with examples of new tissue biomarkers promising to predict responses to therapy in cancer patients. However, few of these progress from the laboratory to the clinic. An exception to this is biomarker quantification in breast cancer, where oestrogen receptor (ER) and HER2 expression are both measured routinely in clinical practice by immunohistochemistry. In this chapter we discuss some of the reasons why more tissue biomarkers proposed in the research setting have not entered the clinic, using breast cancer biomarker development to illustrate. We discuss a selection of biomarkers which are in development and which may be candidates for clinical application using standard molecular pathology techniques, such as immunohistochemistry or fluorescence *in situ* hybridisation, within the next few years (eg. topoisomerase II, EGFR, AKT, PTEN). In particular, we explore how our ever increasing knowledge of molecular and pathway biology is facilitating hypothesis-driven biomarker discovery, and the statistical considerations which need to be addressed in order to adequately validate new candidate biomarkers.

1.2 Introduction

In the last 35 years only two molecular markers, oestrogen receptor (ER) and HER2, have become standard measurements in the management of breast cancer patients (1;2). The long evolutionary cycle of predictive biomarkers seems at odds with the number of published articles on the subject, suggesting the need for a new, and more rigorous approach to this area (3). At the time of writing a simple literature search for 'predictive markers in breast cancer' returns over 150 papers in English in the last year alone, which represent over twenty new molecules, all of which associate with disease-free or overall survival reflecting the bias towards identification of "novel" markers and the lack of investment (both financial and intellectual) in translation of these findings into clinical settings. In spite of massive investment in biomarker discovery, only one new biomarker has been translated into clinical practice in the past twenty five years (HER2). The aim of this chapter, therefore, is not to provide a

comprehensive overview of candidate predictive biomarkers but to explore the driving forces behind biomarker application and discovery, the techniques which are being used in biomarker validation, and the considerations which need to be taken into account in order for new biomarkers to be a clinical success. We will illustrate the 'hottest' biomarker research topics along the way, which with appropriate and directed research effort, may form part of clinical diagnostic decision-making over the next 3-5 years using the tools currently available in standard histopathology laboratories.

1.3 Drug-driven tissue biomarker discovery

The success of the archetypal predictive biomarkers ER and HER2 in breast cancer was driven by the availability of agents and knowledge of how they interact with their targets. There has been limited evidence over the past 20 years of the application of similar mechanistically targeted biomarker discovery approaches. However, the same rational pharmacotherapy paradigm is gradually being applied to both existing chemotherapeutic agents as knowledge of their mechanism of action emerges, and newer targeted "biological agents" as molecular biology is factored into early phase trials during the development of novel pharmacological agents

1.3.1 Existing agents – teaching old dogs new tricks

The current thinking within clinical oncology is that, whilst biologically targeted agents offer significant hope for the future, at least for the next 5-10 years, these agents are likely to be targeted either on specific sub-groups of patients, as with trastuzumab, and/or given in combination with conventional chemotherapeutic agents, as with Avastin. There remains, therefore, a significant debate as to the optimum scheduling and combination of current chemotherapeutic and endocrine agents, which is fuelled by two distinct thought processes. Firstly, it is clear that many patients who receive systemic therapy for breast cancer do not, in fact require such treatment (Oxford overview (4)). It is an inability to identify such patients prior to treatment, rather than an expectation that all patients derive benefit, which drives

the treatment of significant numbers of breast cancer patients with often aggressive chemotherapy. The identification of novel *prognostic* markers (ie markers which inform about clinical response in the absence of therapy) is key to the solution of this dilemma. Secondly, it is becoming increasingly apparent that the biological diversity of breast cancer (cf gene expression signatures of Perou *et al* (5)) underpins not only potential differences in the natural history of the disease but also differences in response to current adjuvant chemotherapy regimens. Thus it is entirely possible, and indeed highly likely, that some tumours which are insensitive to taxanes may in fact respond to anthracycline-based chemotherapies and vice versa. Thus the search for an optimal chemotherapy schedule and combination must in the future include the expectation that this optimum will be different for different patient subgroups and that these groupings will be defined by the presence within breast cancers of molecular targets for specific chemotherapeutic agents. As a result a key objective of research into predictive biomarkers in the near future will be the identification of markers which identify the optimal chemotherapy regimen. This research priority was in fact the second most important goal, second only to identification of prognostic markers to identify patients not requiring treatment, identified in a recent multinational focus group document aimed at identification of the top ten most important research questions in breast cancer (The Top Ten Programme: http://www.toptenresearch.org/).

This process has, in the past, been hampered by the lack of a cohesive approach to the development of predictive biomarkers (3;6) and by the lack of appropriate, clinical trials-based, sample banks in which such biomarkers must be validated. Recently, however, significantly more emphasis has been placed upon the collection of biological samples in the context of clinical trials. Many trials, including the UK TACT, TACT2, TANGO, TEAM, SUPREMO and the BIG-1-98 trials have included prospective tissue collection whilst others including ATAC and NEAT have made significant efforts to retrospectively access tumour samples. These biorepositories represent invaluable resources for the validation of predictive biomarker profiles. Research is ongoing in many of these studies which either has reported or will report in the next 1-3 years.

Two key areas of biomarker research in breast cancer are amongst the first to be addressed using these repositories. Firstly, is there an optimal signature for discriminating patients who may benefit from frontline treatment with aromatase inhibitors (AIs) from those who may derive benefit from tamoxifen followed by an AI? Secondly, are their patients for whom either taxanes or anthracyclines may be omitted without reducing their benefit from adjuvant chemotherapy?

Tamoxifen resistance has, for many years, been associated with gene amplification or overexpression of the HER2 oncogene or lack of expression of the progesterone receptor in ER positive breast tumours (1;7-9). Research in progress in the ATAC, BIG-I-98 and TEAM trials is addressing this question (see below). Coupled with further biomarker research (10-14) it is likely that we will, in the coming years, finally be in a position to identify de novo endocrine resistant cancers, and possibly to identify the optimal endocrine treatment regimen for distinct biological sub-groups.

For chemotherapy, key research in the TACT, TANGO and NEAT trials, within a UK wide collaborative network, should provide insights into biomarkers relating to benefit from taxanes and anthracyclines. Although the first anthracyline was first discovered in the 1950s, its mechanism of action was not elucidated until 1984 (15). Amongst other activities, anthracyclines inhibit the topoisomerase IIα (TIIα) enzyme, which results in double stranded DNA breaks and initiates apoptosis. Since anthracyclines have a low therapeutic index, and patients frequently experience treatment-related cardiomyopathy and secondary leukaemias, biomarkers which select for anthracyline-responsiveness would be of benefit in reducing morbidity in patients receiving adjuvant chemotherapy. Several retrospective studies have separately analysed, on the one hand, TIIα or HER2 expression, gene amplification or deletion, and on the other, more conventional markers of response such as proliferation (16-21). These studies suggest that TIIα aberrations, particularly amplifications, may predict for improved outcome on anthracyline-based regimens relative to tumors with a normal TIIα status. However, the water is muddied by the

fact that the TIIα gene is located close to that for HER2 on chromosome 17q12-21. Amplification of HER2 is associated with TIIα gene aberrations (22), making it difficult to be clear which gene is most closely associated with anthracycline sensitivity. Previous studies suggest HER2 together with TIIα are both potential predictive markers of anthracycline sensitivity (17;20;21;23-25). More recent data, from the BR9601 trial (26), suggests that HER1 and HER3 provide additional information when analysed with HER2. Therefore whilst TIIα remains a promising candidate biomarker the possibility remains that HER2, or even complex molecular panels may be of more practical value in determining eligibility for anthracyclines (see below). Future data from the NEAT study and an ongoing meta-analysis may provide further insights in this area.

1.3.2 Novel agents, novel approaches – the rationale for rational biomarker-driven trials

Even though HER2 and ER have only marginally improved patient selection, by excluding non-responders, lessons have been learned, particularly by the pharmaceutical industry, about the need to decipher the biological basis of response or risk seeing agents prematurely shelved. The most notable example of this is the response of non-small cell lung cancer (NSCLC) to gefitinib (Iressa), an epidermal growth factor receptor (EGFR) tyrosine kinase inhibitor, which showed promising results in pre-clinical studies, but far more modest responses in clinical trials (10-19%) (27;28). Discovery of mutations within the tyrosine kinase domain of the EGFR in NSCLC patients showing dramatic responses to gefitinib caused much excitement that the basis and a marker for sensitivity could be elucidated (29), but the initial enthusiasm was tempered when it became clear that these mutations occur at low frequency, and rarely in smokers (30), who most commonly develop the disease. Since immunohistochemical (IHC) detection of EGFR was not associated with gefitinib response (31;32), it became apparent that methods of patient selection needed to be refined and standardised, in the same way that issues surrounding the detection and criteria for treatment in HER2-overexpressing tumours have evolved since early trials (33). Debate continues as to the optimal approach for selecting

tumours likely to benefit from HER targeted therapies; high EGFR gene copy number detected by fluorescence *in situ* hybridisation, gene mutation and protein overexpression are all candidates in NSCLC (34), suggesting that similar approaches could be explored when using EGFR-targeting agents, such as gefitinib and lapatinib, in the treatment of breast cancer. Although the expression levels of EGFR in breast cancer have been investigated extensively, precise estimates of figures for EGFR 'positivity' have been hampered by the methodological differences between studies, including the use of different assays targeted against DNA, RNA, protein, and activated phosphorylated proteins (35). However, it appears that EGFR is positive in approximately 45% (range 14-91%) of all breast cancers (36;37), and expression is associated with high grade, hormone-receptor negative tumours and increased in vivo proliferation (38)'(39). Expression of EGFR is also enriched in basal-like breast cancers and breast tumours from BRCA1 mutation carriers, with up to 70% of basal-like breast cancers expressing EGFR (40;41). Furthermore, EGFR expression is seen by immunohistochemistry in metaplastic breast carcinomas and in the stromal compartment of phyllodes tumours (80% and 19% respectively) (42;43). These data suggest that there are a number of patient groups who could benefit from EGFR-targeted therapy. However, activating mutations within the kinase domain of EGFR are not seen, and gene amplifications are only detected in up to 6% of invasive breast cancers, although this increases to 25% of those with a basal-like phenotype (44). Nevertheless, and especially due to the close association with hormone-receptor status and the potential targeting of hormone-refractory breast cancer, EGFR-inhibitors have been used in a number of Phase I and Phase II clinical studies (45). Responses to single-agent therapy with gefitinib in hormone-resistant breast cancer has been disappointing, with low clinical benefit rates terminating one trial early and low numbers in another making interpretation of response rates difficult. Likewise, and in spite of early data suggesting that combined therapy with gefitinib and the aromatase inhibitor anastrozole could induce disease stabilisation in 20% of patients, recent reports in the neoadjuvant setting have shown that gefitinib has neither a biological nor a clinical effect when added to anastrozole (46). The majority of these trials, however, did not select their patients prospectively on the basis of EGFR expression status and were small, and therefore any sub-group benefit may not have

been detected. Other members of the HER2 gene family may influence response to therapy and clinical outcome (9;38;47) and results from single-agent studies with lapatinib, as small-molecule inhibitor of EGFR and HER2 tyrosine kinases and dimerisation inhibitor, in which patients are treated on the basis of biomarker expression, are promising (48). Given the increasing knowledge of HER-family biology, similar hypothesis-driven enrichment of patient populations to be treated with EGFR-inhibitors should also be carried out, and detection and interpretation of EGFR standardised.

1.4 Looking beyond the target: pathway-driven tissue biomarker discovery

It is naïve to think we will be able to accurately stratify all patients into responders and non-responders on the basis of single biomarker approaches, even if the biomarker is known to be the drug target. Existing biomarkers are surrogates for complex tumour biology in which multiple, non-linear pathways are (abnormally) activated, within heterogeneous tissues. This means that resistance mechanisms may occur at the level of the target itself (such as presence or absence of activating mutations in EGFR), downstream of the target (such as loss of PTEN in Herceptin resistance), or secondary to the heterogeneity of the tissue itself; ie not all cells within the tumour express the target, so that the agent selects for resistant clones. In addition, other mechanisms may contribute to the effectiveness of the agent which are not directly related to the biology of the molecule that they inhibit, such as the potential contribution of inflammatory responses to Herceptin efficacy.

We have already discussed the role that specific EGFR mutations may have in gefitinib sensitivity in NSCLC. Recently, it was shown using a screening approach *in vitro* that other existing RTK-inhibitors may be used to successfully target imatinib (Glivec) resistant tumours, paving the way for mutation-specific treatment (49), which would necessitate mutation-specific biomarker analysis. However, since most of these mutations are probably rare events in breast cancer, there are currently two approaches to predictive biomarker validation for new agents in clinical trials. The

first is the 'bottom-up' approach, in which the targeted pathway is reconstructed from the literature, and multiple candidate biomarkers tested in neoadjuvant and adjuvant clinical trials with supporting evidence from *in vitro* and *in vivo* experiments, although rarely in a systematic manner. The second is the 'top-down' approach, where predictive signatures are produced from statistical analysis of gene expression array data.

The precedent for the 'bottom-up' approach has come from the investigation of the role of PTEN in Herceptin resistance (50;51). PTEN (phosphatase and tensin homolog deleted on chromosome 10) is a tumour suppressor protein which is frequently downregulated, although not usually mutated, in breast cancer (52). PTEN opposes the action of phosphatidylinositol 3-kinase (PI3K) and downstream AKT to attenuate signalling through this critical growth-promoting pathway, which is known to be inhibited in response to Herceptin and contribute to its anti-tumour action (53). Based on this knowledge of the underlying pathways, Nagata and colleagues showed that loss of PTEN contributes to Herceptin resistance through activation of PI3K signalling, and this has since been substantiated in other studies (50;51). This raises the possibility that PTEN and possibly AKT/PI3Kinase signalling would be an excellent candidate biomarker for validation in the clinical trial setting, although this has only been tested in small numbers of patients and is yet to be tested in the context of Phase III trials. AKT amplifications are rare in breast cancer, however a number of PI3kinase mutations (in the *PIK3CA* gene) have been described (54). Therefore, molecular profiling of the HER2/PTEN/PI3Kinase pathway should be prioritised for future biomarker profiling in Herceptin resistance.

More recently we have taken a similar approach to predictive biomarker analysis of a new agent being used in the treatment of breast cancer, RAD001, a mammalian target of rapamycin (mTOR) antagonist (55-60). mTOR is a 289kDa serine/threonine protein kinase that belongs to the phosphatidylinsotide-3OH kinase related kinase (PIKK) family. It exists in two distinct complexes within the mammalian cell, one containing mTOR, GβL and raptor, (known as mTORC1) and the other containing mTOR, GβL and rictor (mTORC2). These two mTOR complexes have distinct roles

in intracellular signalling, with both direct and indirect effects on AKT activity. Both inhibition and activation of AKT are seen, depending on which complex is inhibited. By reconstructing the pathway and measuring activated (phosphorylated) protein expression levels of candidate biomarkers in biopsies from patients treated with RAD001 for two weeks prior to surgery, we have shown that pre-treatment phospho-AKT (serine 473), but not total or phospho-mTOR, correlate with decreases in proliferation with treatment as measured by Ki67 proliferation indices. This counterintuitive result highlights how rational, pathway-driven biology can reveal new targets for predictive biomarker analysis beyond measurement of the drug-target alone. However, more sophisticated approaches to interrogating these pathways may be required in order to adequately deconvolute the inherent biological complexity. This is discussed in Chapter 2.

1.5 Beyond discovery – biostatistics in biomarker validation

Throughout this chapter we have highlighted contradictory results and some failings in the journey of new biomarkers from 'bench to bedside'. We believe that one of the key aspects of successful and speedy biomarker validation in current research and clinical practice is to ensure the appropriate statistical test and the appropriate statistical power is available prior to reporting of major clinical data sets, in order to ensure robust validation and reduce misleading results. Whilst small sample sizes or retrospective tumour studies are invaluable for hypothesis generation, it is imperative that for biomarkers to be appropriately validated *a priori* hypotheses are correctly defined and powered prior to commencing analysis.

Early reporting or reporting of inadequately powered studies, even within the context of large phase III clinical trials, may not inform and may in fact lead to inappropriate conclusions being drawn. This is particularly critical for studies reporting negative findings. As with other measures of outcome, where underpowered studies in which no evidence of benefit is observed are recognized as providing relatively little value,

we need to recognize similarly rigorous interpretation must be applied to biomarker analyses.

Two key examples illustrate this. Firstly, the potential predictive value of *HER2* gene amplification or overexpression with respect to tamoxifen treatment and the potential for *HER2* to act as a predictive biomarker for response to aromatase inhibitors. There is extensive *in vitro* and *in vivo* evidence to support the role of HER2 as a mediator of resistance to tamoxifen (9;61) and neoadjuvant studies suggest that in fact HER2 positive cancers may derive greater benefit from AIs than tamoxifen (62). However, a recent analysis of the BIG-I-98 trial, whilst suggesting that HER2 was indeed predictive of early relapse, failed to substantiate the interaction between HER2 and treatment with AIs (63). Critically, the authors correctly note that despite the large sample size of this study (7707 samples) the low rate of HER2 positivity (ca 5%) and low event rate to date (3.7%) in this low risk ER-positive population provided insufficient power to address the question of interactions between HER2 status and treatment modality. Therefore, *in this respect*, this study is unable to provide a definitive answer and further analysis or meta-analysis of the major adjuvant AI trials is awaited.

A second example relates to the potential interaction between HER2 and or topoisomerase IIα and response to anthracyclines, as previously mentioned. Several conflicting studies have been published with no clear evidence to suggest whether the interaction between response and biomarkers is attributable to topoisomerase IIα or HER2 (reviewed in (64)). Two conflicting reports relating to the BCIRG 006 trial were presented at the San Antonio Breast Cancer Symposium in 2005 and 2006. In the first report, based on the interim analysis of almost 60% of cases recruited to the BCRIG006 trial, a potential interaction was suggested between topoisomerase IIα and benefit from anthracycline treatment (65). The second analysis, based on analysis of over 90% of cases, and with increased follow up, failed to identify any interaction (8). Two potential explanations exist for this difference, observed within the same study population and reported by the same group. Firstly that the first interim analysis was, in some way, biased by the inclusion of only a small proportion

of patients within the total trial population. Secondly, that in fact the interaction between biomarkers and treatment outcome is in some way time dependent. This is discussed in greater detail in Chapter 2 Further analysis of the BCIRG006 and other datasets will be required to investigate these possibilities.

These examples, however, serve to underline the fact that biomarker analysis is a complex field and one where simplistic answers are hard to come by. For appropriate studies to be designed and correctly interpreted statistical approaches no less rigorous, and potentially more complex, than those employed for the analysis of primary endpoints of response must be employed. Treatment interactions with biomarkers, where treatment response may differ between biomarker positive and negative cases, require multivariate analyses which increase the required sample size. Agreed analytical procedures, which address the potential for interactions between biomarkers and treatments and the potential for such interactions to change over time will need to be determined for future biomarker analyses. Finally, caution must be applied to inappropriately powered studies and, where biomarkers may select small subgroups of cancers, meta-analysis of compatible trials may be required in order to provide definitive answers to some questions.

1.6 Conclusions

In this chapter we have highlighted some of the hurdles which have to be jumped before predictive biomarkers can be considered for clinical practice, with regards to current approaches to tissue biomarking in breast cancer and candidate biomarkers which are likely to be tested in the clinical arena in the relatively near future. Even biomarkers such as TIIα, which have been recognised as potential markers for several years and tested within large Phase II trials, are courting controversy. We have shown how the 'biomarker journey', from bench to bedside, should be underpinned by sound biological hypotheses. Predictive biomarker development will need to change from 'survival of the fittest' (ie value based on publication frequency), to a structured, multi-tiered approach, including the use of preclinical

models, neoadjuvant clinical models, properly designed retrospective studies, and validation within prospective clinical trials. The development of robust and accurate diagnostic assays should precede, not follow, the identification of a potential clinical role for biomarkers.

Predictive marker development requires the coordinated effort of multiple academic institutions and industry to cover all the aspects of development. It takes many years, large investments, and the risk for failure is high because of the nature of drug development. That may be the reason why so few new markers have been introduced in recent years despite major research, development efforts and new techniques. However, there is cause for optimism for the future, provided rigorous scientific procedures are followed in biomarker analyses. Some new advances in reducing risk and increasing success are discussed in Chapter 2.

Chapter 2: Systems Pathology – taking molecular pathology into a new dimension.

2.1 Background

In Chapter 1 we discussed the current state of biomarker development in breast cancer, which has been driven largely by the will of the oncology and translational science community. Arguably, there has not been consistent and well-funded input from pathology into this interface between biomarker discovery and oncology. In this chapter we discuss the role that modern molecular pathology and systems biology might play in overcoming some of the problems which were discussed, such as effective preclinical testing and a lack of systematic interrogation of the underlying biology, using cutting edge approaches and techniques. The wealth of morphological, histological, and molecular data from human cancers available to pathologists means that pathology is poised to become a truly quantitative systems science. By measuring morphological parameters such as tumour stage and grade, and by measuring molecular biomarkers such as hormone receptor status, pathologists have sometimes accurately predicted what will happen to a patient's tumour. While 'omic' technologies have seemingly improved prognostication and prediction, some molecular 'signatures' are not useful in clinical practice because of the failure to independently validate these approaches particularly when applied outside the setting of a clinical trial, and because many tests have a low positive predictive value. Many associations between gene 'signatures' and clinical response are correlative rather than mechanistic and are poor predictors of how cellular biochemical networks will behave in perturbed, diseased cells. Using systems biology, the dynamics of reactions in cells and the behaviour between cells can be integrated into models of cancer. The challenge is how to integrate multiple data from the clinic into tractable models using mathematical models and systems biology, and how to make the resultant model sufficiently robust to be of practical use. In this chapter we also discuss the difficulties in using mathematics to model cancer, and review some approaches in systems biology and experimental pathology which may be used to see systems biology successfully applied in the clinic.

2.2 Introduction

New mathematical models exploit what is known about signalling networks and therapeutic mechanisms to produce a dynamic system, which can be personalized and used to simulate the natural history of a tumour and responses to therapy. In addition to being a practical tool to aid patient management, it is also a powerful hypothesis-generator, exploiting what is known about molecular tumour pathology and what is not known and worthy of further investigation.

Kinetic modelling of complex biological systems, however, is still perceived as esoteric and not clinically applicable because there are very few successful examples of when such modelling has changed practice (66). One notable exception is modelling of ion-channels in the heart which has helped explain the previously ill-defined action of the drug ranolazine (67-69). These modelling data were subsequently used within an FDA submission as supportive evidence for mode of action ((70) and http://www.fda.gov/bbs/topics/news/2006/NEW01306.html). In oncology, systems biology has not yet made the same impact, but with the increased use of therapies targeted against the products of cellular oncogenes, the practical and clinical implications of more in-depth understanding of deregulated signalling pathways is starting to impact on clinical practice. For example, activating mutations in the oncogenic *PIK3CA* and inactivation of the tumour suppressor gene *PTEN* are known to regulate phosphotidylinositol 3-kinase signalling and cell proliferation and survival pathways, which have a role in resistance to anti-HER2 therapies in breast cancer (as already discussed in Chapter 1 and (71;72)). Recent advances in histopathology, molecular pathology, and computational biology make it feasible to test the hypothesis that systems biology can predict responses to cancer therapy in real patients using data from existing clinical trials. A dynamical systems approach to integrating multifaceted and complex data from cancer cells and tissues is more than simply consideration of histological pattern recognition, grade, stage, and genetics, proteomics, and molecular pathology data. Here we suggest ways forward using mathematical and biological models, clinical tissue samples, and methods of data generation, which have allowed this area to evolve, and we also discuss some of the challenges that remain. The molecular basis of breast cancer is particularly well

understood and is therefore data-rich compared to other solid-organ tumours. Predictive pathology tests (such as ER and HER2 immunohistochemistry) are used routinely in the clinic in breast cancer, but there is room for improvement. It is therefore a good disease on which to discuss some of the issues surrounding mathematical modelling and response prediction.

2.3 Making predictions from histopathological snapshots

Cancer is a complex, dynamic disease characterized by the ability to become autonomous in growth, evade death, sustain angiogenesis, invade surrounding tissues, and to metastasize (73). Currently, pathologists generate data from a single pathological snapshot, which acts as a surrogate of the intrinsic biology of the tumour (Figure 2.1), and forms part of the clinical record from which treatment decisions are made. This approach is remarkably powerful and has stood the test of time for prognostication; however, it does not meet the challenge of predicting individual responses to treatment. The most common classification of tumour stage is the TNM classification, which is based on tumour size, and the presence of nodal or distant metastases (74). The tumour stage gives an estimation of the amount of time, or degree of tumour progression, between tumour initiation and resection. The longer the time period between tumour initiation and resection, the greater the chance that the tumour will have undergone clonal evolution and acquired a set of unfavourable characteristics, such as greater size, ability to invade lymphatics or blood vessels, or metastasize to distant sites. In breast cancer, the grade of the tumour is a semi-quantitative composite of mitotic activity, nuclear pleomorphism, and tubule formation (75), which is an indication of the intrinsic biology of the tumour. A high-grade breast tumour with a pushing border, prominent lymphocytic infiltrate, central necrosis, metaplastic elements, and brisk apoptotic rate is likely to belong to the 'basal-like' group of breast cancers (76;77), although it is unclear whether this is really a distinct histological or biological group (78). Clinically, these tumours are associated with a poor prognosis and comprise 20% of the total invasive ductal carcinomas. Data generation from tissue has been further refined by advances in molecular classification of cancers by whole-genome expression and analyses of

gene amplification or gene loss (79;80), and pathologists can make even more detailed assessment of intrinsic pathway biology based on morphological features alone. Tumours of the basal group of breast cancers are likely to express low or no levels of ER, are HER2 negative, but have a high incidence of EGFR protein overexpression or amplification at the genomic level (77). These tumours are likely to harbour overexpression or mutation of p53 and therefore have abnormal cell survival responses (77). If the tumour has occurred in a patient younger than 50, the patient is likely to harbour a germ line mutation in *BRCA1*, and she and her family should undergo genetic counselling and testing (81). The tumour is likely to respond to treatment with platinum-based or taxane chemotherapy (82;83), and would be a promising candidate for enrolment in an EGFR-inhibitor trial.

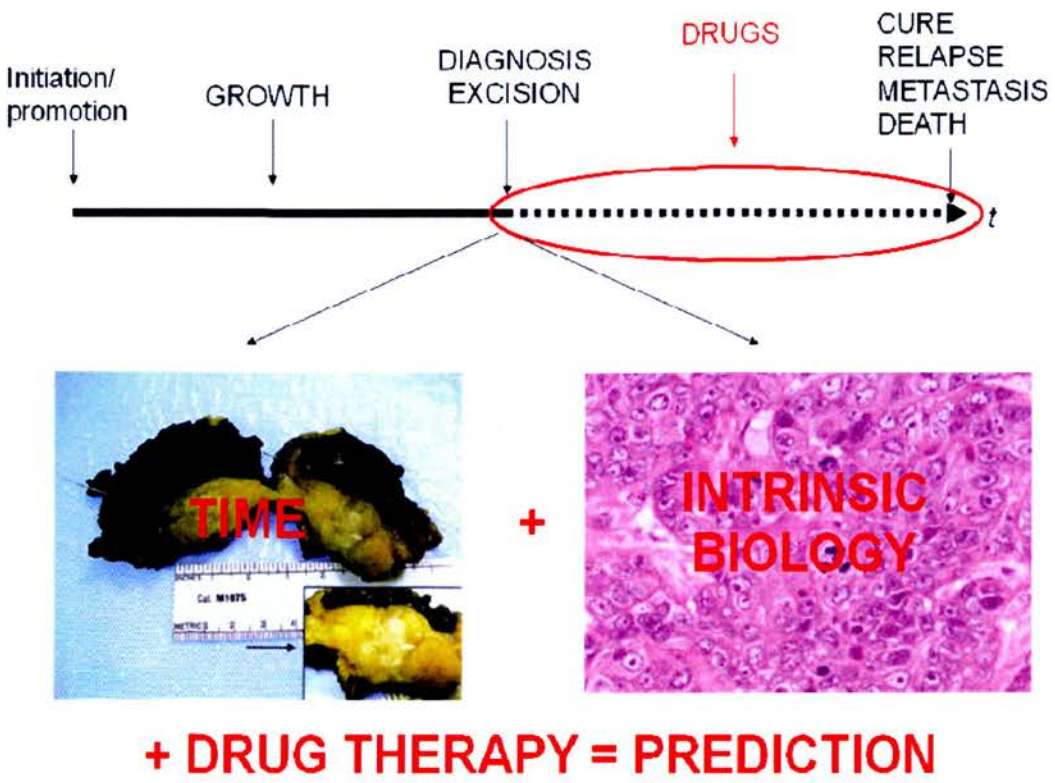

Figure 2.1: The current state of pathology. Therapeutic outcome is inferred from stage (macroscopic data) and grade (microscopic data), which are surrogates of time passed and intrinsic biology. Systems pathology, applied to oncology, mathematically describes tumour behaviour after diagnosis (dashed line), allowing simulation of the effects of disease modifiers (ie drugs) on outcome or, in the reverse causal direction, what combination of drugs in a particular tumour are needed to produce a desired effect (ie decreased proliferation, increased apoptosis, or decreased DFS or OS).

Therefore, from static measurements alone pathologists are good at estimating dynamic processes such as prognosis through the integration of grade and stage, and this is rarely surpassed in multivariate analysis by ancillary methods such as immunohistochemistry for tissue biomarkers or flow cytometry for DNA content (84). In a limited numbers of cases, such as in basal-like carcinomas with characteristic morphological features, the static morphological snapshot broadly defines the activation status of up to five pathways implicated in carcinogenesis (i.e. EGFR, ER, HER2, p53, and BRCA1). It has been proposed that the 80 or so mutations found in solid cancers can be reduced to a limited number of abnormal pathways (85). Therefore, traditional morphological pathology can already comprehensively define the molecular pathology of the tumour in these cases, and this information can be used to plan the management of patients, and be exploited for targeted and combinatorial therapy (85;86).

2.4 Improving predictions from molecular markers

With the advent of 'targeted' therapies that recognize and target cellular oncogenes such as trastuzumab (Herceptin) that targets the HER2 receptor, there is a need for accurate characterization of the underlying oncogenic signalling pathways (72). We need to know not only the structure of these pathways, but also how manipulation of a part by a drug might affect the dynamics at the cellular and tumour level. To date, this approach has relied on static pathological measurements. Morphology alone is powerful, but reflects pathway biology only in a very limited sense, due to the remarkable heterogeneity of solid tumours, lack of distinct clinicopathological entities, and lack of comprehensive molecular classification of the majority of diseases. Although traditional histopathology has enabled rigorous validation of histological prognostic features to clinical endpoints such as relapse and survival, the management of patients with cancer based on prediction of how the patient will respond to any given treatment is now almost as heterogeneous as the tumour it is designed to treat.

As a result of the complexity of tumour biology, patients tend to be over-treated, on the premise that offering a therapy with a small chance of success is still preferable to offering no treatment at all. Thus, 60% of patients with breast cancer unnecessarily receive endocrine therapies (87), and the benefit derived from trastuzumab is only seen in 30–40% of patients who receive it (88). As discussed in Chapter 1, with the exception of ER and HER2, no other predictive tissue biomarkers have been widely adopted in oncology, despite the plethora of literature that indicate new predictive markers for assessing responses to agents (84). We have already discussed, as have several articles, the reasons for this situation (84;89), but essentially the current approach to translational research by the analysis of candidate biomarkers, even within large trials, requires re-evaluation. The emerging evidence indicates that failure to recognize dynamic properties of signalling can result in costly mistakes. For example, loss of feedback inhibition in tumours treated with mammalian target of rapamycin (mTOR) inhibitors results in induction of AKT signalling, and may be responsible for the disappointing efficacy of mTOR antagonists in the clinic (90). Negative feedback signalling mechanisms are likely to contribute to the poor efficacy of agents when studied in phase II and phase III cancer trials and to the high rate of attrition of drugs (approximately 30% due to efficacy), which is both time consuming and expensive (91). Empirical testing of every possible agent or combination of agents in the preclinical or clinical setting would be prohibitively expensive and impractical.

Kinetic mathematical models, therefore, offer the potential to relate molecular-level knowledge to outcome at the cellular and tumour level. Essentially models provide the opportunity to perform trials *in silico* (that is via computer simulations), not necessarily to provide a definitive answer but to contribute to a body of evidence in order to make informed decisions about predicted efficacy. Utilizing dynamic models as predictive tools, therefore, holds promise for reducing treatment failures. Nonetheless, progress in the development of mathematical models suitable for implementing pathology has been slow, as discussed below.

2.5 Why has it been difficult to mathematically model cancer?

We have reviewed the current approaches to modelling cancer elsewhere (92) and have identified both limitations and potential opportunities. With particular regard to pathology, we can identify a number of challenges facing such approaches that must be overcome for the oncology field to progress.

2.5.1 Network complexity

Cancer is a heterogeneous and complex set of diseases, resulting from the accumulation of multiple genetic defects resulting in aberrant pathway activation and disordered growth and survival (73;93;94). At the cellular level, the network of interactions between the various signalling and regulatory pathways governs cell behaviour. In general, the interactions between the components of the cell network are non-linear. This means that small uncertainties in relationships between pathways and the defining parameters of their interactions leads to disproportionate errors in predicted dynamics (95). Given that we will never know the exact details of the network, and that these will vary between patients and at different times in the progression of the disease, it seems improbable that precise definition of metabolic and signalling pathways in cancer is either possible and may not even be desirable.

2.5.2 Cancer measurements are static, not dynamic

Based on grading and staging, the rate of proliferation, and the invasiveness of tumours are major determinants of prognosis (74). The behaviour of cancer is most often characterized pathologically in terms of data collected at a single time point (e.g. from a treatment-naïve diagnostic biopsy or resection specimen) or at relatively few time points in *in vitro* cell-line studies. These data are considered along with other data such as imaging and clinical staging. In essence, clinicians infer underlying dynamics from a single or at best relatively few snapshots of the system.

2.5.3 Spatial heterogeneity

The phenotype of a tumour is not governed only by the epithelial component but also but the tumour environment, that is other cells in contact, the mesenchyme, and inflammatory infiltrate, because these components determine the net inputs to the cell, which includes ligands, cell-cell adhesion molecules, metabolites, oxygen, and drugs. It is important to know how to characterize and quantify the spatial heterogeneity at a given time to inform our understanding of the dynamics. This includes the collection and interpretation of measurements of both the intracellular and extracellular environment. On a finer scale, the intracellular regulatory network is imbedded in a complex spatial context within the cell (96). Many key processes occur on surfaces or across membranes and this spatial compartmentalization within cells has a profound impact on the dynamics of signalling within cells and therefore their response to the environment (96). Relatively little information is available on the spatial organization of key proteins within cells, although recent imaging techniques offer the potential of high-resolution measurements of the spatio-temporal dynamics of large numbers of proteins (97).

2.5.4 Uncertainty and incomplete knowledge

Perhaps the incomplete knowledge of the underlying biology contributes to our lack of understanding of complex biological systems. There is no *a priori* reason why system behaviour should not be highly sensitive to the specific functions of the signalling network. Indeed the efficacy of targeted therapies result from such sensitivities (98;99), and many serious consequences and adverse effects can arise from relatively few, though coordinated, point mutations in key target genes involved in signalling pathways (85). A combination of the strength of the interactions, the complexity of the networks and the dynamics of the systems, means that a full characterization of the interaction network implicated in cancer could require a prohibitive quantity of data.

2.5.5 Combining qualitative and quantitative data

There are a large amount of data and knowledge relating to cancer, but much of it is difficult to integrate for mathematical modelling (for instance sequencing data, copy number gains and losses from array comparative genomic hybridization, high-throughput transcriptional data, quantitative PCR data, biochemical data from *in vitro* and cell based assays, animal models etc), because it is not quantitative, generated in different experimental models, related to a single timepoint, or generates inconclusive results. Thus a range of bioinformatics approaches and new data standards are being developed to address this problem, particularly with respect to high-throughput data and standards within systems biology (100;101). Much of our knowledge concerning biological systems is qualitative but later we propose ways to move pathology towards more-accurate quantification of molecules and their dynamic interactions in tissues.

2.5.6 Physiology versus pathology

Computational systems biology has allowed us to test our understanding of the dynamic behaviour of a few well-characterized pathways using computational models to predict their behaviour (102-108). These models have proven to be extremely useful in helping us to understand the behaviour of quite complicated intracellular signalling pathways, for instance the canonical MAPK and PI3K growth and survival pathways (103;106;109), and changes in the cell cycle (102), in response to physiological stimuli such as growth factors (102-105;110). However, such models have not been so helpful for understanding therapeutic interventions. 'Bottom-up' approaches (in the context of systems biology) are when cell signalling pathways are reconstructed from the literature, whereas 'top-down' approaches are where network structure is constructed from high-throughput, high-density datasets such as transcriptional profiles. Bottom-up approaches have contributed extensively to the foundations of systems biology by modelling physiological pathways and describing systems behaviour such as emergent properties (e.g. thresholds, oscillations and signal duration) (95). However, bottom-up approaches have focused

on physiological rather than pathological systems (such as EGFR signalling and PI3K signalling), which are simpler. Such approaches frequently fail to include important oncogene and tumour suppressor nodes, which are known to be fundamental to breast carcinogenesis and proven resistance proteins (such as HER2, PTEN, and SRC in PI3K and MAPK signalling models). Currently, no dynamical models incorporate ER signalling as a core module, which is clearly essential to understanding anti-estrogen responses in breast and ovarian cancer.

2.6 Proposed solutions

A full description of mathematical techniques for kinetic modelling employed in cancer is beyond the scope of this review, and more-comprehensive descriptions have been published elsewhere (95;110;111). As a means of illustrating a vision for systems pathology, we outline broad illustrative mathematical techniques in dynamic modelling, which would allow pathology to be embedded in a systems framework, either indirectly by contributing to decision-making in translational medicine, or by the direct use of molecular pathology data in mathematical models. Initially such models might be used along with other forms of evidence, such as preclinical testing and data from early phase trials in order to obtain rationally selected biomarkers or to choose or reject certain drug combinations over others. In time, computational modelling would run in parallel with ancillary tests and form part of the pathology report and decision-making process. Since no single systems biology approach is universally appropriate (108), we suggest that there are advantages for progressing complementary hypothesis-driven and data-driven methodologies. Each approach offers advantages over the other, but each has their own limitations.

2.6.1 Hypothesis-driven approaches

Hypothesis-driven approaches that are relevant to the study of the dynamics of cell networks include those where the network is prescribed *a priori*, such as mechanistic, deterministic ordinary differential equation-based mathematic models (e.g. those describing EGFR signalling) (103;105). The intricacies of the interaction

network is often the subject of investigation in itself, and so any prescribed network should be taken as a working hypothesis. Except in a few cases, the quantitative details of the interactions are unknown and so it is necessary to hypothesise relevant forms of the equations governing the interactions and estimate the values of the associated parameters. A major challenge of this approach is that the level of detail demands knowledge of a large number of parameters to fully characterise the dynamics of all the interactions. For this reason, hypothesis-driven approaches have generally only been applied to relatively small networks where comparatively large amounts of quantitative data are available (95). However, as many new therapies in preclinical or early phase trials are targeted against well-characterised pathways (e.g. mTOR inhibitors, PI3K inhibitors, RTK inhibitors) for which models exist but which are missing key oncogene or tumour suppressor nodes (e.g. PTEN in EGFR signalling models, or mTOR module), it would be relatively straightforward to extend these models to investigate resistance factors, or interrogate network behaviour. In this way, unwanted signalling feedback from mTOR to pAKT would be determined before clinical testing (90), and candidate sensitivity and resistance biomarkers may be prospectively selected with a greater level of evidence and confidence, such as PTEN in trastuzumab resistance (see Chapter 6 and (51;71)).

Some have argued that hypothesis-driven approaches have no rational limit to the level of detail needed, and that the demand for quantitative dynamic data is unattainable, making this approach unlikely to succeed. In other words there is simply no end to the requirement for data. There are data indicating that as complexity grows, the behaviour of the network becomes insensitive to the details of many of the interactions (112). This outcome would indicate a logical limit to the level of detail required, beyond which additional complexity does not contribute significantly to the predicted dynamic behaviour of cell systems. If this is true, then we need not be limited to 'small' ordinary differential equation-based mathematical models, which are descriptions of relatively small parts of the regulatory network of the cell. Instead, we can build larger ordinary differential equation-based mathematical descriptions that are sufficiently comprehensive to link combinatorial approaches spanning multiple pathways and pathology (113). Thus, systems pathology can maintain a pragmatic approach to the complexity of data generation

guided by its ultimate usefulness for diagnosis, prognosis, and prediction of response to therapy.

We often want to be able to ask questions in the reverse-causal direction such as "how do we need to change the system to realize this (qualitative) result?" As an example, a systems model for breast cancer can be developed using data obtained from tissue measurements obtained from a given patient (e.g. quantitative measurements of HER2 amplification status, ER and PTEN expression levels). For a given set of potential drugs, we can use the model to predict combinations and doses of the different drugs that return the cell to a normal, non-proliferating state (Figure 2.2; reproduced with permission of Robert Clyde, University of Abertay, Dundee). An advantage of this approach would be to use the model to predict the consequences of each of the drug combinations found to be consistent with the desired outcome on cancer cells, and predict their consequences for healthy cells. Hence, the model could be used to predict drug regimens tailored to individual patients that are most likely to have a good outcome with minimal toxicity. Although this approach would require additional compartments in the model to deal with the relevant pharmacokinetics, the result can be achieved by using the model for different combinations of drugs and applying optimisation approaches (e.g. genetic algorithms) to converge on combinations that are consistent with the desired dynamical outcome, such as a pro-apoptotic response in cancer cells that harbour oncogenic mutations, and no response in normal tissues. It is likely that as this kind of model becomes more quantitative and our knowledge increases, so too will the need for quantitative, quality-assured molecular pathology data.

The interaction networks implicated in cancer not only include those within cells (e.g. EGFR or PI3K signalling networks), but between cells and their environment, and other regulatory networks including the endocrine and immune systems. Any systems approach must be consistent with incorporating higher levels of organisation as required by the particular application. The simplest way to do this is to abstract the system into relevant functional modules that interact with each other. Examples include the cell, the cell environment, the vascular system, and the endocrine network, similar to that already described for the heart (68). In this way

heterogeneity at the tumour level can be accommodated by representing a number of different (evolvable) cell types interacting via a dynamic environment. This model approach is only possible if the associated interactions can be characterized sufficiently accurately to allow reliable prediction. Techniques exist for deriving the set of parameters of a given model that are consistent with a given set of data (114).

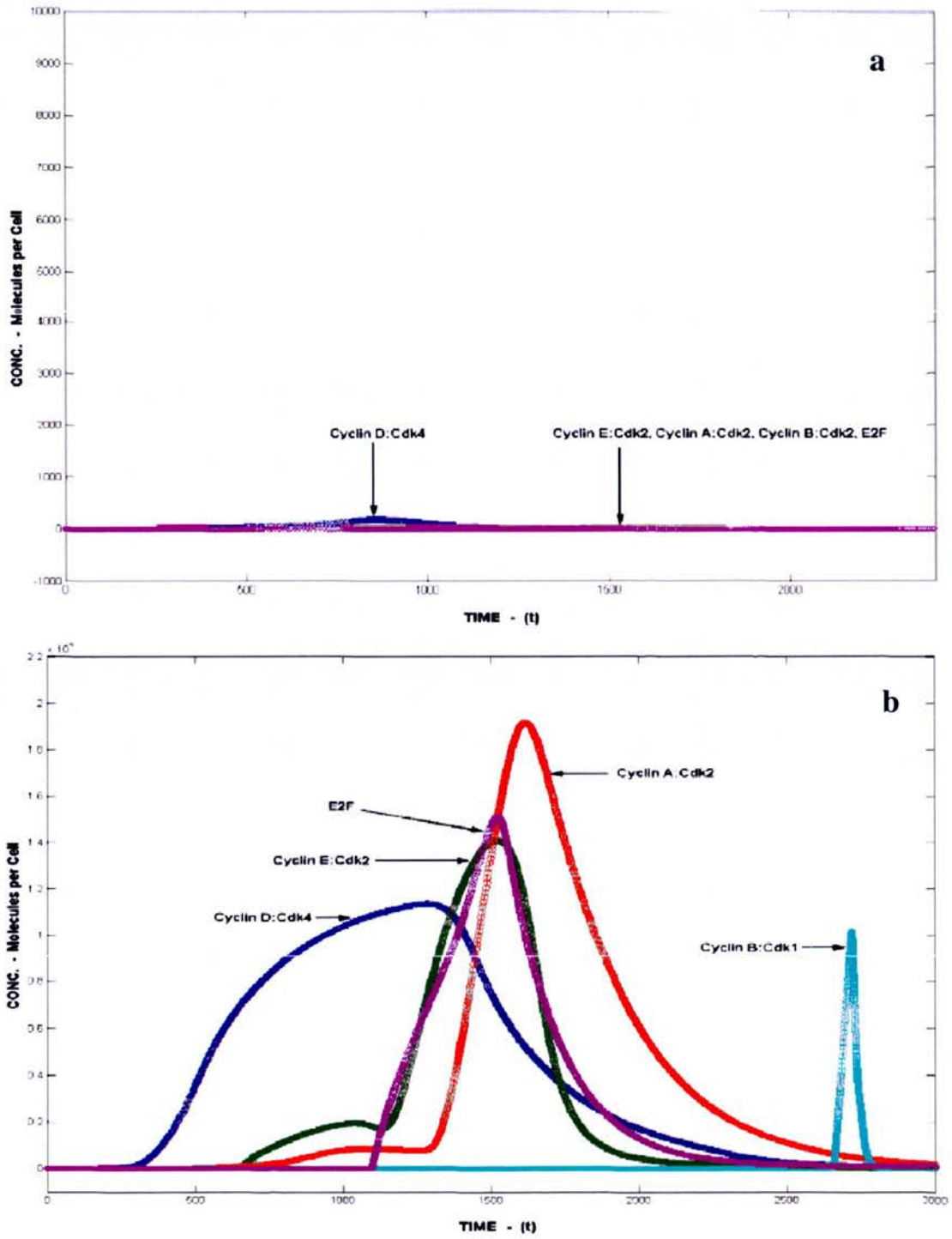

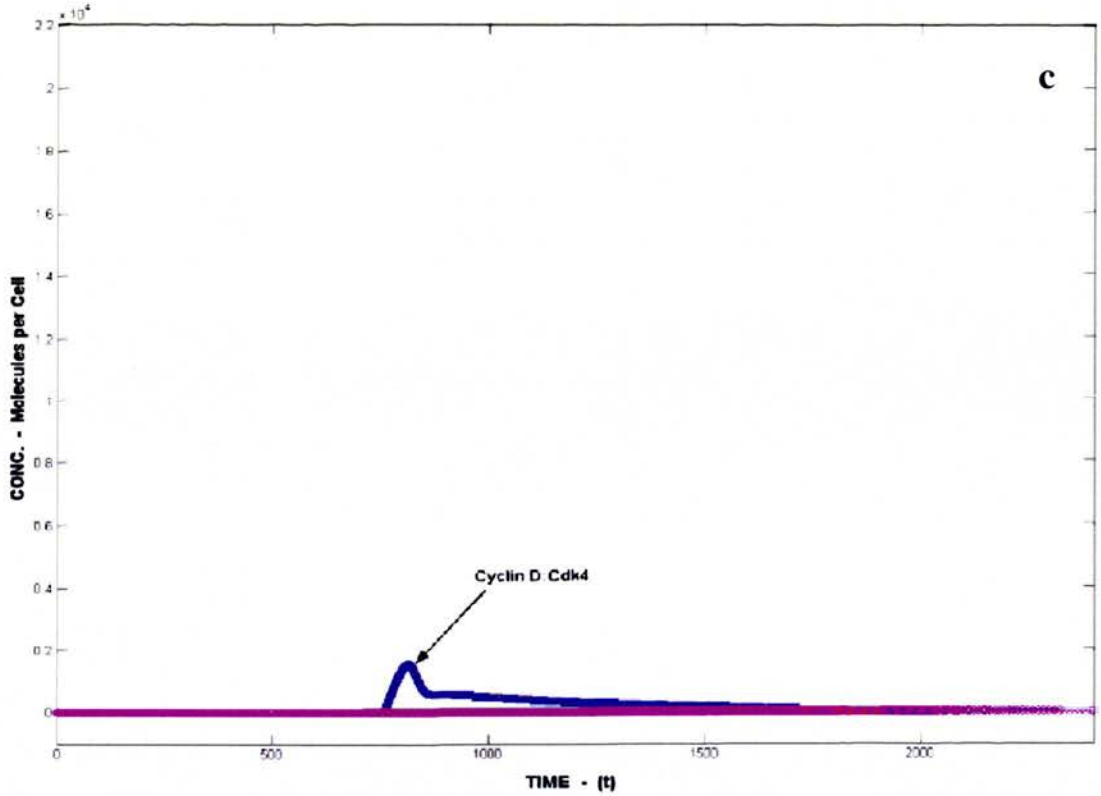

Figure 2.2: Simulation of molecular activity in ER+Her2+ breast cancer using a 'large' (>200 species) ordinary differential based model. Lines represent concentrations of cell cycle proteins in the cell over time. a. A 'normal' breast epithelial cell has very little cell cycle progression under resting conditions. b. The same cell, when harbouring commonly found aberrations in endocrine pathways, oncogenes, and tumour suppressor genes (ER, HER2 and PTEN) shows ordered cell cycle progression and proliferation. c. The same cancer cell after treatment with a combinatorial drug regimen consisting of tamoxifen, an mTOR inhibitor, and trastuzumab identified by a search algorithm. There is almost complete inhibition of proliferation under these conditions, which would be expected to translate into clinical benefit.

Where these approaches employ genetic algorithms to evolve or define the parameter, the target behaviour of the model can be expressed both quantitatively and qualitatively. Given the majority of existing data is qualitative, this is an important advantage.

2.6.2 Data-driven approaches

Important examples of data-driven approaches are general power-law formalisms (a set of mathematical tools for the approximation, modelling, numerical simulation and analysis of nonlinear systems) including Biochemical Systems Theory (115) and Metabolic Control Analysis. Power-law formalisms have been employed in the study of biological networks for more than 30 years, although Metabolic Control Analysis has only recently been applied in the study of cancer (116). Data-driven approaches, including power-law formalisms, are essentially local approximations of the cell and its microenvironment. This means that any resulting analyses are only valid when the cells are infinitesimally close to their state at the time of measurement. The Biochemical Systems Theory is based on an underlying S-system (which is a mathematical representation of non-linear systems, based-on power laws) approach that explicitly represents the dynamics of the network in terms of differential equations that describe the rate of change of variables such as protein concentrations or gene-expression levels (117). The equations characterise the rate of change of the variables in terms of the interaction between components of the system as products of power-laws of the concentrations (or expression levels) of these components. It can be shown that any kind of interaction can be approximated by this form, at least locally.

Using an S-system approach, one can derive an interaction network for a given set of measured variables by deriving the values for the power-law exponent by fitting the equations to time series data (any form of data in which kinetics are described by making a series of measurements over time). Where this fit returns a value of zero, one can infer that the variable in question is independent of that component. By noting only those non-zero exponents for each variable in the system, one can build up the network of interactions between them. As shown in Figure 2.3, this network can be visualized to indicate those links that most sensitively affect the rate of change of connected components. In this sense, the derived network can be used to identify components as potential targets for changing the dynamical state, such as a new drug target or tumour-suppressor nodes. The prediction is valid provided the system is not changed too much from the dynamical state in which the

original measurements were made or where combination therapies are being considered. To our knowledge, the S-system approach has not been applied to the study of cancer, because currently the use has been restricted to a relatively limited number of theoreticians. However, it is beginning to be used in relevant areas of biology such as the analysis of experimentally-derived time courses of cDNA gene expression array data, albeit in yeast (118). This is promising since it is proof of principle that indeed the technique may be used in gene expression data generated from cancer specimens, such as those taken at different timepoints in a neoadjuvant trial.

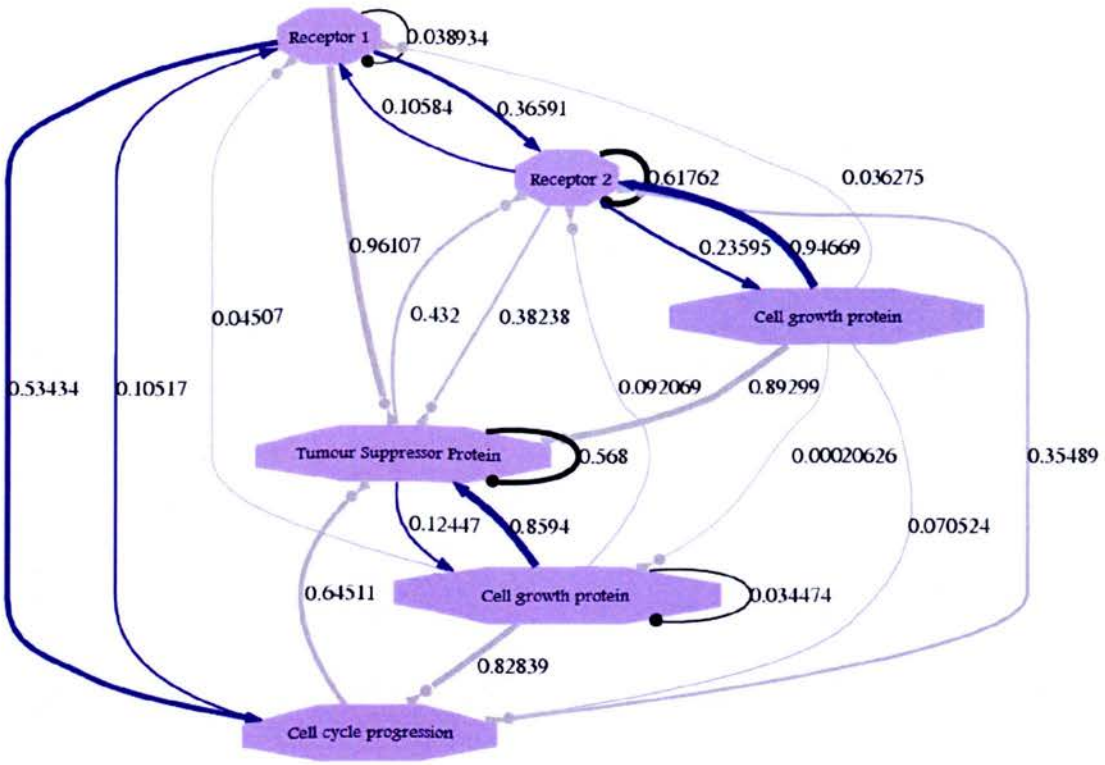

Figure 2.3: Network interactions in cancer, derived from quantitative protein time-series data in vitro using the S-systems Biochemical Systems Theory approach. In response to extracellular ligand, a network diagram is constructed which accurately reconstructs network biology (receptor dimerisation, positive and negative feedback loops). The tumor suppressor role of the tumor suppressor protein (centre) is readily appreciated through multiple inhibitory links to cell growth proteins, and suggests that loss of this key 'node' will result in uncontrolled proliferation. For new networks this leads to new hypotheses, or druggable targets. Blue lines = activation/phosphorylation, grey lines = inhibition/dephosphorylation, black lines = autophosphorylation, numbers = strength of interaction. Reproduced with the permission of Michael Idowu, University of Abertay, Dundee.

An interesting and recent alternative data-driven approach that can be used when qualitative and/or imprecise measures are present exploits fuzzy logic (119), a mathematical term used to describe decisions or biological readouts which have a continuous range between 0 and 1, that is they are imprecise but within boundaries, in contrast to binary logic, when the decision is discrete, either 0 or 1. The state (eg of a probe measuring gene expression on a cDNA microarray) may be imprecisely but qualitatively defined and the rules mapping the state to a future imprecise/qualitative state are based on a set of probability-like functions. The limitations of the approach are similar to those for the other data-driven approaches described above, and their application to large, highly interconnected, networks can result in an unmanageable volume of data required to calibrate the models.

2.7 Data requirements

Although the past few years has seen massive increases in the amount of data generated from biological samples, particularly in the form of gene-expression microarrays, embedding pathology and tissue-based analysis within the systems framework may offer new opportunities for prediction in patients with cancer. If powerful systems tools are to be adopted by the clinical community, it is critical that those individuals involved in clinical trials (particularly oncologists) are aware of these challenges, since they must be specifically addressed in the trial design and planning stages. By doing so, the quality and quantity of pharmacodynamic and pharmacokinetic data may be vastly improved.

2.7.1 Achieving spatial resolution

In tissues, two spatial levels must be specifically resolved; tissue compartments or variability within compartments (i.e. epithelial, stromal, inflammatory component, vascular, and interstitial) and cellular compartments (e.g. immediate extracellular environment, membrane, cytoplasmic, nuclear and organelles). We use two strategies to combine compartment-specific analysis with high-throughput molecular analysis; microdissection and *in situ* protein quantification. Microdissection is becoming a

standard strategy in gene-expression microarray (120) and genomic hybridization protocols (121) in order to enrich for epithelial-cell populations, either to overcome the inherent limitations of sensitivity of the assay (as in array CGH) or in order to infer compartment-specific biology (as in the case of gene expression) (120;121). Microdissection might mean a relatively crude dissection of the epithelial area of a tumour by hand under a dissecting microscope, or alternatively the use of laser capture/catapult microdissection techniques in order to obtain populations of pure cells (122). The latter approach may be more suited for systems biology because the methodology can also be extended to separate any tissue compartment (e.g. blood vessels, stroma), and also morphologically heterogeneous elements within the epithelial areas of tumours, which have differential gene and protein expression signatures and therefore potentially different responses to therapy. The second method we are using is *in situ* protein quantification on automated image analysis platforms for total and phosphorylated (usually active) states of proteins within signalling pathways of interest (see Chapter 4, 5 and 6 and Figure 2.4) (123). These methods multiplex antibodies against particular compartments (e.g. epithelial) with one or more targets of interest, so that compartment-specific protein expression can be quantified. The advantage of this technique over microdissection methods is the ability to discriminate protein expression levels at compartmental and subcellular levels. However, disadvantages include the limited number of targets that can be measured from a single section (which is governed by the number of filters (usually up to five) on the fluorescence microscope), availability of high-quality specific antibodies, tissue auto-fluorescence, and difficulties with absolute quantification. In addition, most histopathology labs use colorimetric techniques rather than immunofluorescence for biomarker quantification, and do not have access to this cutting-edge technology. We have therefore also used immunohistochemistry-based quantification to measure ER in tissue sections from breast cancers, which may be more readily applicable to clinical pathology laboratories in the near future (see Chapter 3). While most *in situ* methods are limited to protein techniques, all macromolecules may be extracted from microdissected tissues, including RNA, microRNA, DNA, and protein. Each macromolecule is amenable to high throughput array-based technologies and, in the case of protein, the tantalizing prospect of

reliable clinical mass-spectrometry proteomics (124) can offer quantitative advantages or assessment of functional post-translational modifications (e.g. phosphorylation or acetylation).

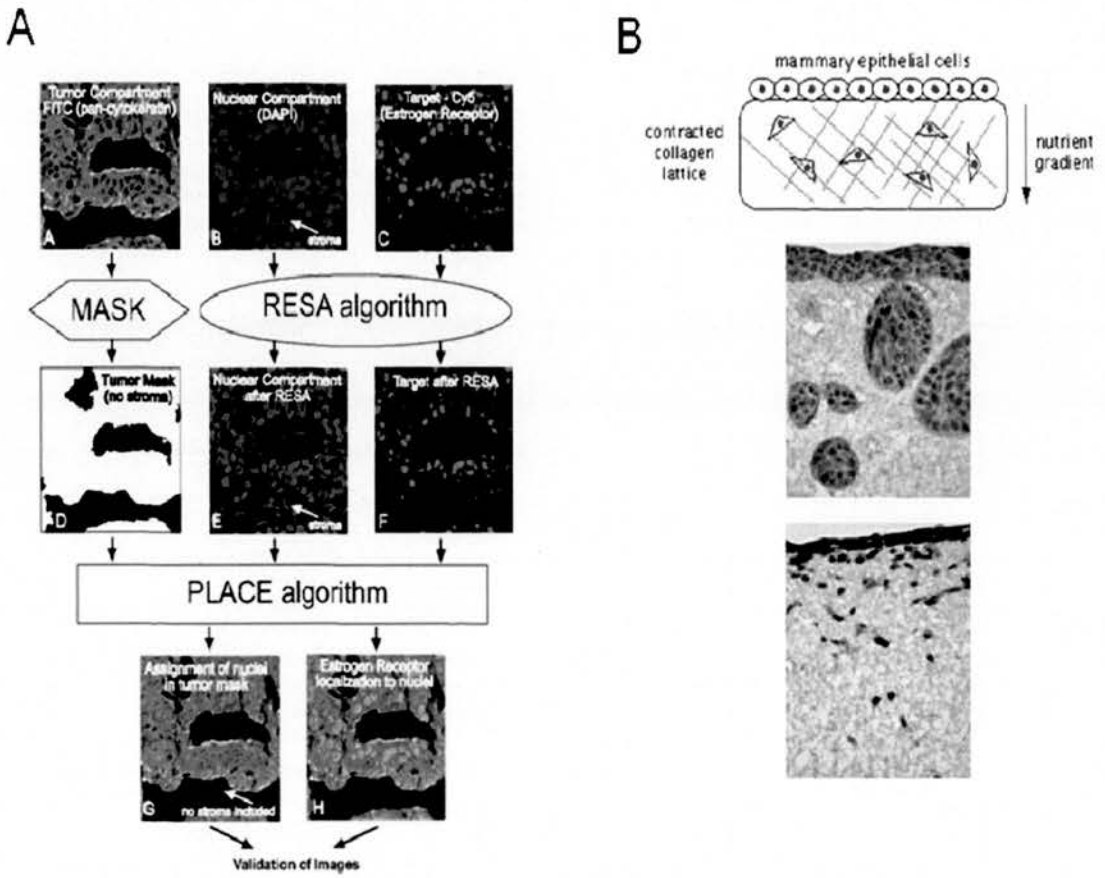

Figure 2.4: New analytical tools and biological models for systems biology. (A) The AQUA image analysis system uses proprietary image analysis software (RESA) and algorithms (PLACE) to quantify protein expression in tissue compartments, which may be used in mathematical models (reproduced with permission from Marisa Dolled-Filhart, Yale School of Medicine). (B) Contracted collagen matrix model for investigating epithelial/stromal interactions *in vitro*. Changes in phenotype may be modelled under different epithelial (middle and lower panes) and stromal conditions and over time (reproduced with permission from Elad Katz, Edinburgh Breakthrough Research Unit).

2.7.2 Achieving temporal resolution

Although increasing temporal resolution seems straightforward for *in vitro*-based experiments it is more difficult within the clinical setting. There are a range of biological models available for analyzing complex biological systems. Nonetheless, even the simplest *in vitro* models require reconsideration of design in order to generate data of sufficient quality to populate mathematical models. While it is relatively trivial to increase data points in an experiment examining pathway responses to targeted therapy *in vitro*, it is only recently that downstream assays are sufficiently 'high-throughput' to generate robust, quantitative data of sufficient quality and quantity to be used to populate mathematical models. This situation is readily appreciated for protein assays; for example, if more than 10–15 samples are assessed by western blotting it becomes increasingly difficult to maintain accuracy, reproducibility, and (more importantly) quantification both within and between blots. If a simple time course with 10 time points for 10 pathway biomarkers is assessed, inclusion of appropriate total protein controls would produce 200 data points, which highlights the issue of non-scalability of data. Although robotics can help to meet the demands of high-performance throughput, new techniques need to be considered to meet the data-rich demands of systems approaches.

Since many of the components assessed within mathematical models are proteins and their activated forms, newer protein assays may be used in order to address the problems outlined above. Reverse-phase protein arrays (RPPA) are high-throughput, high-density protein arrays in which protein lysates from *in vitro* or *in vivo* biological samples are immobilised as spots on nitrocellulose-coated glass slides and protein targets are detected with specific antibodies, similar to immunohistochemistry or immunofluorescence (125). In this way, hundreds to thousands of lysates (including technical and biological replicates) can be assayed under the same conditions on a single slide. As only picoliter quantities are spotted on each spot, tens to hundreds of identical slides may be produced for multiple target analysis from a single cellular or tissue lysate, particularly if robotic spotting is used. In addition, since each lysate is spotted as a dilution series, the signal detected can always be guaranteed to be in the linear range of detection (that is while signal

intensity is still unsaturated), which is rarely the case for western blotting, and if recombinant peptide or protein controls are spotted on the same slide, accurate quantification is possible. As well as facilitating high throughput protein analysis *in vitro*, the small amount of lysate required and the high number of assays that can be performed make this a useful technique for assessing clinical material. This means that large models, requiring tens to hundreds of biological measurements (e.g. the ordinary differential equation-based approach) may be populated with ease. We have used this technology in order to populate a new mathematical model of PI3K signalling in Chapter 6.

The second most important challenge to achieving sufficient temporal resolution for systems approaches is selection of appropriate *in vitro* or *in vivo* models. While transgenic mice offer the attraction of stable genetic perturbations that can be applied to computational models, the long generation times and high numbers of time points required do not lend themselves to the iterative nature of systems biology ie the need to refine the model on the basis of re-experimentation, in order to improve it. Nevertheless, if coupled with live imaging techniques, such as the relatively new technique of intravital microscopy, which has been used to image tumour cell invasion in real-time (126), these animal models may become attractive models for detailed pharmacodynamic studies. We have used a combination of 3-dimensional *in vitro* primary and human adenocarcinoma cell line cultures on contracted collagen matrices (127) and cell line xenografts to model the pharmacodynamics of targeted therapies (Figure 2.4B, reproduced with the permission of Elad Katz, Edinburgh Breakthrough Research Unit). Three-dimensional culture simplifies the tumour context but offers flexible analysis of epithelial and stromal compartments, where both compartments may be genetically manipulated and subjected to both destructive and non-destructive temporal analysis, such as by reverse-phase protein arrays and immunofluorescence. Primary and cell-line xenografts capture the complexity of whole tissues but what makes these models ideal for high-throughput, spatially resolved analyses is their ability to assess tumours from multiple time points, and the availability of abundant tissue for fresh frozen and formalin-fixed paraffin-embedded analysis. In addition, cell lines are readily manipulated *in vitro* for knockdown or overexpression of specific targets with

small hairpin RNA and stable transfection of genetic constructs, respectively, and are then ready for re-implantation and re-testing of the system with specific perturbations. These models are an important intermediate step in validating computational models before they are sufficiently reliable to be used in clinical decision-making.

The real challenge lies with achieving sufficient temporal resolution using real human disease as the model. Nevertheless, there is now extensive experience in gathering tissue and biological samples from three time points in the neoadjuvant setting in individual patients with breast cancer, such that limited pharmacodynamic studies may be performed. In this model, patients are given endocrine or chemotherapy for 3 months prior to definitive resection and samples taken at diagnosis, 2 weeks, and 3 months at the time of resection (128). If basic pathological endpoints such as proliferation (immunohistochemistry analysis of Ki67 expression levels) are measured, then the proliferation index at 2 weeks (but not at diagnosis) is predictive of long-term survival in response to aromatase inhibitor therapy (129;130). Breast cancer is amenable to this type of temporal intervention, since there is the added benefit that tumour shrinkage in the neoadjuvant setting can result in the use breast-conserving surgery rather than mastectomy. Nevertheless, other cancers may also be amenable to multiple sampling, such as ovarian tumours treated with intra-peritoneal chemotherapy (131), or colorectal tumours treated with pre-operative radiotherapy (132), which may be achieved with minimal discomfort or inconvenience to the patient. By exploiting carefully selected human models, we can begin to determine the true nature of the dynamics of tumour responses and move away from inferred biology from static biomarker analysis. In the short term gathering high quality, temporal data from real clinical material is essential to populate and validate computational models. In time, such mathematical models are likely to become applicable and may avoid the need for multiple biological measurements.

2.8 Conclusions

The increasing availability of high throughput molecular techniques offers an unprecedented opportunity to complement existing histopathology approaches to better characterize tumours for predicting prognosis and improving treatment of cancer. At the same time, our understanding of the molecular basis of tumours is improving to the extent that large parts of the regulatory networks are now well characterized. For targeted therapies that modify the network at the single pathway level, the challenge is to link tissue data to modifications at the molecular level that will improve outcomes. This chapter highlights why measurements at a single time point do not encapsulate the required information, and points to the need for measures that characterize the dynamical state of the underlying pathobiology. The resulting complexity of the description necessitates a mathematical modelling approach, and we identify potential methodologies that may be suitable, along with the necessary experimental measures that are required. Pathology as a recognised specialty is at a point where it may be possible to integrate quantitative methods and predictive tools to aid in the diagnosis, prognostication, and prediction of response in patients with cancer. The consensual platform that is provided by the explicit expression of understanding in a systems model offers the possibility for a more-rational approach to data collection and interpretation. Whilst we find that larger, more-comprehensive models for the regulatory network are required, this need not translate into a demand for larger volumes of data. Indeed, a major benefit of such a platform is in identifying where data is critical and where it is not, and where high temporal resolution is required and where it is not. Perhaps of most importance is a platform based on explicit molecular-level modelling, properly integrated with appropriate pathological data, could help to ensure that future research in this area progresses in a more coordinated and self-consistent manner than has been possible before.

Chapter 3: Refinement of conventional quantitative histopathology with automated image analysis.

3.1 Introduction

In the preceding chapters we have discussed the need for validation of appropriate biomarkers in sufficiently powered clinical trials, and the need for accurate quantification. In this chapter, we bring these themes together and investigate the use of semi-automated biomarker analysis in a trial setting. In doing so, we validate an immunohistochemistry-based image analysis system, which may be more readily applied to pathological practice than immunofluorescence-based systems. We show this in the setting of the TEAM trial, which is powered to investigate differences in responses to endocrine therapies according to tissue biomarker status. Central to these responses is the expression of ER and PR, which are known to influence responses to endocrine therapy (133;134). We therefore sought to establish whether ER and PR could be quantitatively measured using image analysis, so that quantitative expression could be assessed within the wider trial.

The Tamoxifen versus Exemestane Adjuvant Multinational (TEAM) trial is an open-label, multinational, phase III trial which recruited 9746 postmenopausal women with ER positive and/or PR positive early breast cancer. Randomisation was to either five years exemestane or 2.5-3 years tamoxifen followed by 2-2.5 years exemestane. A prospectively powered pathology sub-study is underway, recruiting 5000 cases from 5 countries to prospectively test two molecular hypotheses: (1) PR poor tumours relapse early during tamoxifen treatment and may benefit from early treatment with AIs, (2) Type I receptor tyrosine kinases (HER1-3) abnormalities are associated with resistance to tamoxifen and HER1-3 positive cases may also benefit from early treatment with AIs (135-137). These biomarkers are currently being measured by immunohistochemistry (IHC) and FISH (in the case of HER2) in this trial. IHC has been previously shown to correlate well with biochemical assessment of steroid receptors in breast cancer tissues (138). Analysis of ER and PR expression levels is conventionally performed using manual assessment of staining patterns using the histoscore or simplified scoring systems (such as the Allred score) and despite evidence that such approaches can be robust (139), novel high-throughput image analysis technologies offer the opportunity to produce consistent, accurate and reproducible results without the potential for human error (139-141). This is

especially critical since it is emerging that response to therapy is often a quantitative phenomenon dependent on the concentration of protein within the tissue, suggesting robust and quantitative methodologies are important in such analyses (142;143).

Computer-assisted image analysis systems have been used to improve quantification and reproducibility of IHC almost since the introduction of ER IHC into clinical practice 20 years ago (144-147). Although staining intensity by computer-assisted measurement is more consistent than human assessment due to lack of interference by variability in ambient light or fatigue, there remain challenges in analysing complex tissues containing both epithelial and stromal compartments and infiltrates of benign cells such as inflammatory cells. However, over the last few years, hardware and software advances have made semi- automated computerised image analysis a viable option for high-throughput analysis of protein biomarkers in tissue sections and tissue micro-arrays.

Here we validate a semi-automated image analysis approach using the Ariol system (Genetix Applied Imaging) for standard chromogenic immunohistochemical assessment of ER and PR in nearly 600 patients from the TEAM study in tissue microarray (TMA) format.

3.2 Methods

3.2.1 Samples and TMA construction

All patients recruited into the UK TEAM trial were approached prospectively for written informed consent to donate tissue samples to the pathology sub-study. Where consent was given, tissue blocks were retrieved from the local pathology laboratory and sent to the central pathology laboratory. Following H&E sectioning, tumour areas were marked for TMA construction and 0.6mm^2 cores placed into 6 separate TMA replicates for each sample. For this validation study, samples from 3 TMAs were used, containing 595 cases. Full sections of cases from one TMA (containing 198 cases) were cut and stained for ER and PR respectively, for comparison with TMAs.

3.2.2 Immunohistochemistry

IHC was performed according to standard protocols. Briefly, tissue sections were dewaxed in xylene and rehydrated. Antigen retrieval was performed using heat treatment under pressure in a microwave oven for 5 min (ER) in Tris-EDTA buffer pH8.0 or 4 min (PR) in citrate buffer pH6. Sections were blocked for endogenous peroxidase followed by incubation with anti-ER or PR antibodies (ER clone NCL-L-ER-6F11; Novocastra, 1:50 dilution, PR clone 636; Dako, 1:50 dilution) for 60 min at room temperature. Staining was developed using EnVision (Dako, Denmark) and DAB (Dako, Denmark) before slides were counterstained in haematoxylin, dehydrated and mounted in DPX. Stringent quality control was adhered to reduce run to run variation.

3.3.3 Manual evaluation of ER, PR

Two observers scored all whole sections and TMA cores for ER and PR staining intensity following training in IHC as described previously (139). For each section or core the percentage of cells staining 0, 1+, 2+ and 3+ were recorded and a histoscore (0-300) for IHC staining was produced.

3.3.4 Image analysis

For image analysis the TMAs were scanned onto the Ariol SL-50 image analysis system, as previously described (148). Briefly, three-colour filtered images were captured on a black-and-white CCD camera and reconstructed by the supplied proprietary software. Tumour areas were marked by one observer and quality controlled by a second observer and pathologist. The system was trained on the basis of the cellular characteristics (shape, size, and colour) of epithelial, stromal, and infiltrating non-tumour cells to produce a trained classifier applicable to all nuclear stains, which would largely exclude any contaminating cells (stromal cells or

lymphocytes) from the analysis. For both ER and PR an analytical algorithm was trained using one TMA set of 198 cases (stained in sextuplet), after which analysis was performed without human intervention (other than for tumour marking) i.e. once parameters were set these were used for the rest of the study.

3.3.5 Statistics

Histoscores from automated analysis of TMAs were calculated from the sum of cells from all cores (2-6 cores/case), not by averaging histoscores from each replicate core. Automated histoscores were excluded from analysis if they were derived from <100 objects (cells), with 2 cores/case this led to the exclusion of a significant number of cases due to low cell numbers. The inter-observer variation between the scoring of nuclear ER and PR by manual and automated methods was assessed by measuring both Pearson regression coefficients (PRC) and Inter Class Correlation Coefficients (ICCC) statistics. ICCC is a measure of bias assessing the amount of systematic data variance by comparing the variability of each independent observer for each case with the overall variation between all scores, as previously described (149-151), (139). For all PCCs, p values were less than 0.0001.

3.4 Results

3.4.1 TMA analysis is representative of whole section scoring.

All sections and TMAs included in this study were manually scored by two pathology technicians (TR and CK) trained in the assessment of immunohistochemical staining using identical criteria as for pathologist assessment, prior to commencing this analysis both observers demonstrated excellent intra and inter-observer consistency in scoring in line with our previously published criteria (152). Pathological QA ensured that scoring was always performed on invasive tumour. Observer variation, as assessed by PRC and ICCC, was excellent. An

excellent to good correlation between observers for whole section analysis was observed for ER (PRC 0.92, ICCC 0.87, n = 189) and PR (PRC 0.95, ICCC 0.91, n = 197). For TMA analysis correlation between observers was also good for both ER (PRC 0.88, ICCC = 0.85, n = 394) and PR (PRC 0.97, ICCC = 0.94, n = 393).

The correlation between manually scored TMAs and manually-scored sections was assessed for both PR and ER. An excellent correlation was observed between TMA scores for PR (6 replicate cores: PRC = 0.91, ICCC = 0.90, n=197, Figure 3.1A) and an adequate correlation for ER (6 replicate cores: PRC = 0.80, ICCC = 0.56, n=189 Figure 3.1B). These correlations also held for fewer numbers of cores (3 replicate cores: PR PRC = 0.90, ICCC = 0.88, n=196, ER PRC = 0.79, ICCC = 0.60, n=188). The correlation for ER was biased by the small number of ER poor cases (<5%). As reported previously (153;154), TMAs are an excellent high-throughput methodology for clinical trial biomarker analysis and representative of whole section analyses, even for biomarkers such as PR which have traditionally been considered particularly heterogeneous.

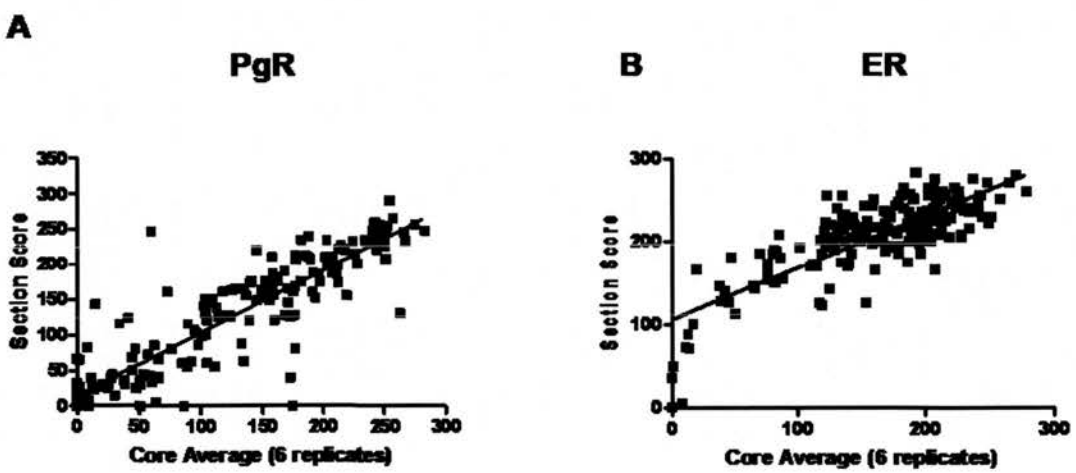

Figure 3.1: XY plots and linear regression analysis of comparison between whole sections and TMA cores (six replicates) for PR (A) and ER (B).

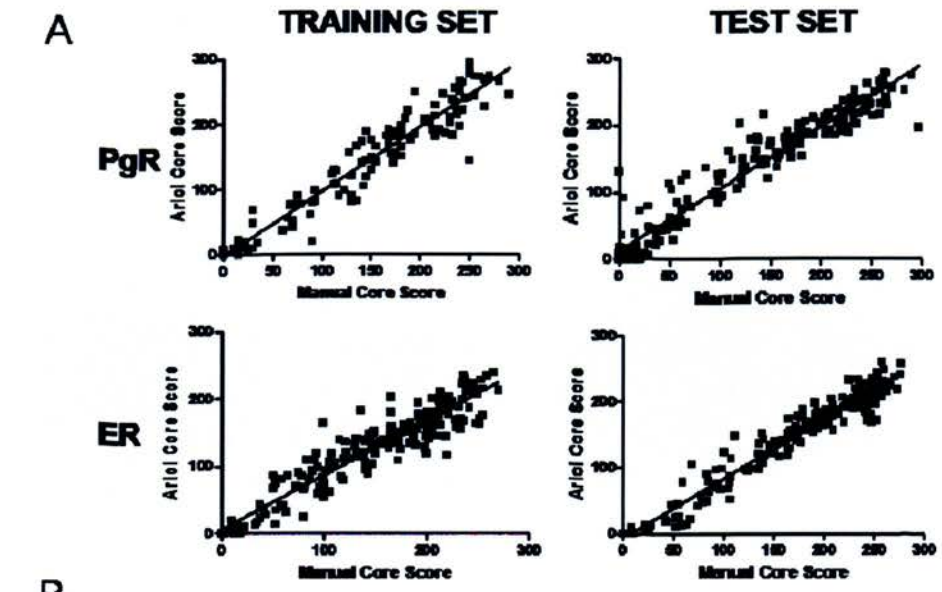

B

PgR	# cores	n	PCC	ICCC
	1.	343 (58)	0.97	0.96
	2.	456 (77)	0.96	0.95
	3.	516 (87)	0.95	0.93
	4.	551 (93)	0.96	0.95
	5.	565 (95)	0.96	0.95
	6.	572 (96)	0.96	0.95

ER	# cores	n	PCC	ICCC
	1.	403 (67)	0.92	0.82
	2.	508 (85)	0.93	0.85
	3.	562 (94)	0.94	0.89
	4.	570 (96)	0.95	0.89
	5.	576 (97)	0.94	0.89
	6.	578 (97)	0.95	0.89

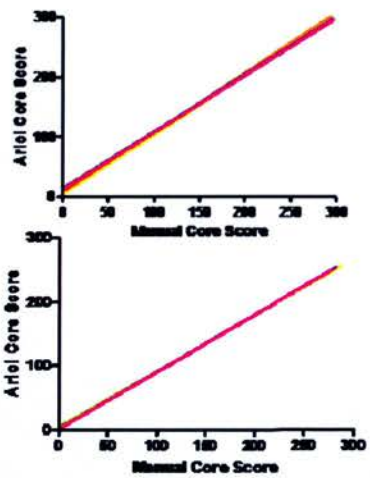

Figure 3.2: Comparison between manual and automated scoring methods. (A) XY plots and linear regression analysis of training and test TMAs for PR and ER show excellent reproducibility when training classifiers are applied to an independent test-set. (B) Number of assessable cores, number of cases (n) (% in brackets) and correlations between manual and automated TMA scores (left) and changes in linear regression (right). Only slight benefit in correlation coefficients is observed when greater than one core is analysed, but more cores are required in order to overcome loss of cores and missed cases.

3.4.2 Manual scoring versus automated image analysis.

Cell classifiers for both positive (DAB stained) and negative (haemotoxylin stained) tumour cells were defined on a training set of tumours (n = 198 (n=186 and n=190

available for analysis for PR and ER respectively); Figure 3.2A, left panels). Manual versus automated histoscores showed excellent correlation for both PR (PRC = 0.95, ICCC 0.95) and ER (PRC = 0.94, ICCC = 0.87). These classifiers were then applied to a second independent test set (n = 199 (n=193 and n=194 available for analysis for PR and ER respectively); Figure 3.2A, right panels), and excellent correlations for both PR and ER were preserved (PR: n = 193; PRC = 0.96, ICCC 0.96, ER: n = 194; PRC = 0.97, ICCC 0.91). Finally, the same classifiers were applied to a larger cohort of tumours including the test set and a third TMA set of 198 cases (n = 384 and 388 for PR and ER respectively). Excellent and good concordance were again demonstrated for PR and ER respectively (6-core replicates, PR; PRC = 0.97, ICCC = 0.96, ER; PRC = 0.95 ICCC = 0.93).

3.4.3 How many cores recapitulate the ER/PR expression seen in tumours?

For both ER and PR we used 6 replicate 0.6mm^2 cores (a total 3.6mm^2). In order to assess the number of replicates required to accurately recapitulate manual results we performed regression analysis between manual and automated scores for both ER and PR (Figure 3.2B). The inclusion of a greater number of cores did not reveal marked improvements in correlations between manual and automated scores for either PR or ER. However, the number of cases with sufficient data to report rose markedly from an average of 81.2% with 2 cores assessed to 94.1% with four cores and 97.2% with 6 cores, because of the exclusion of cases with less than 100 nuclei counted by the automated system. Cases with less than 100 nuclei were deemed unrepresentative of the tumour and were excluded from analysis.

3.5 Discussion

A comparison of manual and automated image analysis techniques on TMAs shows that image analysis is an excellent alternative to manual scoring for ER and PR nuclear stains. There were no significant improvements in correlation when more

than 1 core was analysed, but this was offset by the lower number of cases available for analysis when fewer replicates were used, due to the stringent exclusion parameter of 100 nuclei. The PCCs and ICCCs for PR and ER were always excellent (>0.94 and >0.90, respectively). Semi-automated image analysis can be used in place of manual scoring for ER and PR performed on TMAs in clinical trials with potential for greater consistency and quantification.

The analysis of tissue biomarkers within large patient cohorts by *in situ* methods (for example immunohistochemistry, ISH, proximity ligation assays (148;155;156)) requires consistent, accurate and reproducible high-throughput methods. Tissue microarrays have advantages in improving the consistency of analysis by requiring far fewer staining runs, reducing run to run variation and improving throughput. For example this approach allows the analysis of the 5000 cases for ER/PR in the TEAM trial in 6 IHC runs rather than the approximately 150 runs required for whole section staining. However, it is critical that such methods be appropriately validated. It has previously been shown that consistent and accurate scores can be obtained by manual observers in relatively small data sets (100's of cases) (139), but clinical trial databases often contain several thousand samples. Image analysis, with appropriate quality control, may provide a simple and consistent assessment of staining with greater precision, lower variation between runs, and ultimately yield additional data not previously captured by manual observers. We have validated the analysis of nuclear biomarkers, in particular ER and PR, by replicate TMA core analysis within the context of the TEAM trial using the Ariol automated image analysis system to capture images, quantify both DAB positive (stained) and negative (unstained) nuclei, and process case scores for ER and PR staining intensity in the context of quality assured ER and PR assays performed to GCLP standards. IHC methods and interpretation were standardised in a centralised laboratory.

Data presented here supports the use of TMAs to recapitulate whole section scores for PR and ER (see Figure 3.1) as has been previously reported by other observers (154). Secondly, and more critically, we have evaluated the use of semi-automated image analysis for the quantitative analysis of ER and PR staining using both training and validation sets for both markers. We have shown that consistent results can be

obtained when comparing ER and PR scores from two trained manual observers with those obtained using the Ariol Image analysis system. We note that as few as 2 cores give consistent results between manual and machine analysis.

The population analysed forms part of the pathology sub-study within the Tamoxifen versus Exemestane Adjuvant Multicentre (TEAM) Trial which recruited ER positive breast carcinomas to a trial investigating the potential benefit of upfront versus switch strategies for treatment of hormone receptor positive breast cancer with the aromatase inhibitor Aromasin. Results for both ER and PR staining in both the training and validation sets used in the current study showed excellent correlations between manual and machine derived scores across the observed expression range. Also we observed that the use of image analysis allowed a greater discrimination between the staining intensity of strongly staining ER positive cells (which was not observed by manual scoring), enhancing the information derived from ER quantification, which could reflect the fact that human observers often group together observationally distinct 'strong' and 'very strong' nuclei. This resulted in slightly lower automated scores for tumours with high ER expression. Whilst the biological significance of this added discrimination achieved by image analysis is not yet clear, it provides an important potential improvement in assessment of ER staining by IHC methods.

A second, potentially highly significant, advantage of the image analysis approach is results are based upon the quantification of expression in individual cells rather than broad categorisation. All manual interpretation systems currently used for ER and PR analysis rely on human observers estimating the percentage of stained cells and the intensity of staining. This estimation requires the grouping of results into categorised scoring systems (Allred, Quick Score); even the Histoscore, which represents the best attempt at approximating quantification of expression, is a categorised variable (albeit with 301 potential sub-categories). By integrating results from individual cells using a continuous scale for estimation of staining intensity image analysis systems evaluate marker expression as continuous variables based on cell by cell data. This

provides significant advantages over categorised estimates, the full potential of which remains to be explored.

However, one continued challenge remaining with image analysis is the progression to fully automated systems. Whilst the Ariol system provided excellent consistency with manual observers based on automated analysis of staining intensity and frequency, it was not able to accurately discriminate between tumour and non-tumour components within tissues. Each tissue sample was individually marked for tumour content by trained pathology technicians and quality assured by a second trained individual, with reference to a pathologist where appropriate. This task is highly time consuming but at present remains an essential step to ensure accurate determination of tumour marker expression. Preliminary data suggest modification of counter staining procedures may ultimately allow for fully automated analysis which will greatly expedite future sample analysis.

A large recent study has shown that automated quantification by Ariol automated analysis of ER in breast cancer has similar prognostic significance to pathologist-scored ER values, and that concordance between machine and pathologist, and machine and biochemical assay, were high (148). Our data supports the use of both TMAs and image analysis, with appropriate quality assurance procedures, for the assessment of steroid hormone receptors in large breast cancer clinical trial databases. Indeed image analysis provides a more detailed quantification of biomarkers and may provide additional information about concentration dependent alterations in ER and PR and the biology of breast cancer. In this regard there are similarities between this approach, the analysis of DAB stained biomarkers and immunofluorescence approaches such as AQUA (123). Although fluorescent-based analysis offers theoretical advantages over IHC in terms of wide dynamic range and linearity of detection signal, and has shown significant promise in the research setting, immunofluorescent assays are not yet standard for diagnostic histopathology. However, while Ariol analysis is sensitive and specific for nuclear biomarkers, significant challenges exist in image analysis using this system when trying to discriminate other compartments, both at tissue (epithelial vs stromal) and

subcellular (ie membrane and cytoplasmic) level. Immunofluorescence-based techniques such as AQUA offer significant advantages in this regard, since molecular markers detected on different channels (such as cytokeratin for epithelial cytoplasmic compartments) accurately delineate both subcellular and epithelial compartments. Direct comparisons between quantitative conventional immunohistochemistry and immunofluorescence will be required to determine which approach is most valuable in the management of breast carcinomas in the long term.

ER and PR are critical biomarkers for the evaluation of breast carcinomas. The use of both tissue microarrays and image analysis are appropriate for the analysis of large data sets where quantitative information on ER and PR expression is required. Further comparisons with immunofluorescence would be of significant value, and these approaches may be of benefit in generating high-throughput data for systems biology approaches.

Chapter 4: Describing Pathways (1): The reductionist approach.

4.1 Introduction

In Chapters 1 and 2 we discussed the need for a more systematic analysis of pathway biology in order to understand therapeutic responses to targeted therapies, and in Chapter 3 one approach to improving quantification from tissues. In order to accurately describe network topology (ie the structure of the interactions between molecules), reductionist cellular and molecular biology still plays a role in filling in the detail of these interactions. Existing models (including our own, see Chapter 6) of receptor tyrosine kinase (RTK) signalling focus on the immediate phosphorylation events of kinases within signalling cascades, but these are only accurate over a few minutes since other mechanisms, such as transcriptional feedback, are soon activated. In order to pave the way to expanding existing models of RTK signalling to include such transcriptional events which are known to feed-back onto RTK pathways, we investigated the control of Sprouty-family proteins, which are negative regulators of PI3K and MAPK signalling, and activated as delayed early genes. In doing so we also investigated the effects of Sprouty proteins on trastuzumab sensitivity and resistance.

Although the HER2-targeting RTK inhibitor trastuzumab has clinical efficacy in both early and metastatic breast cancer, measurement of HER2 protein expression or gene amplification status is a poor predictor of response with a low positive predictive value (157;158). The documented benefit of adjuvant trastuzumab combined with chemotherapy vs chemotherapy alone in terms of overall survival in HER2 positive patients is modest (96% vs 95% respectively at 1 year) (157) and 91% vs 87% respectively at 4 years (158). A large proportion of patients therefore unnecessarily receive ineffective and expensive treatments with toxic side-effects, and mechanisms of resistance need to be elucidated in order to more efficiently select patients who will respond to therapy. As previously mentioned, suggested mechanisms of *de novo* and acquired resistance to trastuzumab include *PIK3CA* activating mutations, *PTEN* inactivation, *IGF1R* over-expression and expression of p95 HER2 isoforms (71;72;159). Although much attention has been paid to 'forward-signalling' mechanisms of pathway activation such as activating mutations

in cellular oncogenes (eg *RAS*, *RAF* or *PIK3CA*), it is as likely that loss of negative feedback control also causes aberrant pathway activation, such as is the case with mutation or decreased protein expression of PTEN. We hypothesised that one of the best characterised and potent EGF-induced negative feedback regulators, the Sprouty-family of proteins (160-166), also may be activated as a feedback inhibition programme downstream of HER2 receptor, and therefore contribute to sensitivity or resistance to trastuzumab.

To date there have been no reports implicating Sprouty in therapeutic sensitivity or resistance. The only published report of expression of Sprouty in breast cancer showed decreased expression at transcript level of Spry1 and Spry2 in 78% and 96% respectively of a small panel of breast cancers (n=50) (167). In spite of persistent attempts to establish the underlying mechanism for decreased expression, the exact cause remains elusive and may be different for specific orthologues in different cancers. In prostate cancer, there is conflicting evidence regarding the epigenetic regulation of *Spry1*, *Spry2* and *Spry4*, with some authors showing that *Spry2* and *Spry4* are downregulated by hypermethylation (168;169), although in a separate study no hypermethylation of the promoter region of *Spry2* was identified (170). Likewise, loss of heterozygosity (LOH) of *Spry2* has been found in prostate cancer (168), but not in other cancers. In breast cancer, none of the Sprouty family members are downregulated by either LOH or epigenetic mechanisms. Given the dynamic nature of Sprouty expression in response to ligand drive, it is possible that detection of low expression levels reflects the activation state of the signalling network rather than a genetic or epigenetic phenomenon.

Our objectives were to establish: (1) whether Sprouty-family members are associated with established clinicopathological parameters in breast cancer, (2) whether Sprouty-family members are dynamically regulated as a delayed early genes response downstream of the HER2 receptor, similar to that seen with EGFR, FGFR, and VEGFR, and (3) establish what role, if any, Sprouty expression levels play in therapeutic resistance and sensitivity to trastuzumab. In addition, these data may be used in the future to expand mathematical models of RTK-signalling.

4.2 Methods

4.2.1 Microarray analysis from meta-analysis on ONCOMINE database.

The expression of Sprouty-family transcripts in breast cancer tissues was obtained from meta-analysis of cancer gene microarray meta-analysis public database, representing analysis of over 390 microarray studies (171). Statistical analysis of differences was performed using ONCOMINE algorithms to account for the multiple comparisons among different studies, similar to a meta-analysis, as previously described (171). Comparison of normal tissue and breast cancer were performed on (172) (n=47; 7 normal vs 40 breast carcinomas), grade comparisons on (173) (n= 60; 3 grade 1 vs 39 grade 2 vs 18 grade 3) and HER status on (174) (n=50; 32 HER2 negative vs 18 HER2 positive).

4.2.2 Cell culture and western blotting.

MCF-7, MDA-MB-231, MDA-MB-361, MDA-MB-453, MDA-MB-468, SKBr3, ZR75-1, BT20, and BT474 breast adenocarcinoma cell lines were grown as monolayer cultures in DMEM supplemented with 10% heat-inactivated foetal calf serum (FCS) and penicillin / streptomycin (100IU/mL) in a humidified atmosphere of 5% CO_2 at 37°c, except for MCF10A (MEBM with hydrocortisone, hEGF 10 µg/ml, insulin, cholera toxin and horse serum). Time course experiments were set up by plating cells into 10cm ø petri dishes and leaving for 48h. Cells were then briefly washed in PBS before transferring to phenol red-free DMEM containing 5% double charcoal-stripped serum supplemented with penicillin / streptomycin (100IU/mL) and glutamine (0.3mg/mL) for a further 48h prior to treatment. Paired lysates were prepared by first treating relevant dishes with pertuzumab (100nmol/L; a kind gift from Roche, Basel, Switzerland) immediately followed by the addition of heregulin-β (1nmol/L). Samples were collected at time points of 1, 2, 5, 10, 30, or 60 min, washed in PBS, and immediately lysed in ice-cold isotonic lysis buffer supplemented with aprotinin (10 µg/mL) and protease inhibitors (Roche, 11836153001). Protein

lysates were electrophoretically resolved on either 10% or 12% SDS-PAGE and transferred overnight onto Immobilon-P membranes (Millipore, Bedford, MA). Primary antibodies used for western blotting were: anti-phospho-AKT (Ser^{473}) (Cell Signaling Technology, #4060) at 1:1000; anti-phospho-p44/42 MAP Kinase (Thr^{202}/Tyr^{204}) (Cell Signaling Technology, #9101) at 1:1000; anti-phospho-HER2 (Tyr^{877}) (Cell Signaling Technology, #2241) at 1:1000; anti-phospho-HER3 (Tyr^{1289}) (Cell Signaling Technology, #4791) at 1:1000. Immunoreactive bands were detected using enhanced chemiluminescent reagents (Roche; 1520709) and Hyperfilm ECL film (GE Healthcare, UK), and Integrated Optical Density (IOD) absorbance values were obtained by densitometric analysis using Labworks (UVP Life Sciences, Cambridge, UK).

4.2.3 RNA extraction and reverse transcription

Total RNA was extracted from cell lines using RNA extraction kits, as recommended by the manufacturer (Qiagen, GmBH, Hilden, Germany). RNA was treated with RNase-free DNase I (Qiagen) for 30 min at room temperature. Reverse transcription reactions were performed according to manufacturers' protocols with 1 µg of DNase-treated RNA, using the High Capacity cDNA Archive Kit (Applied Biosystems), 25°C for 10 min, 37°C for 120min, 85°C for 5s.

4.2.4 Quantitative Real-Time PCR

For each PCR reaction, 2µl of cDNA was mixed with 1 ml 20x primer assay mastermix containing a final concentration of 900nM of each primer and 250nM FAM dye-labeled TaqMan MGB probe (hSPRY1 assay ID Hs00398096_m1, amplicon size 78bp, hSPRY2 assay ID Hs00183386_m1, amplicon size 86bp, hSPRY3 assay ID Hs00540086_m1, amplicon size 73 bp; TaqMan Gene Expression Assay, Applied Biosystems), 10 µl 2x TaqMan Universal PCR MasterMix, and 7 µl distilled water. Reactions were carried out using the Applied Biosystems 7900HT Real Time PCR system according to manufacturers' instructions. Reactions were carried out in triplicate. Relative changes in gene expression were calculated using

the ΔΔCt method between untreated controls, MCF10a cell lines and RPL37a (reference) gene products.

4.2.5 Constructs, transfection, and cell viability.

The FLAG-hSpry2 and FLAG-HSpry2^{Y55F} constructs were a kind gift from Dr Graeme Guy (Signal Transduction Laboratory, Institute of Molecular and Cell Biology, National University of Singapore) and used as previously described (175;176). In addition, empty pXJ40FLAG vector was constructed by digesting hSpry2-containing pXJ40FLAG vector at BamH1 and BglII restriction sites. Both mutant and normal sequences were verified by DNA sequencing, and empty vector confirmed by gel electrophoresis. At 70% confluence, cells were transfected with 1–2 μg of FLAG-tagged plasmid DNA using Lipofectamine 2000 reagent (Invitrogen) according to the manufacturer's instructions. On the following day, the cells were trypsinised and plated into 96-well plates at a concentration of 1000 cells/well. The cells were treated with or without trastuzumab (10 μg/ml) for 24 or 48 h. Cell viability was measured using the AlamarBlue reagent (AbD Serotec), according to manufacturer's instructions.

4.2.6 Samples and tissue microarray construction.

The population characteristics of the trastuzumab-treated cohort is summarised in Appendix A. *HER2* gene amplification status was determined by fluorescence *in situ* hybridisation (FISH; DAKO HER2 FISH PharmDx, Ely, Cambridgeshire. The study was approved by the Lothian Research Ethics Committee (08/S1101/41). Overall survival was calculated from date of initial diagnosis to date of death by any cause. Following H&E sectioning of representative tumour blocks, tumour areas were marked for TMA construction and 0.6mm^2 cores placed into 3 separate TMA replicates for each sample, as previously described (177).

4.2.7 Immunofluorescence and AQUA automated image analysis.

A detailed description of the AQUA HistoRx methodology is available elsewhere (123;178). Briefly, slides were incubated with primary antibodies diluted in 0.025% PBST for 1 h at room temperature (AE1/AE3 mouse monoclonal cytokeratin antibody, rabbit polyclonal to hSpry2 (Novus Biologicals) diluted 1:100 and 1:25 respectively. Pan-cytokeratin antibody was used to identify infiltrating tumour cells and normal epithelial cells, DAPI-counterstain to identify nuclei, and Cy-5-tyramide detection for target (hSpry2) for compartmentalised (tissue and subcellular) analysis of tissue sections. hSpry2 antibody specificity was determined by a single band on western blot and correct (epithelial) cellular localisation.

4.2.8 Statistics

AQUA scores were averaged from replicate cores, and cores containing <5% malignant epithelium were excluded. We used the software programme, X-Tile, to determine the optimal cutpoint while correcting for the use of minimum *P* statistics (179), which is known to inflate type I error when used incorrectly (180). Two methods of statistical correction for the use of minimal *P* approach were utilised, the first calculation of a Monte Carlo *P*-value and for the second, the Miller-Siegmund minimal *P* correction (180). Overall survival was subsequently assessed by Kaplan-Meier analysis with log-rank for determining statistical significance. Relative risk was assessed by the univariate and multivariate Cox proportional hazards model. Comparison of differences in means *in vitro* was performed using the Student's T-test. All calculations and analyses were two-tailed where appropriate and done with SPSS 14.0 for Windows (SPSS, Inc., Chicago IL).

4.3 Results

4.3.1 Sprouty-family members are differentially expressed in clinicopathological subgroups of breast cancer and in breast cancer cell lines in vitro.

We first interrogated published gene expression profiles to assess the expression of Sprouty-family proteins according to clinicopathological parameters (Figure 4.1). Sprouty 3 was omitted from the analysis since this is considered a minor orthologue. *Spry1*, *Spry2* and *Spry4* show decreased gene expression in invasive breast carcinomas compared to normal breast, consistent with previous reports (167). Loss of *Spry1* and *Spry2* expression is significantly associated with high grade tumours, in contrast to *Spry4* gene expression, where increased expression is present in high grade disease. *Spry1* and *Spry* 4 show increased expression in HER2-positive breast tumours, while *Spry2* is decreased.

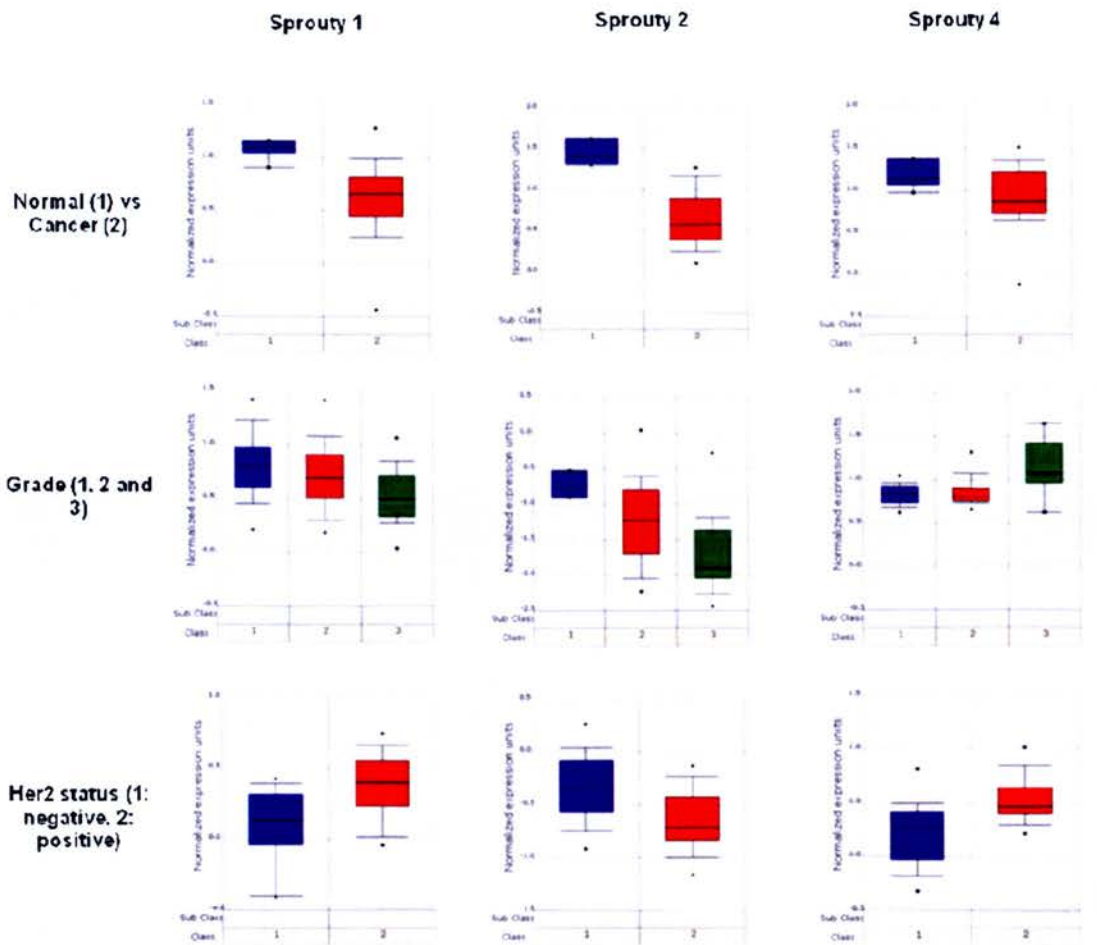

Figure 4.1: Gene expression of Sprouty-family members according to the clinicopathological parameters, using the ONCOMINE online resource. Comparisons between groups were analysed as previously described (171), and differences between groups were highly significant ($p<0.001$).

We next investigated whether similar gene expression patterns were present in breast adenocarcinoma cell lines. Quantitative gene expression analysis of *Spry1*, *Spry2* and *Spry4* confirmed >2-fold downregulation of *Spry1*, *Spry2* and *Spry4* in 60%, 70% and 80% of cell lines respectively when compared to the immortalised 'normal' MCF-10A breast epithelial cell line (Figure 4.2a). The magnitude of downregulation was frequently large, with 20%, 60% and 30% of cell lines showing >100 fold downregulation of *Spry1*, *Spry2* and *Spry4* respectively. We next investigated whether the differential gene expression of Sprouty in $HER2^{low}$ vs $HER2^{high}$ tumours occurred *in vitro*. Decreased expression of *Spry2* (Student's T-test, p=0.036; Figure 4.2b), but not *Spry1* or *Spry4* (p=0.10 and p=0.37 respectively) was observed in cell lines expressing high levels of HER2 protein measured semi-quantitatively by western blotting.

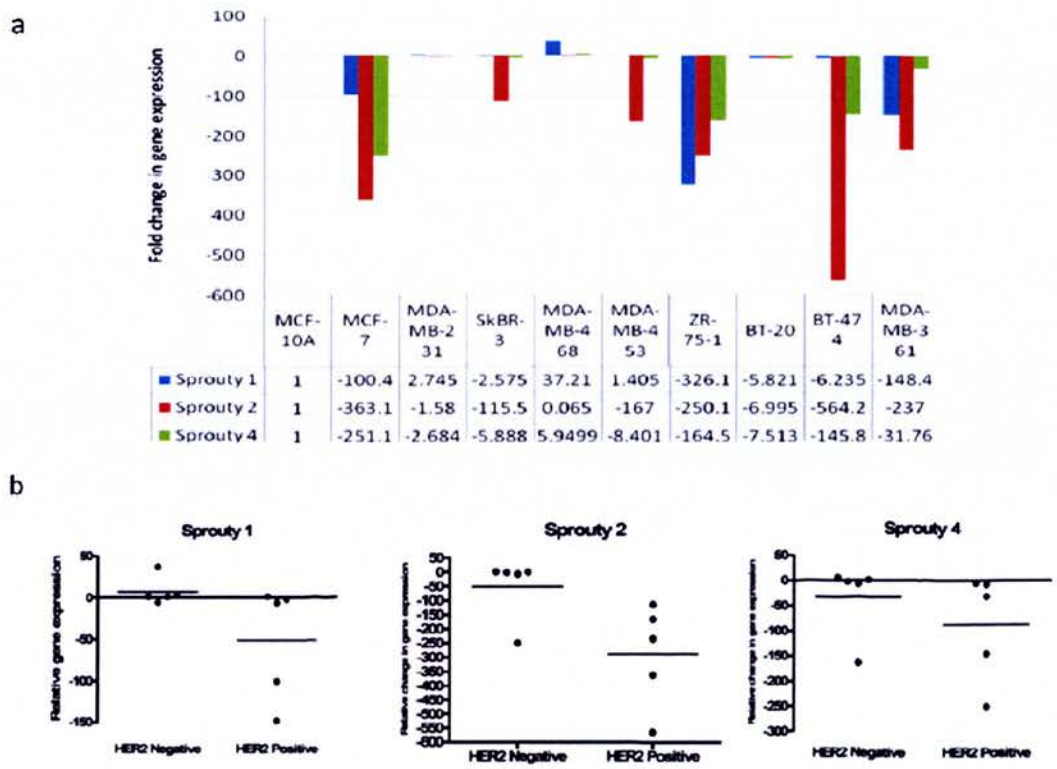

Figure 4.2: In vitro analysis of Sprouty gene expression. a, Analysis of cell lines by quantitative real-time PCR shows profound downregulation of *Spry1, Spry2* and *Spry4* in a high proportion of breast cancer cell lines when compared to the immortalised 'normal' MCF-10A breast epithelial cell line. **b,** *Spry2* (Student's t-test, p=0.036), but not *Spry1* or *Spry4* are associated with increased protein expression of HER2.

Although the HER2-amplified cell lines SKBr3, BT474, and MD-MBA-361 all showed >2-fold reduction in gene expression, several others also showed large-magnitude downregulation. We reasoned that since Sprouty was associated with HER2 protein expression, and that Sprouty is infrequently mutated or epigenetically silenced in cancer, Sprouty gene expression could be dynamically regulated through HER2-directed growth signalling pathways as well as through EGFR-mediated pathways (181-183).

4.3.2 Sprouty-family members are dynamically expressed as delayed early genes downstream of HER2/HER3.

In order to test this hypothesis, we stimulated BT474 cells, which showed the lowest steady-state expression of *Spry2* and intermediate expression of *Spry1* and *4*, with heregulin-β in order to drive signalling through the HER2/HER3 signalling axis. BT474s cells express low levels of HER1 and HER4, and intermediate levels of HER2 and HER3, with low-level amplification of HER2. All three Sprouty transcripts showed an increase in expression by 4 h consistent with a delayed early gene (DEG) response as previously described for signalling with EGF and FGF (Figure 4.3a). To show that the effect was dependent on HER2 signalling, cells were treated with the HER2 dimerisation inhibitor pertuzumab, which completely abrogated the Sprouty transcriptional response (Figure 4.3a).

Since Sprouty proteins are known to feed back onto the canonical MAPK growth factor signalling pathway, which cross-talks with PI3K cell survival pathway via RAF and protein phosphatases, and interact with PI3K signalling directly via PTEN (184), we investigated the dynamics of activation of ERK, PI3K and upstream receptor activation using phospho-specific antibodies to pAKT (Ser^{473}), phospho-p44/42 MAP Kinase (Thr^{202}/Tyr^{204}, and pHER2 (Tyr^{877}) in response to heregulin-β and pertuzumab (Figure 4.3b). pHER2, and pERK were transiently activated with return to low steady-state levels after 24 h, in response to heregulin, while activation of pAKT was sustained at 24 h.

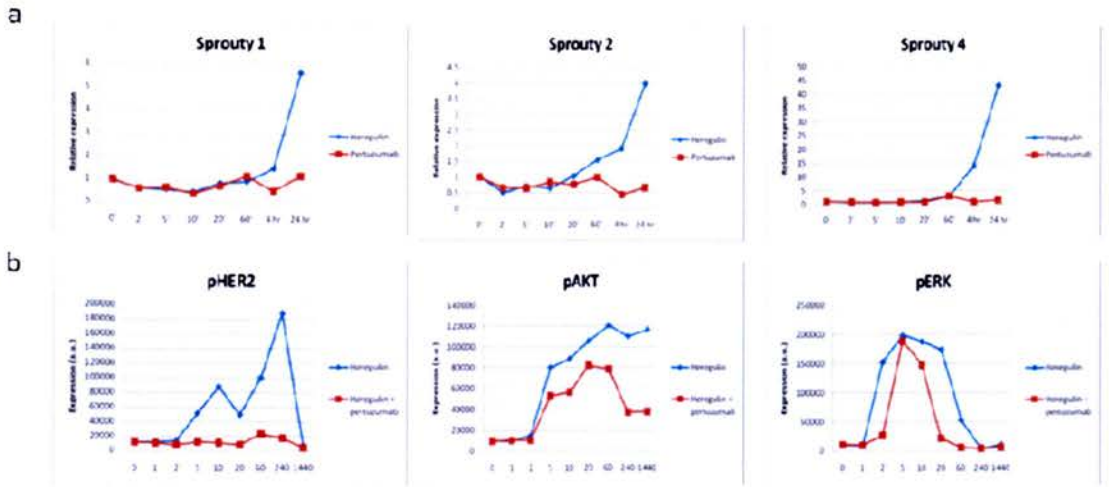

Figure 4.3: Gene and protein expression of Sprouty-family members over time. **a,** Quantitative real-time PCR analysis of dynamic expression of *Spry1*, *Spry2* and *Spry4* over 24 hours in BT474 cells in response to heregulin-β (blue line) and heregulin-β plus pertuzumab (red line) shows that *Spry* is expressed as a delayed early gene. Expression levels are relative expression compared to untreated controls at time = 0 min. **b,** Timecourse profiles of receptor activation (HER2 and HER3), pAKT and pERK over 24 h in BT474 cells.

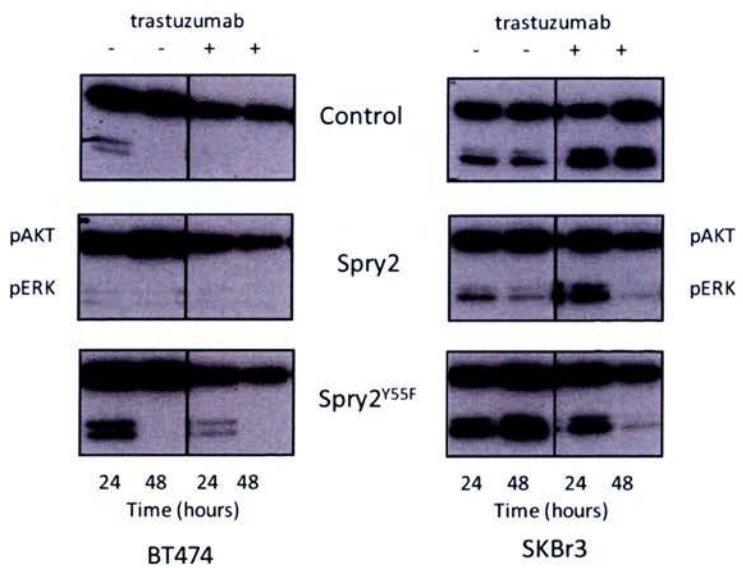

Figure 4.4: Western blots of pAKT and pERK activation at 24 and 48 h in trastuzumab sensitive (BT474) and trastuzumab resistant (SKBr3) breast cell lines. Cells were treated with or without trastuzumab (10mg/ml) in control, Spry2 or Spry2^{Y55F} transfected lines. All experiments were repeated at least twice.

Inhibition with pertuzumab inhibited phosphorylation of HER2 and HER3, consistent with dimerisation inhibition, caused a sustained decrease in pAKT, but had little effect on pERK dynamics. Sprouty expression therefore appears to be temporally decoupled from downstream activation of effector proteins, indicating complex interactions with effector pathways by Sprouty-mediated feedback inhibitory loops in the physiological setting.

Nevertheless, transient expression of full length wild-type and dominant negative Spry2^{Y55F} had the expected effect on ERK signalling, causing decrease and increase in pERK expression at 24 h in both BT474 and SkBr3 breast adenocarcinoma cell lines (Figure 4.4), confirming the regulatory effect of Sprouty under experimental conditions.

4.3.3 Spry2 acts synergistically with trastuzumab to reduce cell viability in vitro, and forced feedback inhibition with chemical inhibitors have a similar effect.

Since *Spry2* is most closely associated with HER2 status, we next investigated what the effect of altering steady-state expression of Spry2 was on cell growth and therapeutic response, using transient expression of wild-type and dominant negative Spry2^{Y55F}. SkBr3 breast adenocarcinoma cell lines were insensitive to treatment with trastuzumab, while BT474s were sensitive at 48 h (Figure 4.5) when grown in full serum conditions. Overexpression of empty vector, Spry2, or Spry2^{Y55F} dominant negative construct resulted in no significant changes in growth in either of the cell lines at 48 h. However, overexpression of Spry2 significantly increased sensitivity to trastuzumab at 48 h in trastuzumab-insensitive SKBr3s, but there was no difference in growth in BT474s with either the full length or dominant-negative constructs. Spry2 inhibited both pERK and pAKT in SkBr3s, but not BT474s, suggesting that Sprouty can synergise with trastuzumab via either inhibition of ERK or PI3K signalling. Re-establishing feedback inhibition in Sprouty-low tumours may therefore be an effective strategy for combinatorial therapy with trastuzumab, and

raises the possibility that in some HER2 overexpressing tumours, high expression of Spry2 may be a marker of response to trastuzumab. We tested the combinatorial approach *in vitro* by substituting the negative feedback control of ERK and PI3K signalling of Spry2 with the chemical inhibitors LY294002 and PD98059, which inhibit PI3K and MEK1 respectively, with and without treatment with trastuzumab. As expected, trastuzumab showed little effect on cell viability alone, but a synergistic effect when SKBr3 cells were pretreated with LY294002, inhibiting growth by 29% at 24 hours (Figure 4.5). Forcing feedback inhibition through combinatorial approaches may therefore be a novel therapeutic strategy in tumours with *a priori* trastuzumab resistance.

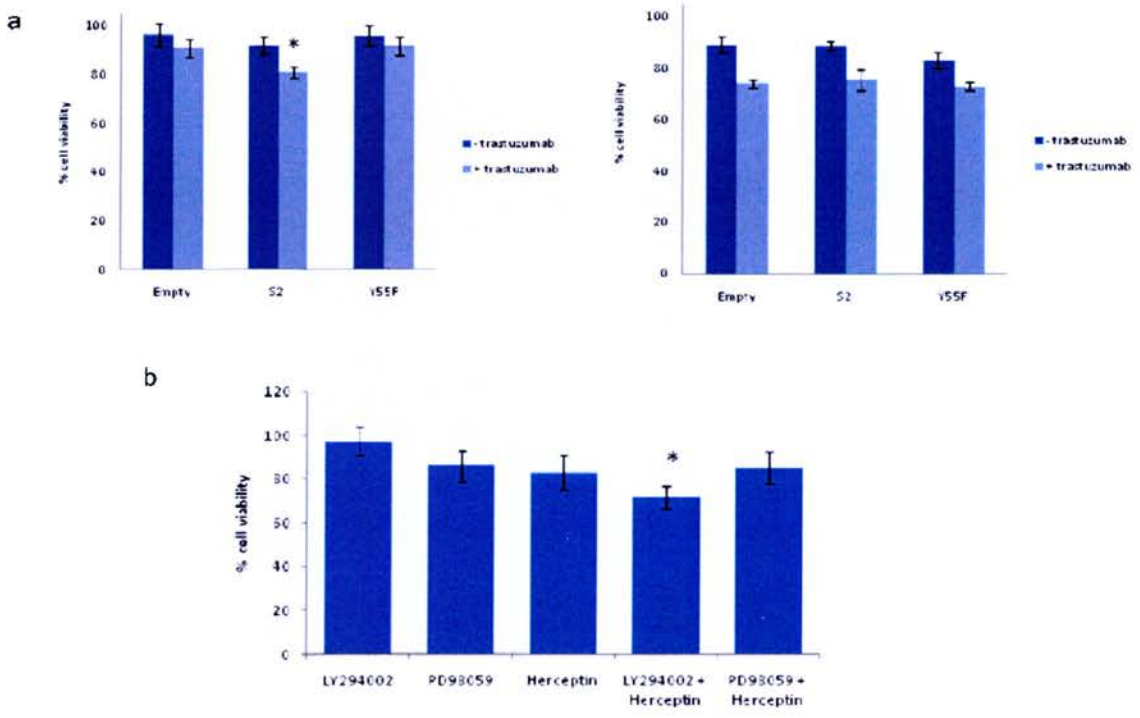

Figure 4.5: Sensitivity of trastuzumab sensitive and resistant cell lines in vitro with variable Spry2 expression. a, Cell viability (AlamarBlue) assays to assess the effect of Spry2 on sensitivity to trastuzumab in trastuzumab resistant SKBr3s (left panel) and trastuzumab sensitive BT474s (right panel). Values are % cell viability compared to untreated controls. Expression of full length Spry2 results in a significant decrease in cell viability (asterisk, Student's t-test, p=0.0008) compared to control or dominant negative Spry2^{Y55F}. **b,** Trastuzumab and LY294002 show synergistic inhibition of cell viability (asterisk, Student's t-test, p=0.042) in trastuzumab-resistant SKBr3 breast cell lines.

4.3.4 Low Spry2 expression is associated with resistance to trastuzumab in trastuzumab-treated patients.

Since higher levels of Spry2 were responsible for increased therapeutic efficacy in the HER2+ SKBr3 breast cell line, we quantified expression of Spry2 in 122 primary breast tumours from patients who had been treated with trastuzumab using the AQUA fluorescence image analysis system (Figure 4.6). This allowed us to test whether high expression levels of Spry2 protein were associated with trastuzumab sensitivity, and low expression levels with resistance, in the clinical setting. The cutpoint for Spry2 expression were calculated as described above, such that as well as showing high significance for difference in survival ($p=0.0069$), the cutpoint for Spry2 expression also maintained good significance with Monte Carlo simulations ($p=0.09$) and correction for type I error (Miller-Seigmund p value = 0.12). In univariate analysis, tumour size, ER status, chemotherapy regimen, and Spry2 expression levels were all associated with significant survival differences (log-rank test, $p<0.05$, Appendix A), but Spry2 remained the only significant predictor of survival in multivariate analysis (Cox logistic regression, $p=0.002$). Consistent with the findings *in vitro*, high levels of Spry2 expression were associated with better overall survival than patients with tumours which expressed low levels of Spry2 (HR = 2.28, 95% CI 1.22 – 4.26; $p=0.008$; mean survival 48 (95% CI 41-54 months) months vs 37 (95% CI 26-40 months) months for high and low Spry2 levels, respectively; Figure 4.6b). This supports the role of Spry2 as a tumour suppressor gene in breast cancer, and its role in therapeutic resistance to trastuzumab.

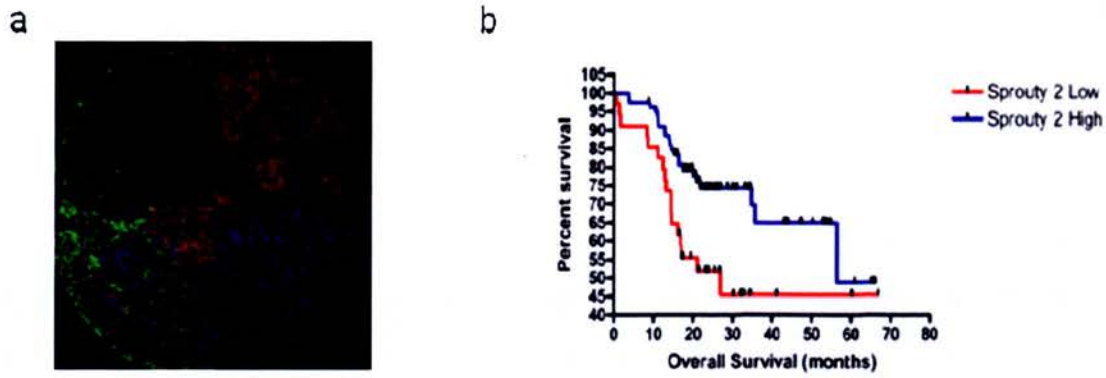

Figure 4.6: Quantitative expression of Spry2 is associated with trastuzumab senstitivity in patients. a, AQUA fluorescent analysis of Spry2 expression in a tissue microarray core, showing cytoplasmic localisation of Spry2 (red) and masking of tumour areas for quantitation by cytokeratin (green). **b,** Kaplan-Meier survival curves for patients treated with trastuzumab for low (red) and high (blue) protein expression of Spry2. Overall survival is calculated from time of initial diagnosis to date of death.

4.4 Discussion

The balance between positive and negative signals is critical in the maintenance of normal cell homeostasis in response to external stimuli, whether the stimulus is physiological (such as ligand drive) or therapeutic (such as with RTK or small molecule inhibitors of cellular signalling). The clinical implications of feedback control are becoming more readily appreciated. Loss of feedback inhibition in tumours treated with mTOR inhibitors (via increased expression of IRS-1) results in induction of AKT signalling, and may be responsible for the disappointing efficacy of mTOR antagonists in the clinic (90). At worst, mechanisms such as unintended negative feedback contribute to the poor efficacy of agents when studied in Phase II and Phase III cancer trials and the high rate of attrition of drugs (approximately 30% due to efficacy), which is both time consuming and expensive (91).

Here we investigated the role of one such feedback mechanism, Sprouty expression, in breast cancer and therapeutic resistance to RTK-inhibitors. In breast cancer, *Spry1* and 2 have been shown to be downregulated at gene expression level compared to

normal breast epithelium (167), which we confirm by meta-analysis of published gene expression data and confirmatory *in vitro* gene expression studies in a panel of breast cancer cell lines. Also consistent with a tumour suppressor function, *Spry1* and 2 expression decreases with increasing histological grade, but *Spry4* increases. Variable Sprouty expression is not uncommon and reflects bimodal or complex functions depending on context or orthologue. For example, Spry2 can have positive effects on ERK signalling as well as negative effects through sequestration of cbl and inhibition of cbl-mediated receptor ubiquitination and degradation (160), and *Spry4* may play a greater role in cell fates other than proliferation or apoptosis, such as cell spreading and motility (185), which would have a greater influence on other pathological endpoints such as invasion and metastasis. Similarly, *Spry1* and 4 were highly expressed in HER2 positive tumours, while *Spry2* showed lower expression. Since Sprouty expression was associated with HER2 status, has been shown to be expressed as a delayed early response (DER) gene downstream of other closely related growth factor receptors such as EGFR and FGFR, we further explored the association with HER2 in order to establish whether Sprouty plays an important role downstream of this therapeutically-targeted receptor. Interrogation of a panel of breast carcinoma cell lines confirmed the expression patterns from array analysis and showed that decreased *Spry2* is associated with HER2 protein expression level. Since HER2 does not have any known ligands, and HER3 is kinase-dead, we exploited the property of heregulin-β to preferentially drive signalling through HER2/HER3 receptor dimerisation (in preference to EGFR heterodimerisation) to show that, similar to delayed early gene expression of Sprouty downstream of FGFR and EGFR, *Spry1*, *2* and *3* are expressed as DEGs with increased expression after 4 h, which was sustained at 24 h. This effect was abrogated by the RTK dimerisation-inhibitor, pertuzumab. Although transient expression of Spry2 or dominant negative $Spry2^{Y55F}$ showed inhibition and induction of ERK signalling as expected, physiological pathway activation with heregulin-β showed pathway activation dynamics which were not obviously related to profiles of *Spry2* gene expression, suggesting that physiological control of signalling is more complicated than forced expression within the experimental setting would suggest. Therefore there is an additional explanation for altered steady-state expression of genes in cancer which

are not mutated, epigenetically silenced by hypermethylation of promoter regions, or have loss of heterozygosity, none of which have been shown for Sprouty in breast cancer. Instead, steady state expression levels represent surrogates for the dynamic state of related signalling pathways at that point in time, in this case *Spry2* expression in the face of HER2 overexpression.

We explored the cooperativity of feedback by Sprouty on overcoming therapeutic resistance to trastuzumab by overexpressing Spry2 or dominant negative $Spry2^{Y55F}$ in trastuzumab-resistant or sensitive cell lines expressing intermediate-levels of endogenous Spry2. Full length Spry2 synergised with trastuzumab to inhibit growth in trastuzumab insensitive SkBr3 cells. In some settings, therefore, reinstating negative feedback can overcome trastuzumab resistance. Since no Sprouty mimetics exist for therapeutic purposes, we used inhibitors of PI3K and ERK signalling, LY294002 and PD98059 in place of Spry2 feedback, since Spry2 can inhibit ERK directly or PI3K indirectly via PTEN. LY294002, but not PD98059, synergised with trastuzumab to inhibit cell growth, suggesting that for cellular proliferation at least, inhibition through PI3K is the dominant synergistic feedback mechanism. Steady state levels of Spry2 were confirmed to have an impact on therapeutic response in a series of 122 trastuzumab-treated breast cancers, with low Spry2 levels significantly associated with decreased overall survival in multivariate analysis. Our data suggest that in a proportion of breast tumours deficient in negative feedback, combinatorial therapy with inhibitors of pathways downstream of RTKs may be an effective therapeutic strategy, and negative feedback proteins such as Sprouty may be useful biomarkers for selecting patients for these therapies.

Although in this chapter we suggest that high levels of Sprouty 2 are associated with trastuzumab resistance, and that Sprouty expression changes at gene expression level in the face of ligand drive, the exact relationship between the first measurement (static) and the second set of measurements (dynamic) in real tissues remains to be determined. Therefore input of equations describing the gene expression of Sprouty, and inhibition of MAPK/PI3K pathway components by Sprouty, may lead to a greater understanding of the relationship between steady-state levels of feedback

proteins and ligand drive. Although not specifically included in our existing models (see chapter 6), delayed early gene responses would be an attractive area for further systems biology work, especially given the potential therapeutic importance of these proteins.

Chapter 5: Describing Pathways (2): The multiple pathway approach.

5.1 Introduction

Although it is clear from our own data (Sprouty (Chapter 4) and PTEN (Chapter 6) and others (71;72;159;186;187) that detailed understanding of canonical growth factor pathways (such as MAPK/PI3K) is beginning to lead to advances in understanding resistance mechanisms with respect to RTK-inhibitors, there also needs to be discovery-driven advances in biomarker biology in order to meet the rapid evolution of therapeutics available to the clinic. Much of this unmet need has come from research using gene expression microarrays, but little of this has resulted in useful clinical tests, for reasons already discussed. Given the complexity of crosstalk between pathways, there is no definite *a priori* reason why some seemingly unrelated pathways might not impact on each other in the face of therapeutic perturbation. Moreover, many of the molecular mechanisms mediating responses to 'traditional' cytotoxic therapies (which are still the mainstay of adjuvant therapy for many cancers) remain to be established. To date there have been few attempts to deconvolute complexity across multiple pathways at protein level. Driven by our desire to understand how different pathways interact at a systems level, and by a need to develop new tools to discover markers of therapeutic response, we sought to investigate how accurate measurements of pathways may be used to re-classify cancers, using quantitative measurements from AQUA fluorescence image analysis.

Survival figures for epithelial ovarian cancer remain poor, with 65% of women dying of their disease at five years (188), in spite of often initially good response rates to chemotherapy (189). This is partly because women with ovarian cancer present with late-stage disease, but also because of a lack of predictive tissue biomarkers coupled with effective therapy in clinical practice or in the pipeline, in contrast to the clinical success stories of ER, HER2 and others in breast cancer (84;190). Most women are treated with cytotoxic chemotherapy (usually platinum +/- taxane) (189), rather than with lower toxicity targeted agents, such as tamoxifen or trastuzumab (Herceptin). There is therefore an acute need to identify markers of sensitivity to existing cytotoxic agents as well as to identify new 'hits' for targeted therapy in ovarian

cancer, which could translate into real clinical benefit if currently available therapies can be more precisely targeted to known dysregulated signalling in ovarian cancer.

Recent evidence suggests that distinct molecular subgroups of ovarian cancer exist, both between (191) and within (192) recognised histopathological subgroups (serous, endometrioid, clear cell, mucinous). This suggests that while histopathology alone provides useful prognostic and predictive information, additional molecular profiling may be able to resolve some of the heterogeneity in response. Molecular classification at protein level may be more informative for therapeutic prediction than gene expression profiling, which so far has only shown benefit in the experimental setting (86). This is because drugs are designed to target proteins rather than genes or transcripts in oncogenic or tumour suppressor pathways, which may show as much as 60% difference to mRNA after post-translational modification. In addition, the measurement of proteins is more readily adapted to clinical histopathology labs, which already use immunohistochemistry as a standard molecular technique, facilitating ready transition to the clinic.

The most useful protein targets to measure to meet these aims remain open to debate. However, an emerging paradigm within cancer biology, and supported by recent large-scale genotyping and transcriptional profiling studies (85), is that the complexity of cancer can be reduced to abnormalities in suppression or activation of only a few pathways, since several different mutations or transcriptional aberrations within the same pathway can lead to similar phenotypes (193). To date, no attempt has been made to classify tumours on the basis of pathway activation status, which may be assessed by measurement of phosphorylated epitopes of key signalling molecules. For example, phosphorylation of the serine 473 epitope of AKT provides a measure of the activation state of the PI3K pathway (194). We hypothesise that since experimental and clinically used agents already exist which target growth and apoptotic pathways, classification of individual tumours by pathways could result in a tumour specific signature which could guide patient-tailored therapy from a number of readily-available and licensed agents, either alone or in combination.

The aim of this part of our study was to (1) quantitatively measure the activation state of eight growth- or survival-promoting pathways which are known targets of current or experimental cancer therapeutics by generating a phosphoprotein profile in cancer biopsy tissue (2) relate this to clinicopathological parameters including histological subtype, proliferation, and apoptosis, and (3) establish whether this approach can generate new testable hypotheses that allow prediction of therapeutic responses.

5.2 Patients and Methods

5.2.1 Study population

The study population consisted of 168 epithelial ovarian tumours (48 serous, 30 endometrioid, 30 clear cell, 10 mucinous, 23 mixed epithelial, and 7 malignant mixed mullerian invasive ovarian tumours, as well as 5 borderline serous and 14 borderline mucinous tumours) treated in the Edinburgh Cancer Centre between 1994 and 2005, as described previously (195). The study was approved by the Lothian Research Ethics Committee (08/S1101/41). Summary patient characteristics are shown in Table 5.1. Standard treatment included cytoreductive surgery followed by platinum-based therapy, with or without combination with paclitaxel. Overall survival was calculated from the date of diagnosis (primary surgery) to the date of death by ovarian cancer, or to the date of last follow-up (censored). Patients who died from disease other than ovarian cancer were censored.

5.2.2 Tissue microarray (TMA) construction

The construction of this TMA has already been described (195). Briefly, four replicate TMAs were constructed using established techniques (196), and three replicates were used for analysis within this study. Where primary lesions showed a mixed histological pattern, representative areas of each histological type were targeted, so that all types were adequately represented within the analysis.

Characteristic	No.	Percent	Log-rank p-value
Number of patients	152	100	
Age			**0.018**
Median	61.0	N/A	
Range	24 - 90	N/A	
1st line chemotherapy regimen			**0.36**
Platinum-based	51	33.6	
Platinum & taxane	44	28.9	
Other/none	28	18.4	
Unknown	29	19.1	
Stage			**<0.0001**
I	29	19.1	
II	20	13.2	
III	52	34.2	
IV	20	13.2	
Unknown	31	20.4	
Grade			**0.019**
Well differentiated	12	7.9	
Moderately differentiated	24	15.8	
Poorly differentiated	80	52.6	
Unknown	36	23.7	
Histology			**0.005**
Serous	46	30.3	
Clear cell	31	20.4	
Endometrioid	29	19.1	
Mixed	23	15.1	
MMMT	7	4.6	
Mucinous	14	9.2	

Table 5.1. Patient characteristics of ovarian cancer cohort.

5.2.3 Immunofluorescence

Immunofluorescence for phosphoprotein targets was performed using methods previously described (197). The antibodies and conditions used within the study are described in Table 5.2. Phosphoprotein specificity was determined by a single band on western blot, positive tissue controls, epithelial specificity, and expected

subcellular localisation, together with omission of primary antibody as a negative control. Antibodies not meeting all of these criteria were rejected.

Target	Supplier	Dilution	Antigen retrieval
pAKT (Ser 473)	CST (#4060)	1:100	Sodium citrate pH6.0
pERK (Thr202/204)	CST (#9101)	1:25	Sodium citrate pH6.0
pER (Ser118)	CST (#2511)	1:500	Sodium citrate pH6.0
pbCatenin (Ser33/37/41)	CST (#9561)	1:25	Sodium citrate pH6.0
pSTAT3 (Ser727)	CST (#9134)	1:100	Sodium citrate pH6.0
pNFkB (Ser529)	CST (#3037)	1:25	Sodium citrate pH6.0
pRB (Ser807/811)	CST (#9308)	1:50	Sodium citrate pH6.0
pH2AX (Ser139)	CST (#9718)	1:50	Sodium citrate pH6.0
pBRCA1 (Ser1524)	CST (#9009)	1:25	Sodium citrate pH6.0
p-p53 (Ser15)	CST (#9286)	1:100	Sodium citrate pH6.0
Ki67	DAKO (M7240)	1:50	Tris-EDTA pH9.0
pHH3	CST (#9701)	1:100	Tris-EDTA pH9.0
Caspase 3	CST (#9661)	1:200	Sodium citrate pH6.0

Table 5.2. Antibodies used for pathway classification, concentrations, and antigen retrieval conditions. Antigen retrieval was for 5minutes in a microwave pressure cooker in all cases.

5.2.4 AQUA automated image analysis

A detailed description of the AQUA HistoRx methodology is available elsewhere (178;197). Pan-cytokeratin antibody was used to identify infiltrating tumour cells, DAPI-counterstain to identify nuclei, and Cy-5-tyramide detection for target for compartmentalised (tissue and subcellular) analysis of tissue sections. Monochromatic images of each TMA core were captured at x20 objective using an Olympus AX-51 epifluorescence microscope, and high-resolution digital images analysed by the AQUAnalysis^{TM} software. If the epithelium comprised <5% of total core area, the core was excluded from analysis.

5.2.5 Protein expression analysis and statistics

AQUA scores were averaged from replicate cores. Protein expression data were analysed in Cluster v2.11 and visualised using Treeview v1.6, as previously described (198). Raw AQUA scores were filtered so that >50% of protein expression data was present for each tumour analysed. K-means clustering was performed on filtered AQUA scores which had been log-transformed, normalised by protein, and mean-centred. Overall survival was subsequently assessed by Kaplan-Meier analysis with log-rank testing to determine statistical significance. To assess whether our clusters provided more accurate predictions than standard clinicopathological parameters, we performed univariate and multivariate analysis using Cox proportional hazards regression models. Comparison of differences in means for proliferation and apoptosis were performed using one-way ANOVA, and differences in distribution of histological subtypes and grade per cluster by Chi-squared test. All calculations and analyses were two-tailed where appropriate and done with SPSS 14.0 for Windows (SPSS, Inc., Chicago IL).

5.3 Results

5.3.1 Patient characteristics

Ovarian tumours were analysed from 168 patients. Of these, 152 patients had sufficient AQUA data after filtering (>50% data present) for subsequent clustering and survival analysis. Clinicopathological details for these patients summarised in Table 5.1. For the whole group, the median overall survival from diagnosis was 42.9 months (range 0.8 – 161.0 months) and the 5 year overall survival was 19.0 percent.

5.3.2 Phosphoprotein expression and pathway activation is heterogeneous within and between histological subtypes

We first sought to quantify and visualise the activation state of eight growth- or survival-promoting pathways (PI3K, MAPK, β-catenin, STAT, NFκB, ER, cell

cycle, DNA damage response; Figure 5.1) by measuring the tissue expression of ten phosphoprotein targets.

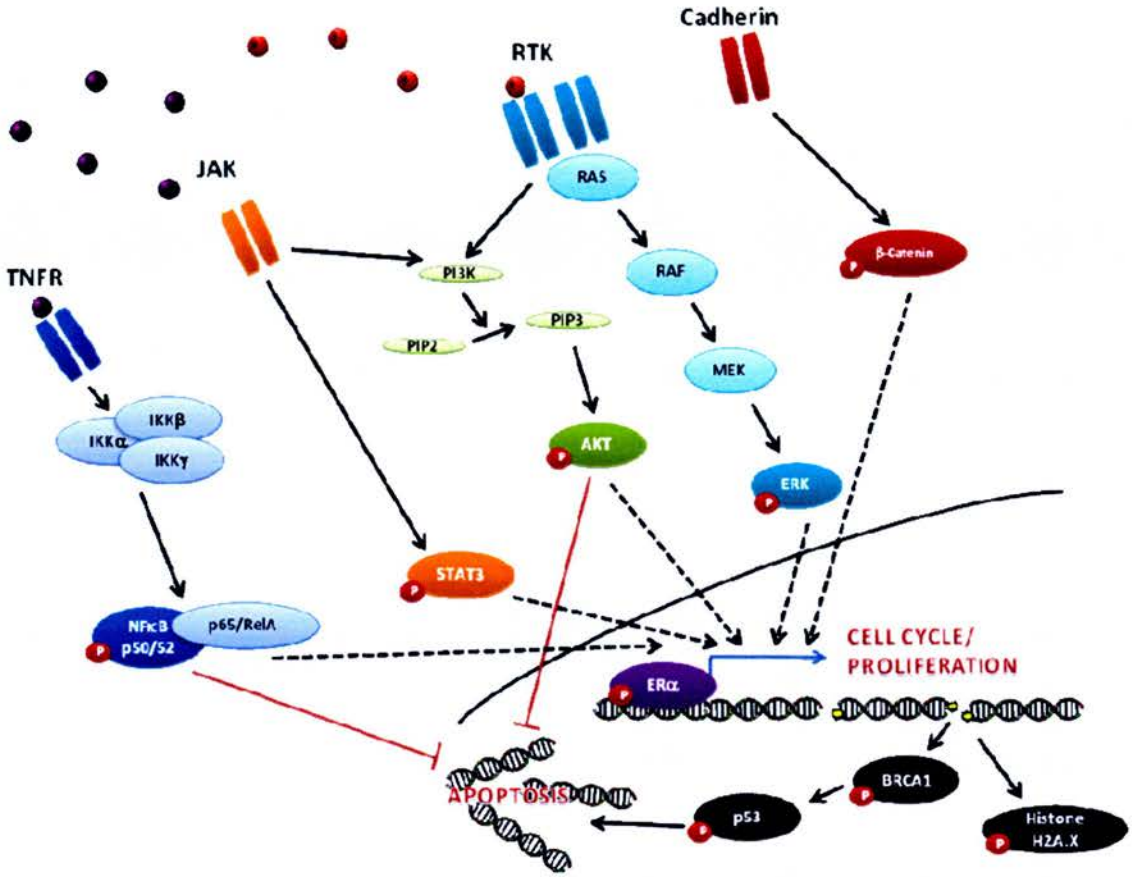

Figure 5.1: Schematic of pathways investigated in this study.

Representative expression across different cancers is shown in Figure 5.2A and in the same cancer in Figure 5.2B, in order to illustrate how the AQUA score relates to *in situ* phosphoprotein expression (Figure 5.1B).

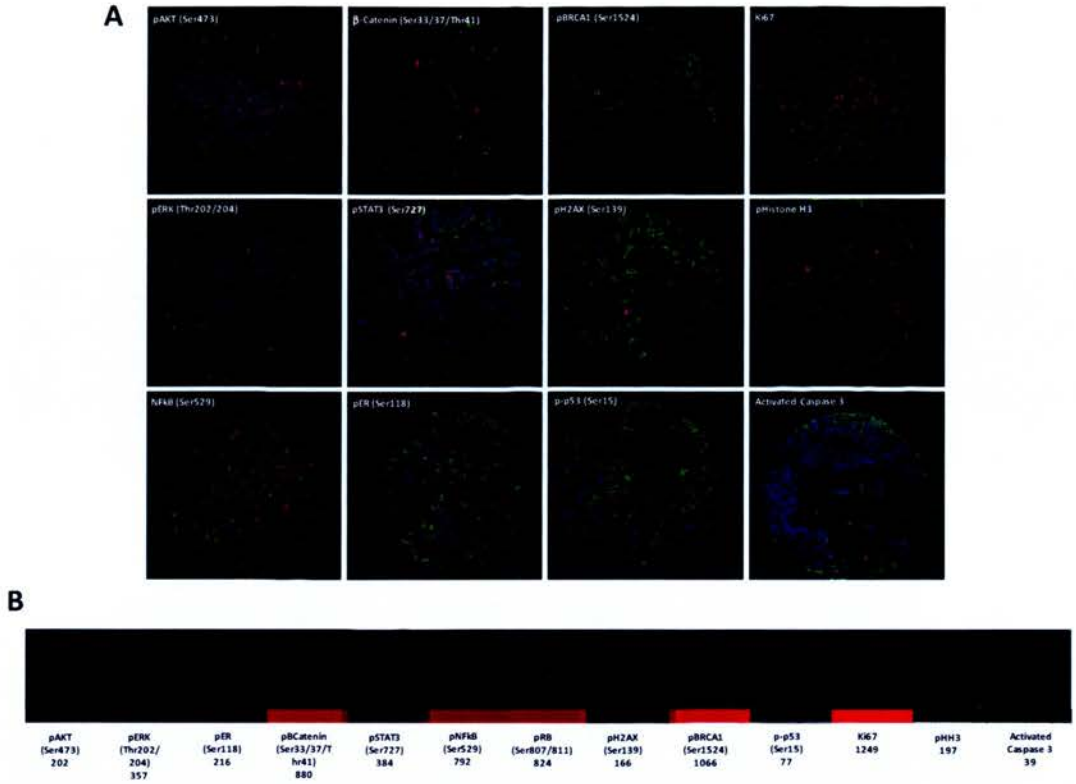

Figure 5.2: AQUA quantitative image analysis. (A) Representative immunofluorescence images of each of the phosphoproteins and pathological markers used within the study. Blue = DAPI nuclear counterstain, Green = cytokeratin tumour mask, Red = target. (B) Representative staining from an individual case, with corresponding AQUA score represented as both a heatmap and whole integer.

Phosphoprotein expression was heterogeneous within (Figure 5.3A) and between (Figure 5.3B) histological subtypes, indicating that similar subtype heterogeneity exists at a functional, phosphoprotein level, to that recently reported for total protein expression in ovarian cancer (191). When analysed for the most common (median) expression difference between histological subtypes (Figure 5.3B), subtypes exhibit differences in phosphoprotein expression and pathway activity. Thus serous carcinomas exhibit relatively high expression of DNA-damage response phosphoproteins (pBRCA1 and pHistone-H2A.X) with low p53 phosphorylation, while clear cell carcinomas show relatively high levels of phosphorylation of the growth and cytokine dependent pathways β-catenin, STAT, and NFκB and the downstream tumour suppressor pRB. However, there are no significant differences in

proliferation (measured by Ki67 and pHH3) or apoptosis (measured by activated caspase 3) between the main histological subtypes (one-way ANOVA; Ki67 p=0.120, pHH3 p=0.066, activated caspase 3 p=0.056). These data suggest that crossover exists between morphology and molecular phenotype in ovarian cancer, but that re-classification of tumours by phosphoprotein signature may refine prognostication and prediction by traditional histopathological parameters.

5.3.3 Regrouping of ovarian carcinomas by phosphoprotein profiling reveals subgroups with distinct pathway activation profiles and pathological properties

In order to determine the value of phosphoprotein profiling compared to traditional histopathological subtyping, we used K-means clustering to organise the tumours on the basis of phosphoprotein expression. Three main clusters were identified (Figure 5.3C). The distribution of histological subtypes in Figure 5.5 confirmed the crossover between morphology and phosphoprotein expression. Cluster 1 contained a high proportion of serous, endometrioid and mucinous carcinomas and cluster 2 a high proportion of clear cell carcinomas. Cluster 3 contained predominantly serous and mixed-histology tumours. Poorly differentiated tumours were distributed equally across phosphoprotein clusters, but cluster 3 tumours had a lower proportion of well and poorly differentiated tumours (Chi-squared test, $p = 0.016$). However, in contrast to histopathological subtypes, phosphoprotein clusters showed significant differences in proliferation and apoptosis (Figure 5.6), with cluster 3 showing significantly higher proliferation (one-way ANOVA; Ki67 $p=0.01$, pHH3 $p<0.0001$) than clusters 1 and 2. Clusters 1 and 3 showed lower apoptosis measured by activated-caspase 3 (one-way ANOVA; $p=0.044$) than cluster 2. Each of the clusters also had distinct profiles of pathway activation (Figure 5.4), with cluster 1 showing low level expression of the markers analysed, cluster 2 high levels of phosphorylation of hormone, growth factor and cytokine-dependent signalling pathways (ER, MAPK, β-catenin, STAT, NFκB) and p53, and cluster 3 activation of PI3K and DNA-damage sensing proteins, but relatively low p53 phosphorylation.

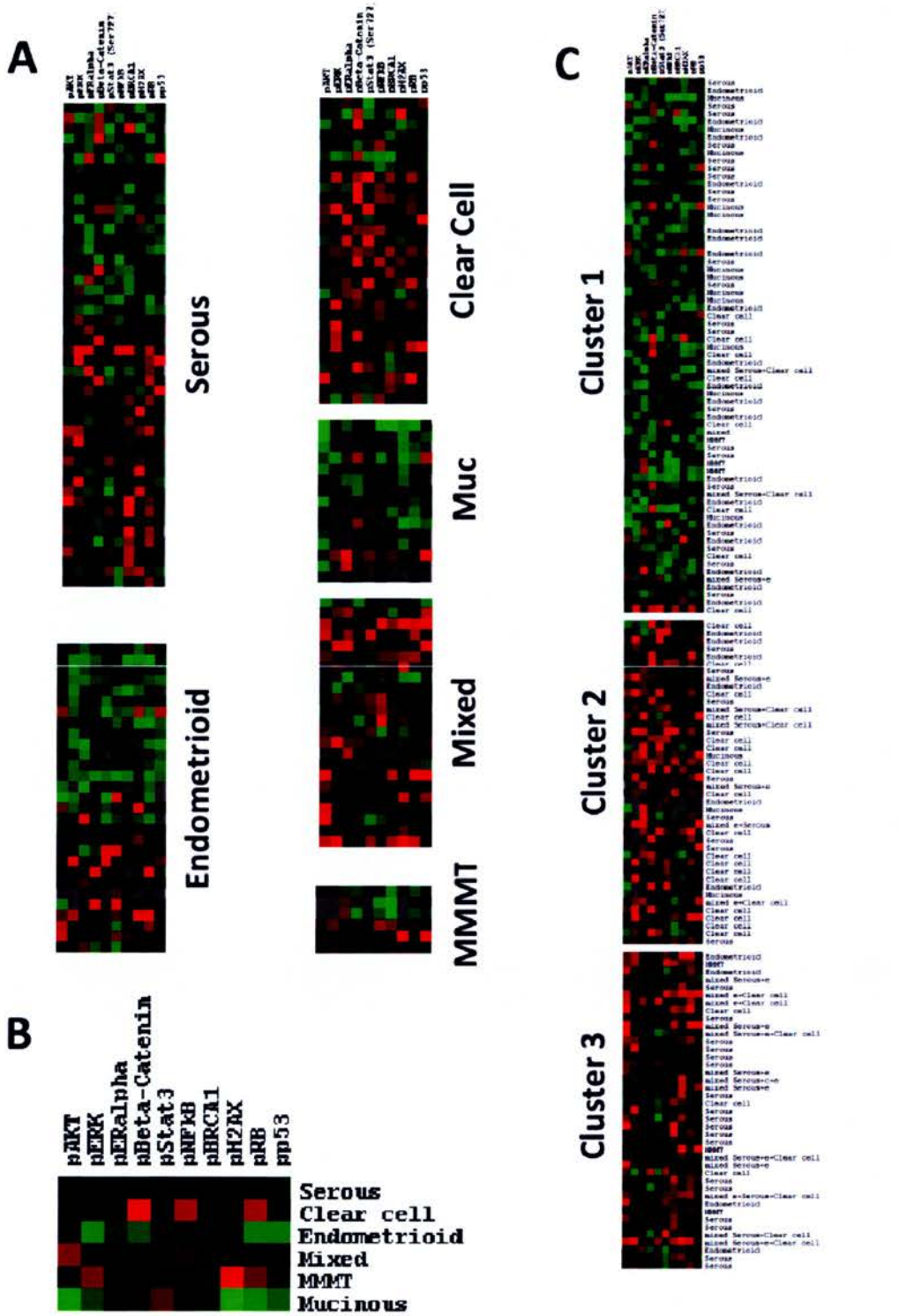

Figure 5.3: Visualisation and analysis of phosphoprotein expression data (1). (A and B) Phosphoprotein expression by histological subtype (median expression levels illustrated in (B)). K-means clustering of (C) produces 3 distinct phosphoprotein clusters with distinct pathway activation (see Figure 5.4).

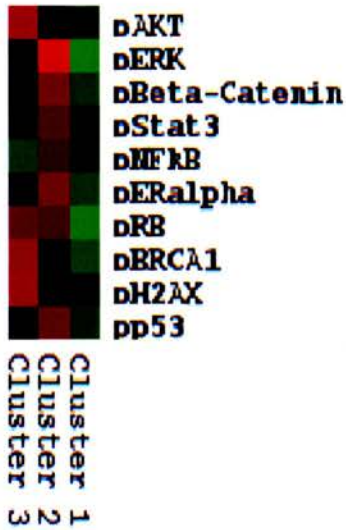

Figure 5.4: Visualisation and analysis of phosphoprotein expression data (2). Pathway activation status of the three phosphoprotein clusters.

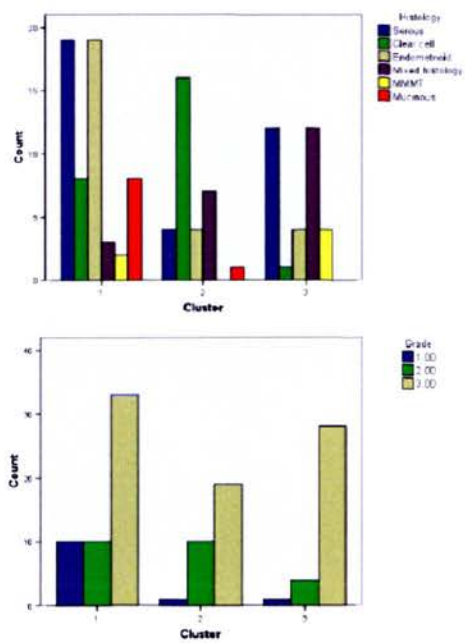

Figure 5.5: Distribution of histological subtype (top) and grade (bottom) per cluster.

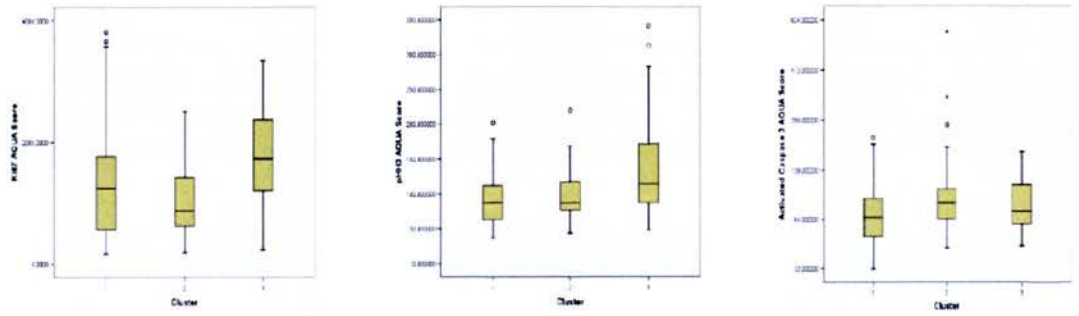

Figure 5.6: Proliferation and apoptosis per phosphoprotein cluster. One-way ANOVA; Ki67 p=0.01; pHH2 p=0.001; caspase 3 p=0.044.

5.3.4 Phosphoprotein profile clusters provide a novel predictive framework for rationalising cancer therapies

Since phosphoprotein clusters differentially express pathway activation markers, we sought to establish whether this approach could be used to predict responses to existing therapy, and therefore potentially also novel therapies. Baseline assessment of prognosis by univariate log-rank analysis for clinicopathological parameters (Table 5.1) and phosphoprotein cluster showed that age, stage, grade, histology and phosphoprotein cluster were all significantly associated with overall survival (Table 5.1 and Figure 5.7). Phosphoprotein cluster was associated with a hazard ratio (HR) of 1.36 (95% CI 1.08-1.72). Survival by stage showed little difference between stage I and II versus stage II and IV, similar to that recently described (191). Only stage remained a significant predictor of overall survival in a multivariate Cox regression model (p=0.011; HR = 1.34; 95% CI 1.06 – 1.69). However, we hypothesised that since cluster 3 showed a pattern of phosphoprotein expression indicating high levels of DNA-damage (high phosphorylation of BRCA1 and H2A.X) but an absent p53 response (low p53 phosphorylation) that tumours contained within this cluster would be relatively insensitive to further DNA-damage induced by DNA-crosslinking agents such as carboplatin and cisplatin. Given the relatively high rate of proliferation rates of these tumours (Figure 5.6), they would nevertheless be expected to be sensitive to spindle poisons such as taxanes. Subgroup analysis of patients treated with platinum alone compared to a platinum and taxane-containing regimen

supported this hypothesis, with significantly poorer survival for patients in cluster 3 relative to clusters 1 and 2 when treated with platinum alone (Figure 5.8; p = 0.006; HR = 1.46; 95% CI 1.11 – 1.92). In patients treated with taxane-containing regimens, survival for cluster 3 tumours was equal to that of clusters 1 and 2. When adjusted for chemotherapy, phosphoprotein cluster and pathological stage were the only two variables which were significantly associated with survival by univariate analysis. In a Cox regression model, only phosphoprotein cluster remained a significant predictor of response to chemotherapy (p=0.015; HR = 1.40; 95% CI 1.06 – 1.84).

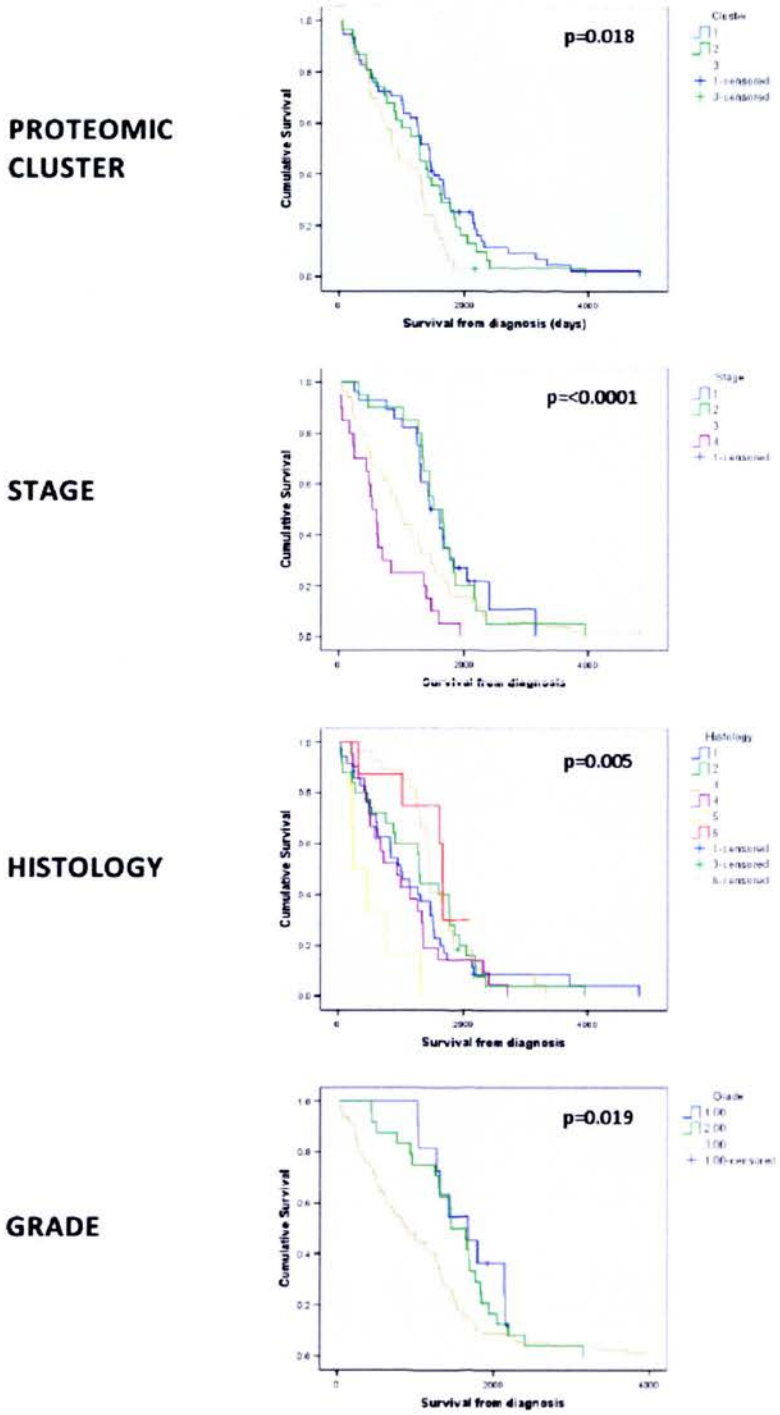

Figure 5.7: Kaplan-Meier survival curves for significant variables (1). For the whole cohort. P values = log rank test.

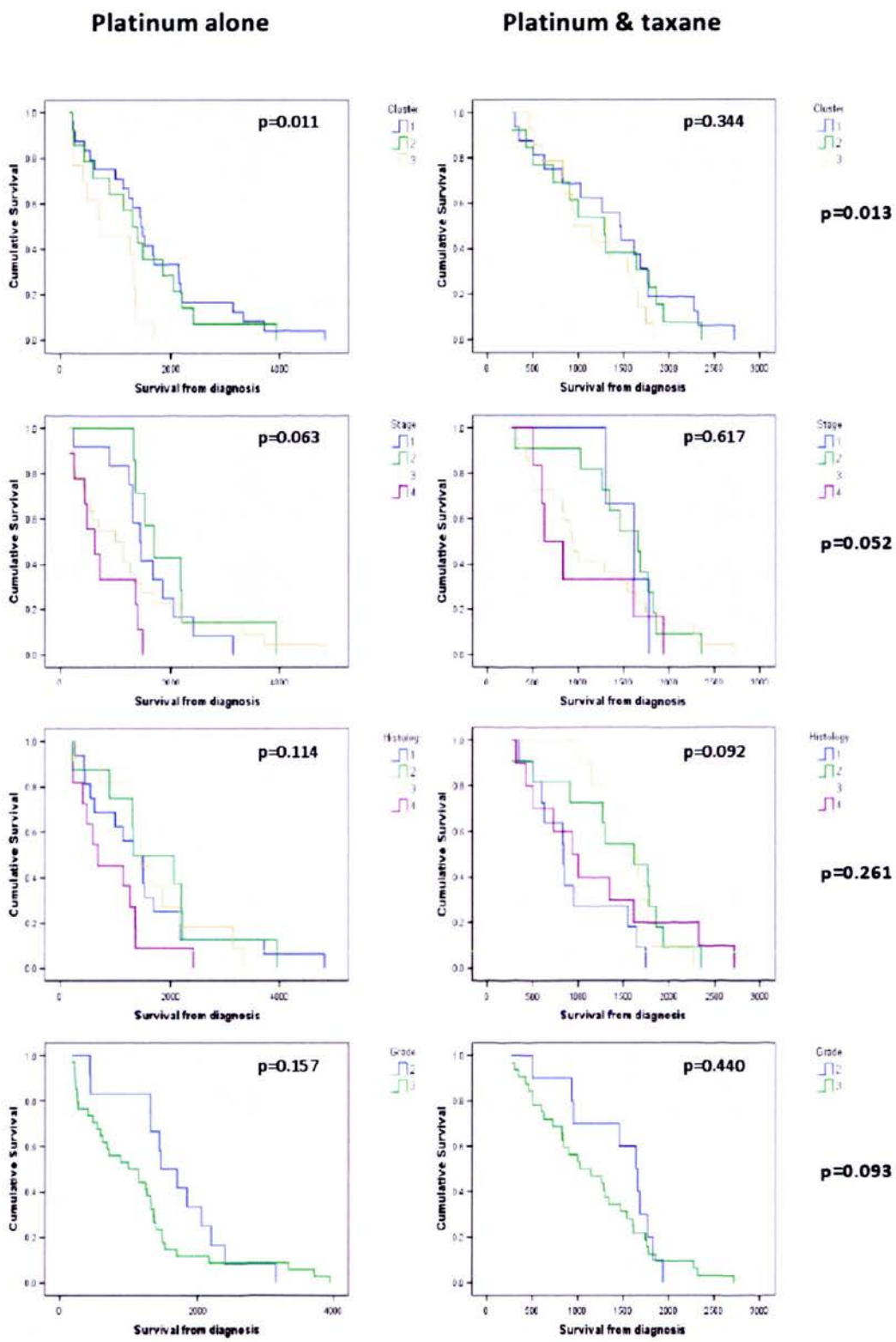

Figure 5.8: Kaplan-Meier survival curves for significant variables (2). By treatment. P values = log rank test.

5.4 Discussion

This study is the first to group human cancers based on the activation state of oncogenic pathways by quantitative phospho-protein expression analysis. We chose ovarian cancer as a model for this approach since the disease is proving resistant to classification by existing approaches (such as gene expression array analysis) (199;200) but there is some evidence to suggest that a few well characterised pathways are aberrantly expressed in different histological subtypes (201). We have shown that while phosphoprotein profiling does show some association with traditional histopathological subtypes, reclassification on the basis of similar phosphoprotein expression by cluster analysis reveals new molecular subgroups which have distinct pathological characteristics in terms of cell fate (proliferation and apoptosis) which are not apparent by histopathological classification alone. These phosphoprotein clusters also provide a means to predict *a priori* which patients may respond better to a particular therapy. In this case, the DNA-damage response profile of excessive DNA damage (high pBRCA1 and pH2AX) in the absence of p53 phosphorylation suggested relative resistance to platinum-based therapy, which was borne out in subgroup analysis of chemotherapy regimens and multivariate analysis. Therefore patients with cluster 3 tumours had a worse overall survival than cluster 1 or 2 tumours when treated with the DNA-crosslinking cytotoxics cisplatin or carboplatin alone, but all three clusters had the same overall survival when treated with a combination of cisplatin/carboplatin and a taxane mitotic spindle poison, which might be expected to kill cells by p53-independent mechanisms such as mitotic catastrophe. Additional therapeutic targets are PI3K inhibitors in cluster 3 and growth factor inhibitors (either alone or in combination) in cluster 2. Therefore it might be reasonable to add a PI3K inhibitor or mTOR inhibitor to taxane-containing regimens in patients with cluster 3 tumours in order to increase efficacy. Validation of the clustering observed within this study within an independent cohort, and further investigation *in vitro* and *in vivo* of the therapeutic targets identified herein, are warranted.

The finding of a DNA-damage response profile predictive of chemotherapy response is in keeping with a growing body of evidence supporting the use of molecular targets within DNA-damage and apoptotic response pathways as predictive tissue biomarkers in ovarian cancer. p53, bcl2, MMR, ERCC1, and BRCA1 have all been implicated in cisplatin resistance (202-207). For instance, BRCA1 plays a complex role in mediating sensitivity and resistance to platinum-based therapies and taxanes, and has been the subject of recent review (207). Functional BRCA1 is associated with resistance to platinum and sensitivity to taxanes (207). No data exists on the *in vivo* role of phosphorylated BRCA1, one readout of the function of BRCA1, in any cancer, although the serine 1524 site measured in this study is known to be phosphorylated in response to DNA damage in model systems (208). One interpretation of the high pBRCA1 (Ser1524) in cluster 3 is that BRCA is functional and can overcome platinum-induced damage. However, given the high p-histone H2A.X expression (which when phosphorylated at serine 139 localises to sites of DNA-damage (209)) and low p53 (Ser15, which is also phosphorylated in response to DNA-damage (210)) pattern observed in cluster 3, we might postulate that DNA-damage has already been sustained but downstream p53-dependent effector mechanisms have failed, and that further DNA-damage is unlikely to trigger apoptosis in a p53-dependent manner. Mutation of p53 (Ser15) is also known to inhibit p53-dependent cisplatin-induced apoptosis (211). The relatively low rate of apoptosis seen in cluster 3 is consistent with this hypothesis. Since taxanes mediate much of their effect in a p53-independent manner, this explains the relative sensitivity of cluster 3 to taxanes in line with previous data. In this way the measurement of phosphoproteins can provide additional functional information about key nodes in signalling pathways beyond that seen by total protein measurements alone.

Our analysis of upstream signalling pathways has revealed potential new targeted and combinatorial therapeutic options. In cluster 3 there is high expression of activated AKT, which is a surrogate for PI3K pathway activation and may be a candidate biomarker for RTK and mTOR inhibitors in breast and other cancers (71;212). Similar biomarker data for ovarian cancer is lacking. An inverse

relationship between pAKT and p53(Ser15) has been observed *in vitro*, and is thought to in part mediate cisplatin-resistance via a p53-upregulated modulator of apoptosis (PUMA)-dependent and p53-dependent mechanism (211), which lends support to the inverse relationship between these proteins seen in this study. These data suggest that the addition of a PI3K/mTOR inhibitor may be a novel combination approach in ovarian tumours harbouring this signature *in vivo*.

Cluster 2 tumours show a phosphoprotein profile which is suggestive of growth-factor dependency, with high levels of phosphorylation of pathways which are known to connect extracellular growth signals from cytokines and growth factors (pERK, β-catenin, STAT, NFκB, ER; see figure 5.1) with cellular growth and survival. Although data exists implicating these pathways in ovarian cancer histogenesis, this is the first time that the activation state of these pathways measured by phosphoprotein analysis have been described in clinical samples. Somatic mutations of *K-RAS* (213-215) and *CTNNB1* (the gene encoding β-catenin) (216) are seen in mucinous and endometrioid ovarian cancers respectively, and aberrant Wnt, JAK/STAT and MAPK signalling has recently been described in serous ovarian cancers by gene expression analysis (192). These data are not directly comparable with phosphoprotein data, but the phospho-MAPK, β-catenin, and STAT expression seen in serous cancers is in keeping with deregulation of these pathways in a proportion of serous cancers, further supporting the validity of the current approach. More importantly, each of these pathways represent either existing or novel therapeutic targets, and the pharmacologial agents which target them are relatively low toxicity compared with cytotoxic chemotherapies. Good biochemical response rates have been seen in tumours treated with aromatase inhibitors in phase II clinical trials (217-219), and Wnt/β-catenin antagonists have shown promising efficacy *in vitro* and are emerging as new therapeutic targets in cancer (220). Much less in known about STAT signalling and ovarian cancer therapy, but one study suggests therapeutic efficacy *in vitro* with the JAK inhibitor AG490 (221).

In conclusion, this part of the study is the first to measure the activation states of a number of pathways by phosphoprotein analysis. This approach offers the

opportunity to represent a sufficient amount of the disease complexity with a relatively low volume of data. It identifies factors of importance in response prediction to existing chemotherapies, but also several new hypotheses about novel targets and approaches to individualised therapies. These findings will need further validation in both experimental and clinical settings.

Chapter 6: Describing Pathways (3): The systems pathology approach.

6.1 Introduction

In the preceding chapters we have extensively discussed the need for accurate measurements so that biological data may be input into mathematical models, in order to predict therapeutic response. In this chapter we use these principles and populate a new mathematical model of RTK-signalling, developed in collaboration with colleagues at the Centre for Systems Biology at Edinburgh, with data generated using reverse phase protein arrays. We validate our findings in a clinical cohort using quantitative protein expression measurements using AQUA image analysis.

As previously discussed, HER2-targeting receptor tyrosine kinase (RTK) inhibitors, such as trastuzumab and pertuzumab, show clinical efficacy in breast and ovarian cancer but measurement of HER2 protein expression or gene amplification status is a poor predictor of response with a very low positive predictive value (157;158). Activating mutations in the oncogene *PIK3CA* and inactivation of the tumor suppressor gene *PTEN* are known to regulate phosphotidylinositol 3-kinase signaling and cell proliferation and survival pathways, and empirically these have been shown to play a role in resistance to anti-HER2 therapies in breast cancer (71;187). However, the evidence supporting the role of PI3K-pathway activation in RTK-inhibitor resistance has only been tested in very small cohorts of patients retrospectively ((71) and (187), n=55 and n=47, respectively). Further evidence is required in order to support the use of PI3K pathway biomarkers in the clinic supported by robust preclinical and clinical evidence.

Kinetic (or dynamic) computational models offer the opportunity to cheaply and efficiently test the efficacy of targeted therapies *in silico* (that is, computationally) as part of the preclinical testing process (89). However, this methodology is still perceived as esoteric and not clinically applicable because there are very few successful examples of when such modelling has changed practice (66). In oncology, systems biology has not yet made an impact, but the use of therapies targeted against the products of cellular oncogenes in signalling pathways lends itself to this approach

since these pathways can readily be modelled using ordinary differential equations (89). To date, canonical pathways such as the epidermal growth factor receptor (EGFR) pathway have only been modelled in order to explain and predict physiological phenomena (102-108). However, such models have not been so helpful for understanding therapeutic interventions, since they frequently fail to include important oncogene and tumour suppressor nodes, which are known to be fundamental to carcinogenesis and proven resistance proteins (such as HER2, PTEN, and SRC in PI3K and MAPK signalling models).

The aim of this study was to address these deficiencies in current models by (1) developing a new kinetic model which could be interrogated to predict resistance to RTK-inhibitor therapies, and (2) directly test predictions *in vitro* and in clinical samples.

6.2 Materials & Methods

6.2.1 Computational modelling

A kinetic model of heregulin-induced HER2/3 signalling through MAPK and PI3K pathways was developed on the basis of the model proposed by Hatakeyama *et al* (13). The whole kinetic model contains 56 ordinary differentials equations (ODEs) (S1.1)-(S1.56) describing the change of the concentrations of 56 biological entities (proteins, receptors, and lipid second messengers) involved in MAPK and PI3K signalling (see 'Appendix C – mathematical model, ODEs'). A detailed modeling methodology and description of the model design is given in B.1 and B.2 (Appendix B – modeling methods and description of mathematical model). The abbreviations used in the text and ODEs are given in the 'Appendix C – mathematical model, ODEs'. All network schemes were designed using the Edinburgh Pathway Editor (222). The computer model construction, fitting and analysis were implemented using the DBsolve package for kinetic modelling (223) and SimBiology modeling software (MATLAB, The MathWorks Inc.). The model parameterisation procedure permitted us to describe satisfactorily experiments of activation in the different

branches of the ERK/AKT signalling network (see Figure S4 in 'Appendix D – figures') and determine a set of kinetic parameters of the model (see Tables S2 and S3 in 'Appendix C – mathematical model, ODEs').

6.2.2 Cell Culture and Collection of Lysates

PE04 and BT474 cells were grown as monolayer cultures in DMEM supplemented with 10% heat-inactivated foetal calf serum (FCS) and penicillin / streptomycin (100IU/mL) in a humidified atmosphere of 5% CO_2 at 37°c. Time course experiments were set up by plating cells into 10cm ø petri dishes and leaving for 48hrs. Cells were then briefly washed in PBS before transferring to phenol red-free DMEM containing 5% double charcoal-stripped serum supplemented with penicillin / streptomycin (100IU/mL) and glutamine (0.3mg/mL) for a further 48hrs prior to treatment. Paired lysates were prepared by first treating relevant dishes with pertuzumab (100nmol/L) +/- bpV(pic) (50nmol) immediately followed by the addition of heregulin-β (1nmol/L). Samples were collected at time points of 1, 2, 5, 10, 30, 45 or 60 mins, washed in PBS, and immediately lysed in ice-cold isotonic lysis buffer [50mM Tris-HCl (pH7.5), 5 mM EGTA (pH 8.5), 150 mM NaCl, 1% Triton X-100] supplemented with aprotinin (10 µg/mL) and a protease inhibitor cocktail (Roche, 11836153001). Lysates were centrifuged for 6 min at 13,000 x g and protein concentrations of supernatants subsequently determined using the BCA assay (Sigma, BCA-1). All cell culture and timecourse experiments were performed at least three times, and representative RPPA and western blot curves were used for the model fitting procedure described above and to validate model predictions.

6.2.3 Western Blotting

Protein lysates were electrophoretically resolved on either 10% or 12% SDS-PAGE and transferred overnight onto Immobilon-P membranes (Millipore, Bedford, MA). After transfer, membranes were blocked with 1% blocking agent (Roche; #1520709) in TBS before probing overnight at 4°C with the appropriate primary antibody made up in 0.5% blocking agent. Primary antibodies used for western blotting were as

follows: anti-phospho-AKT (Ser^{473}) (Cell Signaling Technology, #9271) at 1:1000; anti-AKT (Cell Signaling Technology, #9272) at 1:1000; anti-phospho-p44/42 MAP Kinase (Thr^{202}/Tyr^{204}) (Cell Signaling Technology, #9101) at 1:1000; anti-p44/42 MAP Kinase (Cell Signaling Technology, #9102) at 1:1000; anti-HER1 (Cell Signaling Technology, #2232) at 1:1000; anti-HER2 (Cell Signaling Technology, #2242) at 1:1000; anti-phospho-HER2 (Tyr^{877}) (Cell Signaling Technology, #2241) at 1:1000; anti-HER3 (Cell Signaling Technology, #4754) at 1:1000; anti-phospho-HER3 (Tyr^{1289}) (Cell Signaling Technology, #4791) at 1:1000; anti-HER4 (Cell Signaling Technology, #4795) at 1:1000; anti-PI3K (Cell Signaling Technology, #4249) at 1:1000; anti-PTEN (Cell Signaling Technology, #9552) at 1:1000; anti-phospho-PTEN (Ser380/Thr382/383) (Cell Signaling Technology #9554) at 1:1000. Immunoreactive bands were detected using enhanced chemiluminescent reagents (Roche; 1520709) and Hyperfilm ECL film (GE Healthcare, UK). Bands were scanned using an Epson Perfection 4990 scanner and Integrated Optical Density (IOD) absorbance values were obtained by densitometric analysis using Labworks gel analysis software (UVP Life Sciences, Cambridge, UK).

6.2.4 Reverse phase protein arrays (RPPA)

Denatured and reduced protein lysates were spotted onto nitrocellulose-coated glass slides (Eurogentec, Hampshire, UK), as previously described (224). Three replicates were spotted per sample in eight two-fold dilutions. Slides were hydrated in Whatman wash buffer for 5 minutes, Li-Cor blocking buffer for 1 hour (LI-COR Biosciences, Nebraska, USA), and then incubated with primary antibodies overnight at 4°c in a sealed box containing a damp paper towel. The following day slides were washed in PBS/T at room temperature for 5 minutes (x3) before incubating with far-red fluorescently-labelled secondary antibodies diluted in Li-Cor Odyssey Blocking Buffer (1µL/2mL) at room temperature for 45mins with gentle shaking. Slides were then washed in excess PBS/T (x3) / PBS (x3) and allowed to air dry before reading on a Li-Cor Odyssey scanner at 680nm and 780nm and images exported as TIFF files for further analysis. Slides were stained using the above primary antibodies (matched total and phosphoproteins duplexed on each slide).

RPPA analysis was performed using MicroVigene RPPA analysis module (VigeneTech, Carlisle, MA, USA). Spots were quantified by accurate single segmentation, with actual spots signal boundaries determined by the image analysis algorithm. Each spot intensity was quantified by measuring the total pixel intensity of the area of each spot (volume of spot signal pixels), with background subtraction of 2 pixels around each individual spot. The mean of the replicates was used for normalization and curve fitting. Curve fitting was performed using five parameter logistical non-linear regression using a joint estimation approach ('supercurve method'). The quantification y0 (intensity of curve) or rsu (relative concentration value) of sample dilution curves were normalized by corresponding total protein.

6.2.5 *PIK3CA* mutation analysis and copy number quantification

PIK3CA mutation analysis was performed using the ARMS/Scorpions multiplexed PCR assay as previously described (225) to detect the four most common mutations in *PIK3CA*, (H1047L, H1047R (Exon 20), E545K and E542K (Exon 9)). PIK3CA copy number quantification was performed with primers for PIK3CA and the glucokinase (GCK) gene as the reference gene as previously described (226). Quantitative PCR was performed on the Rotor-Gene 6000 real-time detection system (Corbett Life Sciences, USA), in 15µl reaction volumes containing 2x Power SYBR Green PCR Master Mix (Applied Biosystems, USA) and 1µM forward and reverse primers. PCR conditions were 10 m at 95°C followed by 40 cycles consisting of 10 s at 95°C, 15 s at 60°C and 20s at 72°C. ΔCt was calculated as GCK Ct – PIK3CA Ct and ΔCt>3 was defined as amplified.

6.2.6 Samples and tissue microarray construction

The population characteristics of the trastuzumab-treated cohort is summarised in Appendix A. *HER2* gene amplification status was confirmed by fluorescence *in situ* hybridisation (DAKO *HER2* FISH PharmDx, Ely, Cambridgeshire). The study was

approved by the Lothian Research Ethics Committee (08/S1101/41). Following H&E sectioning of representative tumour blocks, tumour areas were marked for TMA construction and 0.6mm^2 cores placed into 3 separate TMA replicates for each sample, as previously described (177).

6.2.7 Immunofluorescence

Immunofluorescence for PTEN was performed using methods previously described (123). Briefly, 3μm tissue microarray slides were deparaffinized and antigen-retrieved by pressure-cooking in 0.15mM sodium citrate buffer at pH6. Endogenous peroxidases were blocked with 2.5% hydrogen peroxide for 15 minutes and non-specific binding blocked with serum-free protein block for 15 minutes. Slides were then incubated with primary antibodies diluted in 0.025% PBST for 1 h at room temperature (AE1/AE3 mouse monoclonal cytokeratin antibody, rabbit polyclonal to PTEN (Cell Signaling) diluted 1:100 and 1:25 respectively. After washing in 0.025% PBST sections were incubated for 1 hour at room temperature with secondary antibodies, which included an Alexa 488–conjugated goat anti-mouse antibody diluted 1:100 in 0.1M TBS, and prediluted goat anti-rabbit antibody conjugated to a horseradish peroxidase–decorated dextran-polymer backbone (EnVision, Dako). Slides were then incubated for 10 minutes with Cy5-tyramide, which is activated by horseradish peroxidase, to visualize HER2 expression. 4′,6-Diamidino-2-phenylindole (Molecular Probes, Eugene, Ore) was used to stain the nuclear compartment.

6.2.8 AQUA automated image analysis

A detailed description of the AQUA methodology is available elsewhere, and has been described above (123). Pan-cytokeratin antibody was used to identify infiltrating tumour cells and normal epithelial cells, DAPI-counterstain to identify nuclei, and Cy-5-tyramide detection for target (PTEN) for compartmentalised (tissue and subcellular) analysis of tissue sections. Monochromatic images of each TMA

core were captured at x20 objective using an Olympus AX-51 epifluorescence microscope, and high-resolution digital images analysed by the AQUAnalysis software. Briefly, a binary epithelial mask was created from the cytokeratin image of each TMA core. If the epithelium comprised <5% of total core area, the core was excluded from analysis. Similar binary masks were created for cytoplasmic and nuclear compartments based on DAPI staining of nuclei. PTEN expression was quantified by calculating the Cy5 fluorescent signal intensity on a scale of 0-255 within each image pixel, and the AQUA score generated by dividing the sum of Cy5 signal within the epithelial mask by the area of the cytoplasmic compartment.

6.2.9 Statistical analysis methods

AQUA scores were averaged from replicate cores. In order to reduce type I error which can result from using the minimum p-value method for determining the cutpoint value for PTEN expression in Kaplan-Meier analysis (180), we utilised X-Tile, which allows determination of an optimal cutpoint while correcting for the use of minimum *P* statistics (179). Two methods of statistical correction for the use of minimal *P* approach were used, the first calculation of a Monte Carlo *P*-value and for the second, the Miller-Siegmund minimal *P* correction (180). Overall survival was subsequently assessed by Kaplan-Meier analysis with log rank for determining statistical significance. Relative risk was assessed by the univariate and multivariate Cox proportional hazards model. Comparison of PTEN expression class with the clinical and pathological variables (age, tumour and nodal stage, histological grade, ER and HER status, NPI) were made using χ^2 analysis. Comparison of differences in means *in vitro* were performed using the Student's T-test. All calculations and analyses were two-tailed where appropriate and done with SPSS 14.0 for Windows (SPSS, Inc., Chicago IL).

6.3 Results

6.3.1 Development of a mathematical model to predict responses to RTK-inhibitors

In order to systematically assess resistance factors to anti-receptor tyrosine kinase (RTK) therapy in cancer biopsies, we developed a kinetic mathematical model of MAPK/PI3K signalling and used it to predict consequences of anti-HER2 monoclonal antibody therapeutic intervention (a full kinetic mathematical model description is given in Appendix B – modeling methods and mathematical model description). We developed it to describe HER2-inhibitor antibody/receptor binding, HER2/HER3 dimerisation and inhibition, AKT/MAPK crosstalk, and the kinetic and regulatory properties of PTEN (Figure 6.1 and Appendix D - figures S1-S3, S10).

The design of our model was also based on modelling studies of the HER signalling network (105;109;227;228). The inclusion of the tumour suppressor protein PTEN was deemed particularly important since it is a key negative regulator of the PI3K signalling pathway (229), and it has been implicated as a resistance mechanism to trastuzumab in breast cancer (71;187); however, the effect of quantitative decreases in protein expression, which is more commonly seen than mutation or epigenetic regulation, is unknown. The new model, including a PTEN subsystem, explicitly describes the competition between the lipid and protein phosphatase activities of PTEN, autodephosphorylation, and the balance and interchange between the active (PTEN) and inactive (pPTEN) forms of the protein, using experimentally derived kinetic parameters (Figure 6.1 and Appendix D - Figure S10).

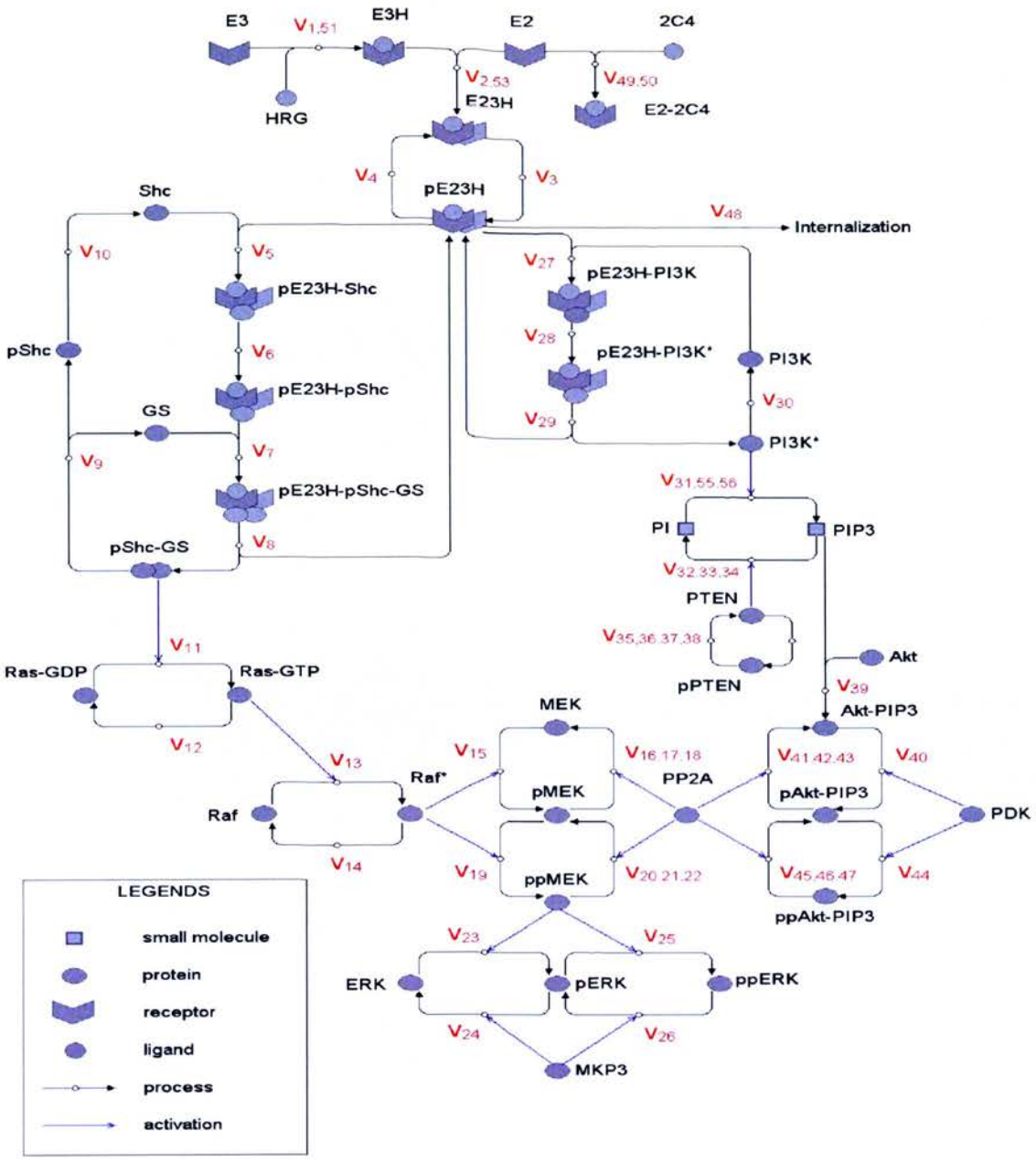

Figure 6.1: Network schema of MAPK and PI3K signalling. a, Schematic representation of mathematical model used to interrogate sensitivity and resistance factors to RTK-inhibitors. The whole kinetic model contains 56 ordinary differential equations and is described in detail in the Appendix B. Abbreviations used within the scheme are shown in Appendix C.

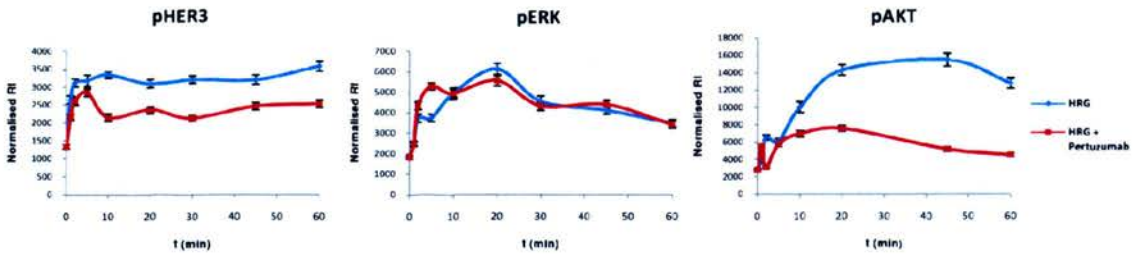

Figure 6.2: Computational model validation and predictions. Time-course plots of experimental data used to parameterise the computational model. Data were generated from reverse phase protein arrays (phosphoprotein normalised by total protein) and are representative of multiple experiments (heregulin-β (blue) and heregulin + pertuzumab (red); error bars represent 95% confidence intervals).

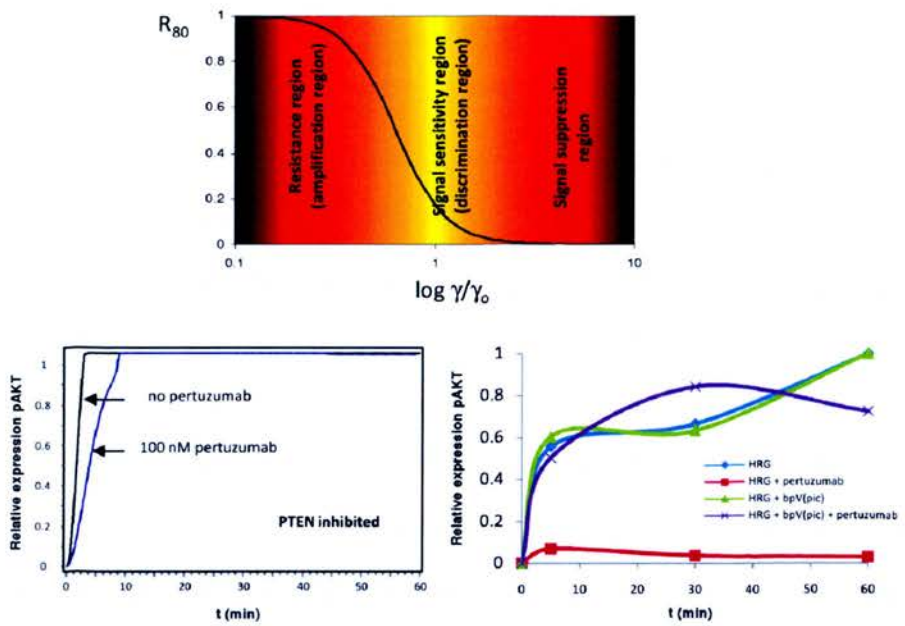

Figure 6.3: The theoretical dependence of therapeutic resistance R80 on the ratio γ of PTEN and PI3K*. (γ = PTEN/PI3K*, see Appendix B for details)**.** The index of therapeutic resistance (R) was defined as follows: R80 = pAKT80/ pAKT0, where pAKT80 - the value of pAKT signal when 80% of RTK receptors are inhibited by the drug, pAKT0 – pAKT signal in the absence of any RTK inhibitors. The value of pAKT signal was taken at 60th min after HRG stimulation. Thus R reflects the non-responsiveness (or resistance) of the pAKT signal to the inhibition of receptors by RTK inhibitors. When R80=1 the resistance is the highest, that means that 80% inhibition of RTK causes no inhibition of pAKT signal. In our model high resistance is observed on decreasing γ 3-5 times regarding to γo set in the model. The value γo=105 corresponds to our theoretical results of 80% inhibition of pAKT signal in response to 80% inhibition of RTK. Lower panels, Predicted effect of PTEN loss on pAKT kinetics (left) in the presence or absence of pertuzumab, and resulting experimental data (right),

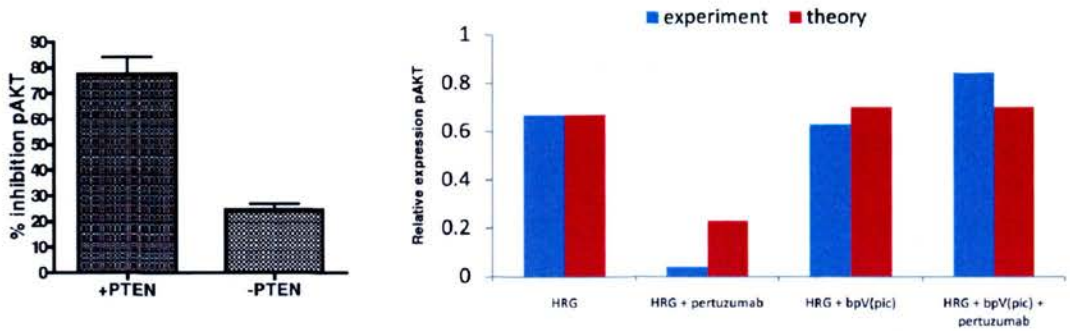

Figure 6.4: Comparison of computational predictions and unseen experiments of steady-state levels of pAKT at 30 minutes. Kinetic and steady-state profiles of pAKT by inhibition of PTEN function with bpV(pic) closely match computational simulations.

The kinetic model (Figure 6.1 and submodels shown in Appendix) was then fit to high-resolution *in vitro* dynamic phosphoprotein expression generated from reverse-phase protein arrays and normalised to total protein expression (Figure 6.2), as well as supportive western blot data Figures in Appendix D: S12, S13). Timecourse data were generated from PE04 ovarian cancer cell lines stimulated with heregulin-β in the presence or absence of the HER2 dimerisation-inhibitor pertuzumab (Figure 6.2 and Appendix D - Figure S12), in order to derive kinetic parameters, as described in Appendix B – modeling methods and description of mathematical model. Additional timecourse profiles of BT474 breast cancer cell lines were studied, but not used for parameterization of the mathematical model, in order to establish qualitative similarities between cell lines and the generality of the approach. Additional model validation was provided by heregulin dose-response experiments (Appendix D - Figure S13). The model satisfactorily reproduced the response kinetics of heterodimerisation of HER2/HER3, pERK, and pAKT activation stimulated by heregulin-β, and the inhibitory effect of pertuzumab. A dominant signalling effect through PI3K with sustained steady-state changes in PI3K signalling in response to heregulin-β after 1 hour in multiple cell lines was observed (Figure 6.2).

6.3.2 Resistance factor γ dictates sensitivity and resistance to RTK-inhibitor therapy

In order to predict which pathway components most influence therapeutic resistance to anti-HER2 therapy, we used the kinetic model to interrogate which parameters most influenced downstream pathway activation in response to endogenous ligand stimulation and inhibition with dimerisation inhibitors. Computational analysis of the model showed that HER2 receptor levels, total PTEN levels, and activation of PI3K by mutation led to dimerisation inhibitor resistance measured by sustained AKT phosphorylation after treatment with the dimerisation inhibitor pertuzumab (Appendix D - Figure S15); however, since the activation of PI3K required to induce resistance was supraphysiological (x10 required to induce resistance in simulations vs x2 activation by mutation as seen *in vitro* (230)), and patients are always selected on the basis of high HER2 expression for receptor tyrosine kinase inhibitor therapy, we focussed on PTEN as potential resistance mechanisms in order to offer a quantitative explanation for therapeutic resistance observed *in vivo* (71). PTEN exists in a signalling cycle with PI3K, such that the balance between the activities of PTEN and PI3K enzymes, PTEN:activated PI3K (integrated resistance factor γ; Figure 6.3 and Appendix B – modeling methods and description of model B.3) dictates the sensitivity of AKT activation to ligand stimulation or inhibition. High γ result in effective inhibition of AKT activation in response to pertuzumab, while low γ predict sustained AKT activation and insensitivity to pertuzumab (Figure 6.3). Thus we found that the resistance to inhibition is strongly γ dependent. At low γ the system amplifies small signals from membrane receptors and becomes insensitive to receptor inhibition. In Figure 6.3b this regimen corresponds to high values of the therapeutic resistance index $R_{80}(\gamma)$. In the range of γ_o (corresponding to the computational results in Figure 2a) signal transduction through PI3K/PTEN cycle is sensitive to inhibition by pertuzumab (pAKT signal can be inhibited by 30-70%). Further increase in γ (more than ten times higher than γ_o) leads to strong inhibition of pAKT signals due to significant weakening the signal transduction through the PTEN/PI3K cycle (see Appendix B – modeling methods and description S3). Our results are in a good agreement with ultrasensitive and signal-transducing regimes of

signalling cascades described earlier for covalent modification (231;232) and kinase-phosphatase cycles (233).

6.3.3 Computational simulations are predictive of unseen experiments of therapeutic resistance caused by resistance factor γ.

We tested the effect of changing the PTEN:PI3K ratio by stimulating with heregulin-β after pre-treating PE04 cell lines with bpV(pic), a potent and specific inhibitor of PTEN which acts by binding to the active phosphatase CX5R motif (234;235). The model was entirely predictive of these unseen *in vitro* experiments, with dynamics (compared by curve comparison and integration of kinetic profiles) and steady-state levels of pAKT activation matching computational simulations, and abrogating inhibition of pAKT with pertuzumab (Figure 6.4). Likewise, increasing the ratio of PTEN:activated PI3K with the PI3K inhibitor LY294002 resulted in dose-dependent inhibition of pAKT, but not pERK, in PE04 cells (Appendix D - Figure S14). This is also in agreement with our theoretical results (see Appendix B – modeling methods and description B.3). Therefore, the model suggests that resistance to RTK inhibitors is dependent on the quantitative balance of both the protein expression of PTEN (which is common in breast cancer (85)) and PI3K activating mutations, which are commonly amplified and mutated in many breast and ovarian cancers (236;237).

6.3.4 The resistance factor γ dictates resistance to pertuzumab in cellular models *in vitro*.

Further validation of the capacity of measurement of PTEN:activated PI3K ratio to predict therapeutic response was sought from cellular models of therapeutic sensitivity and resistance. We measured total PTEN, PI3K mutation status of the four most common mutations in the *PIK3CA* gene (H1047L and H1047R in exon 20, E545K and E542K in exon 9, representing ~90% of *PIK3CA* mutations) and PI3K amplification status in a panel of 13 ovarian carcinoma cell lines to investigate the association of PTEN:activated PI3K with response to pertuzumab (Figure 6.5a). Total PTEN protein expression levels were strongly negatively correlated with both

pAKT and percentage growth inhibition with pertuzumab (Pearson's correlation coefficient 0.68 and 0.74 respectively; Figure 6.5b).

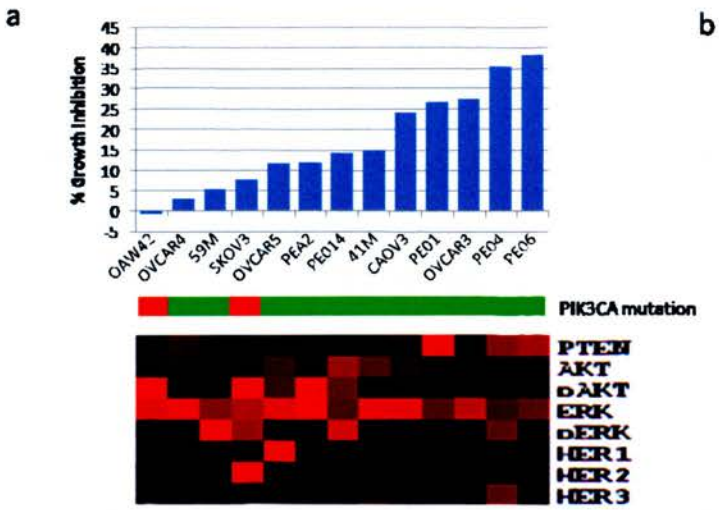

b

	pAKT	Growth inhibition
PTEN	-0.68	0.74
PTEN:PI3K	-0.74	0.76
AKT	-0.29	-0.05
pAKT	1	-0.55
ERK	0.24	-0.54
pERK	0.19	-0.14
HER1	0.04	-0.37
HER2	-0.20	-0.20
HER3	-0.22	0.43

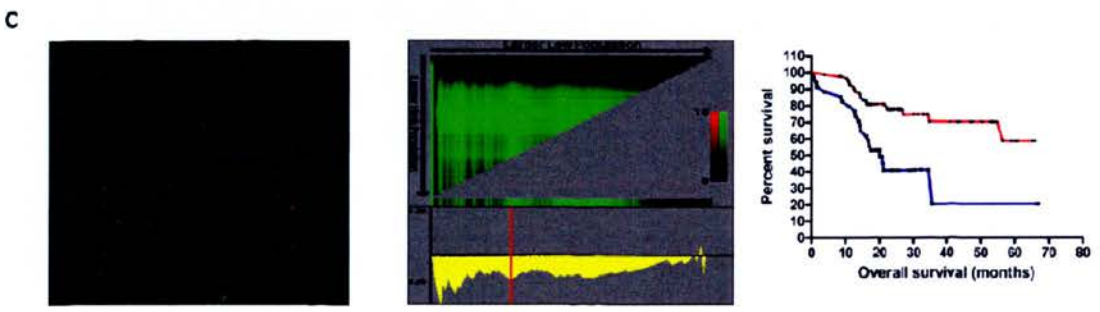

Figure 6.5: Quantitative PTEN protein expression is associated with pertuzumab sensitivity in vitro and trastuzumab resistance in vivo. a and b The relative sensitivity of 13 ovarian carcinoma cell lines to the HER2 dimerisation inhibitor pertuzumab was determined by growth assay (SRB), and expression of PTEN and other MAPK and PI3K pathway components assessed by semi-quantitative western blotting. Sensitivity to pertuzumab is closely correlated with PTEN expression but not with other pathway members. **c, (left panel)** AQUA fluorescent analysis of PTEN expression in a tissue microarray core, showing cytoplasmic localisation of PTEN (red) and masking of tumour areas for quantitation by cytokeratin (green). **(middle panel),** Calculation of optimal cutpoint for PTEN expression. X-tile calculates all possible combinations of results for different cutpoints (upper panel) and corresponding relative risks (lower panel). Cutpoint is selected on the best corrected and Monte-Carlo p-value. **(right panel),** Kaplan-Meier survival curves for patients treated with trastuzumab for low (blue) and high (red) protein expression of PTEN. Overall survival is calculated from time of initial diagnosis to date of death.

Two of the cell lines, SKOV3 and OAW42, showed activating mutations in PI3K but none of the cell lines harboured *PIK3CA* amplifications. Activation by mutation was assumed to increase the activity of PI3K twofold (230), and calculation of PTEN:activated PI3K resulted in small increases in correlation coefficients with pAKT and growth to 0.73 and 0.76 respectively, suggesting that PTEN expression is the dominant factor in sensitivity to HER2 dimerisation inhibition, consistent with recent reports (238), and the relatively weak effect of x2 activity of PI3K on resistance seen in simulations. However, measurement of HER1-3, pAKT, or pERK, were not highly correlated with sensitivity to pertuzumab (Figure 6.5b).

6.3.5 The quantitative expression of PTEN is associated to trastuzumab resistance in the clinic.

Since both computational and cellular modelling strongly suggest that quantitative PTEN protein expression most influences ultimate cellular response to HER2 inhibition, we quantified expression of PTEN in 122 trastuzumab-treated primary breast tumours using the AQUA quantitative image analysis system (Figure 6.5c and Appendix A) on primary breast tumours arrayed on tissue microarrays. Increasing PTEN expression was proportional to decreased relative risk of death when treated with trastuzumab (Figure 6.5c, middle panel), mirroring the effect on the therapeutic resistance index $R_{80}(\gamma)$ by changes in γ. A rigorously defined cutpoint for PTEN expression (see materials and methods) resulted in a mean reduction in overall survival of 21.6 months in $PTEN^{low}$ vs $PTEN^{high}$ patients (Figure 6.5c; uncorrected p=0.0003, Miller-Seigmund p=0.0099, Monte Carlo p=0.01), equivalent to a 3.0 times increase in relative risk of dying from breast cancer after treatment with trastuzumab in $PTEN^{low}$ cases (RR = 3.0; 95% CI 1.6-5.5, p<0.0001). In univariate analysis, tumour size, ER status, chemotherapy regimen, and PTEN expression levels were all associated with significant survival differences (log-rank test, p<0.05, Appendix A), but PTEN remained the only significant predictor of survival in multivariate analysis (Cox logistic regression, p=0.01) and corresponds well to the parameter γ when PI3K expression level assumed to be constant. HER2 expression

and *PIK3CA* mutation status (mutations found in 26/119 (21.8%) available samples) were not predictive of survival.

6.4 Discussion

Our data has shown the successful application of kinetic modelling of the PI3K and MAPK signalling pathways in the selection of resistance factors to RTK-inhibitors. We have shown that PTEN is the dominant resistance factor to RTK-inhibition. As far as we are aware, this is not only the largest series of breast cancers treated with trastuzumab to be analysed for PTEN to date, but the first to demonstrate strong association of the level of PTEN expression with overall survival rather than simply time to progression (71). Our data strongly suggest that PI3K inhibition in PTEN-low tumours should be combined with RTK-inhibitors, as recently shown for lapatinib *in vitro* (239). Similar to quantitative ER positivity in breast cancer (240), our data show that approximately a quarter of HER2+ patients may be spared ineffective, and potentially toxic, treatment if stratified by PTEN expression.

The phosphoinositol 3-kinase (PI3K) pathway mediates key hallmarks of cancer such as growth, proliferation, survival, motility and angiogenesis (186). PI3K phosphorylates the lipid second messenger PI, which recruits AKT and PDK1 to the cell membrane. PTEN is a key negative regulator of the PI3K signalling pathway (229). PTEN mutations are responsible for the hereditary diseases Cowden disease, and partial loss-of-function mutations or loss of heterozygosity (LOH) are common in the majority of cancers, and loss of expression by techniques such as immunohistochemistry or Western blotting is frequently seen. Although recent reports have suggested that *PIK3CA* mutations are important on a PTEN mutant background (241), and PTEN expression may cooperate with *PIK3CA* mutations in breast cancer and mediating trastuzumab resistance (71;238), our data show that PTEN exerts dominant control in downstream pathway activation and resistance to RTK-inhibitors. *PIK3CA* mutations exert a relatively small influence on PTEN:PI3K signalling cycle and resistance, and would have to have a five-tenfold increase in enzymatic activity to mediate resistance, which explains the lack of effect of *PIK3CA*

mutation on trastuzumab resistance seen herein. Previous reports implicating *PIK3CA* mutations in HER2-inhibitor resistance have only been *in vitro* or are very small cohorts of patients (71;187). Other RTK inhibitors such as pertuzumab have also been shown to inhibit PI3K pathway activation (242;243) suggesting that constitutive activation of this pathway through PTEN downregulation may also contribute to pertuzumab resistance *in vitro* and *in vivo*. Given the quantitative nature of these phenomena, a mathematical description and systems analysis of the PI3K pathway has been useful for understanding therapeutic responses, and allow better selection of patients expected to respond to receptor tyrosine kinase inhibitors.

In this chapter, we have successfully demonstrated how a systems biology approach can generate hypotheses that can be tested experimentally in preclinical models and which can then be applied to clinical evaluation. Predictions from this model are consistent with known findings, have been extended within this study, and add weight to the use of PTEN as a biomarker for stratifying patients for HER2-inhibitor or combinatorial therapy, particularly an RTK-inhibitor and PI3K-inhibitor in cancers with low γ. This model provides a foundation for further development and inclusion of more variables that may impact on RTK inhibitor response. Network topology, kinetics, and quantities of molecules dictate cellular, and ultimately clinical outcome. Systems biology approaches, in particular deterministic kinetic models based on experimental data, offer a new approach for integrating molecular pathology and computational modelling in order to more rationally interrogate cancer pathways and predict responses to therapy.

Chapter 7: Conclusions and future directions.

7.1 Conclusions and future directions.

In the preceding chapters we have discussed some of the challenges facing translational scientists in the discovery, testing, and validation of tissue biomarkers in order to predict therapeutic responses in cancer patients. Over the past few years these challenges have been addressed largely by academic oncologists, often in breast cancer research which has, above all other solid cancer research, been driven by effective campaigning, funding, public awareness, and patient advocacy. However, the reality has been that the selection of patients for the right therapy at the right time has fallen short of expectations, as demonstrated by only small gains in survival and the slow adoption of new tests into the clinic. Many other cancers, such as ovarian and pancreatic cancer, still have a dismal prognosis. Too many patients still receive unnecessary, and toxic, therapies.

We propose that systems biology approaches may be a fruitful avenue for preclinical testing of biomarkers, which may complement existing experimental approaches. In doing so, we have highlighted how accurate quantification of proteins in tissues is required to populate mathematical models; a by product of this has been that we have developed new, systematic approaches to interrogating pathways and visualising molecular pathology data (ovarian cancer classification), and have used dynamic timecourse experiments to try and understand how static measurements in pathology relate to dynamic cellular processes (Sprouty 2 in breast cancer). We have used new image analysis technologies to advance more traditional biomarker approaches (Ariol for ER and PR immunohistochemistry quantification in existing clinical trials), and also to investigate novel approaches to biomarker testing and discovery (AQUA for ovarian cancer classification and quantitative PTEN expression). We have started to explore new technologies such as RPPA for high throughput, high accuracy quantification. While molecular pathology sits at the heart of these endeavours they are, by their very nature, multidisciplinary, and require the concerted efforts of teams of professionals beyond those usually associated with biomedical research. In addition to hopefully advancing translational science, the type of multidisciplinary

work described herein can also be a hugely intellectually rewarding, and satisfying experience.

The work described leaves numerous avenues for future research and development. There is no shortage of targeted therapies for which a systems biology approach may usefully be applied and models developed. We have already proposed that Sprouty should be integrated into our existing model so that our findings can be tested *in silico*. This would also be a first step in including gene expression events in kinetic models, such that signalling processes are not restricted to phosphorylation events alone. Another immediate advance would be the addition of mTOR signalling to our PI3K model already developed, since these agents (such as Everolimus, RAD001) are already entering Phase III trials but show uncertain, and sometimes disappointing clinical responses. However, this remains a reactive approach and the real test of systems biology will only come when a new marker or agent not already in late development is tested *prospectively* by experimentation or in early phase clinical trials. It is likely that systems biology will not be the only evidence but complement biochemical, *in vitro* and *in vivo* data to determine whether a particular therapy, combination of therapies, or marker warrants further work or investment.

From a clinicopathological standpoint, the further evidence that PTEN predicts response to trastuzumab, over and beyond HER2 expression, is compelling evidence that a clinical test for PTEN should be developed for the clinic. Further validation of the AQUA cutpoint determined in our study needs testing in an independent cohort of patients, and in the context of an appropriately powered prospective clinical trial. In order to develop a suitably robust test which would show sufficiently low inter-laboratory variation, standards need to be developed which can be measured along with the clinical samples in order to control and normalise fluorescence intensities. These standards might take the form of known cell line standards, or recombinant proteins. The HERA translational study (investigating adjuvant trastuzumab in early breast cancer) may provide an opportunity for PTEN validation. Since some patients still derive benefit from trastuzumab even with low PTEN expression, it is unlikely that treatment would be withheld in these patients. They might, however, be

excellent candidates for combined therapy with a PI3K inhibitor, and further preclinical and clinical testing of this hypothesis should be pursued.

The exploratory study on ovarian pathway classification has resulted in a number of new hypotheses to test for combinatorial therapy and response prediction, and the approach can be applied to any cancer. The findings of the study require validation in an independent cohort of ovarian tumours, and this experiment is currently underway. However, we advocate a more systematic approach to pathway profiling than that described herein, which was candidate-driven, rather than based on primary experimental data. Instead of selecting pathways and markers from the literature, in a follow-on experiment designed to pathway profile breast cancers, we have used phospho-protein antibody arrays (Eurogentec, Hampshire, UK) to profile 250 phospho-epitope targets spanning thirteen pathways in a panel of breast cancer cell lines. Unsupervised analysis of these data has resulted in regrouping of the cell lines into three clusters with distinct pathway phospho-activation profiles, which are similar to, but distinct from, existing molecular classification (luminal, basal, HER2) (Figure 7.1).

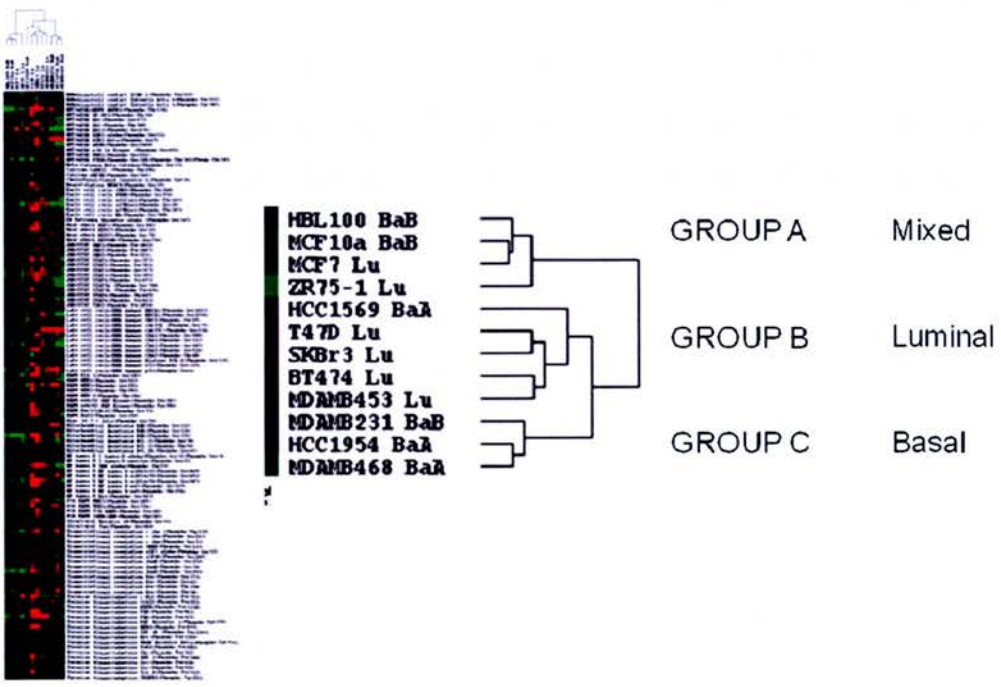

Figure 7.1. Phospho-protein profiling of breast cancer cell lines by phospho-antibody arrays.

These profiles are being validated in a large cohort of breast cancers (n=500) by AQUA and RPPA analysis, and therapeutic targets tested *in vitro* in the same cell lines. A similar set of data is also being generated in ovarian cancer cell lines, in order to establish *in vitro* models in which combinatorial regimens may be tested.

Finally, systems biology is a nascent field which has been hyped as *the* solution to a panacea of ills, from inefficient drug design to famine, but has (quite rightly) yet to gain wide acceptance within clinical medicine. The hype has not been matched with success, partly due to unrealistic expectations. In order for the field to continue and become more clinically relevant, all stakeholders (for instance pathologists, oncologists, pharmaceutical companies, biologists, and funding agencies) require education in systems biology, multidisciplinary approaches, and the opportunities and limitations that systems biology has to offer. Together with real clinical success stories, systems biology may yet realise its promise.

References.

(1) Jordan VC, Brodie AM. Development and evolution of therapies targeted to the estrogen receptor for the treatment and prevention of breast cancer. Steroids 2007;72:7-25.

(2) Slamon DJ, Clark GM, Wong SG, et al. Human breast cancer: correlation of relapse and survival with amplification of the HER-2/neu oncogene. Science 1987;235:177-82.

(3) Bartlett JMS. Biological predictors of tumour response: Natural selection or intelligent design? Advances in Breast Cancer , 1-5. 2005.

(4) Clarke M, Collins R, Darby S, et al. Effects of radiotherapy and of differences in the extent of surgery for early breast cancer on local recurrence and 15-year survival: an overview of the randomised trials. Lancet 2005;366:2087-106.

(5) Perou CM, Sorlie T, Eisen MB, et al. Molecular portraits of human breast tumours. Nature 2000;406:747-52.

(6) Bartlett JMS. Translational reserach and the development of novel biomakers in breast cancer. Advances in Breast Cancer 3, 76-85. 2006.

(7) Tovey SM, Dunne B, Witton CJ, et al. Can Molecular Markers Predict When to Implement Treatment with Aromatase Inhibitors in Invasive Breast Cancer? Clin Cancer Res 2005;11:4835-42.

(8) Johnston SRD, Head J, Pancholi S, et al. Integration of Signal Transduction Inhibitors with Endocrine Therapy: An Approach to Overcoming Hormone Resistance in Breast Cancer. Clin Cancer Res 2003;9:524S-532.

(9) Witton CJ, Reeves JR, Going JJ, Cooke TG, Bartlett JMS. Expression of the HERI-4 family of receptor tyrosine kinases in breast cancer. Journal of Pathology 2003;200:290-7.

(10) Kirkegaard T, McGlynn LM, Campbell FM, et al. Amplified in breast cancer 1 in human epidermal growth factor receptor-positive tumors of tamoxifen-treated breast cancer patients. Clin Cancer Res 2007;13:1405-11.

(11) Kirkegaard T, Witton CJ, McGlynn LM, et al. AKT activation predicts outcome in breast cancer patients treated with tamoxifen. Journal of Pathology 207, 139-146. 2005.

(12) Cannings E, Kirkegaard T, Tovey SM, et al. Bad expression predicts outcome in patients treated with tamoxifen. Breast Cancer Res Treat 2007;102:173-9.

(13) Bergqvist J, Elmberger G, Ohd J, et al. Activated ERK1/2 and phosphorylated oestrogen receptor alpha are associated with improved breast cancer survival in women treated with tamoxifen. European Journal of Cancer 2006;42:1104-12.

(14) Gutierrez MC, Detre S, Johnston S, et al. Molecular changes in tamoxifen-resistant breast cancer: Relationship between estrogen receptor, HER-2, and p38 mitogen- activated protein kinase. Journal of Clinical Oncology 2005;23:2469-76.

(15) Tewey KM, Rowe TC, Yang L, Halligan BD, Liu LF. Adriamycin-induced DNA damage mediated by mammalian DNA topoisomerase II. Science 1984;226:466-8.

(16) Di Leo A, Chan S, Paesmans M, et al. HER-2/neu as a predictive marker in a population of advanced breast cancer patients randomly treated either with single-agent doxorubicin or single-agent docetaxel. Breast Cancer Res Treat 2004;86:197-206.

(17) Di Leo A, Larsimont D, Gancberg D, et al. HER-2 and topo-isomerase II alpha as predictive markers in a population of node-positive breast cancer patients randomly treated with adjuvant CMF or epirubicin plus cyclophosphamide. Annals of Oncology 2001;12:1081-9.

(18) Jarvinen TAH, Tanner M, Rantanen V, et al. Amplification and deletion of topoisomerase II alpha associate with ErbB-2 amplification and affect sensitivity to topoisomerase II inhibitor doxorubicin in breast cancer. Am J Pathol 2000;156:839-47.

(19) Jarvinen TAH, Kononen J, Peltohuikko M, Isola J. Expression of topoisomerase II alpha is associated with rapid cell proliferation, aneuploidy, and c-erbB2 overexpression in breast cancer. Am J Pathol 1996;148:2073-82.

(20) Knoop AS, Knudsen H, Balslev E, et al. Retrospective analysis of topoismerase IIa amplifications and deletions as predictive markers in primary breast cancer patients randomly assigned to cyclophosphamide, methotrexate, and fluorouracil or cyclophosphamide, epirubicin and fluorouracil: Danish breast cancer cooperative group. Journal of Clinical Oncology 23, 7483-7490. 2005.

(21) Pritchard KI, Shepherd LE, O'Malley FP, et al. HER2 and responsiveness of breast cancer to adjuvant chemotherapy. New Engl J Med 2006;354:2103-11.

(22) Tanner M, Jarvinen P, Isola J. Amplification of HER-2/neu and topoisomerase IIalpha in primary and metastatic breast cancer. Cancer Res 2001;61:5345-8.

(23) Paik S, Bryant J, Tan-Chiu E, et al. HER2 and Choice of Adjuvant Chemotherapy for Invasive Breast Cancer: National Surgical Adjuvant Breast and Bowel Project Protocol B-15. J Natl Cancer Inst 2000;92:1991-8.

(24) Di Leo A, Gancberg D, Larsimont D, et al. HER-2 Amplification and Topoisomerase II{alpha} Gene Aberrations as Predictive Markers in Node-positive Breast Cancer Patients Randomly Treated Either with an Anthracycline-based Therapy or with Cyclophosphamide, Methotrexate, and 5-Fluorouracil. Clin Cancer Res 2002;8:1107-16.

(25) Moliterni A, Menard S, Valagussa P, et al. HER2 Overexpression and Doxorubicin in Adjuvant Chemotherapy for Resectable Breast Cancer. Journal of Clinical Oncology 2003;21:458-62.

(26) Poole CJ, Earl HM, Hiller L, et al. Epirubicin and cyclophosphamide, methotrexate, and fluorouracil as adjuvant therapy for early breast cancer. New Engl J Med 2006;355:1851-62.

(27) Fukuoka M, Yano S, Giaccone G, et al. Multi-institutional randomized phase II trial of gefitinib for previously treated patients with advanced non-small-cell lung cancer (The IDEAL 1 Trial) [corrected]. J Clin Oncol 2003;21:2237-46.

(28) Kris MG, Natale RB, Herbst RS, et al. Efficacy of gefitinib, an inhibitor of the epidermal growth factor receptor tyrosine kinase, in symptomatic patients with non-small cell lung cancer: a randomized trial. JAMA 2003;290:2149-58.

(29) Lynch TJ, Bell DW, Sordella R, et al. Activating mutations in the epidermal growth factor receptor underlying responsiveness of non-small-cell lung cancer to gefitinib. N Engl J Med 2004;%20;350:2129-39.

(30) Pao W, Miller V, Zakowski M, et al. EGF receptor gene mutations are common in lung cancers from "never smokers" and are associated with sensitivity of tumors to gefitinib and erlotinib. Proc Natl Acad Sci U S A 2004;101:13306-11.

(31) Cappuzzo F, Gregorc V, Rossi E, et al. Gefitinib in pretreated non-small-cell lung cancer (NSCLC): analysis of efficacy and correlation with HER2 and epidermal growth factor receptor expression in locally advanced or metastatic NSCLC. J Clin Oncol 2003;21:2658-63.

(32) Parra HS, Cavina R, Latteri F, et al. Analysis of epidermal growth factor receptor expression as a predictive factor for response to gefitinib ('Iressa', ZD1839) in non-small-cell lung cancer. Br J Cancer 2004;%19;91:208-12.

(33) Bartlett J, Mallon E, Cooke T. The clinical evaluation of HER-2 status: which test to use? Journal of Pathology 2003;199:411-7.

(34) Hirsch FR, Varella-Garcia M, McCoy J, et al. Increased epidermal growth factor receptor gene copy number detected by fluorescence in situ hybridization associates with increased sensitivity to gefitinib in patients with bronchioloalveolar carcinoma subtypes: a Southwest Oncology Group Study. J Clin Oncol 2005;23:6838-45.

(35) Rampaul RS, Pinder SE, Nicholson RI, et al. Clinical value of epidermal growth factor receptor expression in primary breast cancer. Adv Anat Pathol 2005;12:271-3.

(36) Klijn JG, Berns PM, Schmitz PI, Foekens JA. The clinical significance of epidermal growth factor receptor (EGF-R) in human breast cancer: a review on 5232 patients. Endocr Rev 1992;13:3-17.

(37) Fox SB, Smith K, Hollyer J, et al. The epidermal growth factor receptor as a prognostic marker: results of 370 patients and review of 3009 patients. Breast Cancer Res Treat 1994;29:41-9.

(38) Tovey SM, Witton CJ, Bartlett JMS, et al. Outcome and human epidermal growth factor receptor (HER) 1-4 status in invasive breast carcinomas with proliferation indices evaluated by bromodeoxyuridine labelling. Breast Cancer Res 2004;6:R246-R251.

(39) Rampaul RS, Pinder SE, Wencyk PM, et al. Epidermal growth factor receptor status in operable invasive breast cancer: is it of any prognostic value? Clin Cancer Res 2004;10:2578.

(40) Nielsen TO, Hsu FD, Jensen K, et al. Immunohistochemical and clinical characterization of the basal-like subtype of invasive breast carcinoma. Clin Cancer Res 2004;10:5367-74.

(41) Turner NC, Reis-Filho JS. Basal-like breast cancer and the BRCA1 phenotype. Oncogene 2006;25:5846-53.

(42) Reis-Filho JS, Pinheiro C, Lambros MB, et al. EGFR amplification and lack of activating mutations in metaplastic breast carcinomas. J Pathol 2006;209:445-53.

(43) Kersting C, Kuijper A, Schmidt H, et al. Amplifications of the epidermal growth factor receptor gene (egfr) are common in phyllodes tumors of the breast and are associated with tumor progression. Lab Invest 2006;86:54-61.

(44) Lambros MB, Natrajan R, Reis-Filho JS. Chromogenic and fluorescent in situ hybridization in breast cancer. Hum Pathol 2007;38:1105-22.

(45) Chan SK, Hill ME, Gullick WJ. The role of the epidermal growth factor receptor in breast cancer. J Mammary Gland Biol Neoplasia 2006;11:3-11.

(46) Smith IE, Walsh G, Skene A, et al. Neoadjuvant Anastrozole Alone or With Gefitinib in Early Breast Cancer: A Phase II Placebo-Controlled Trial (Study 223) With Biological and Clinical Outcomes. J Clin Oncol 2007;.

(47) Witton CJ, Reeves JR, Going JG, Cooke TG, Bartlett JMS. Coexpression of EGFr, HER2, HER3 and HER4 in primary human breast carcinoma. Breast Cancer Res Treat 2001;69:32.

(48) Burris HA, III, Hurwitz HI, Dees EC, et al. Phase I safety, pharmacokinetics, and clinical activity study of lapatinib (GW572016), a reversible dual inhibitor of epidermal growth factor receptor tyrosine kinases, in heavily pretreated patients with metastatic carcinomas. J Clin Oncol 2005;23:5305-13.

(49) Carter TA, Wodicka LM, Shah NP, et al. Inhibition of drug-resistant mutants of ABL, KIT, and EGF receptor kinases. Proc Natl Acad Sci U S A 2005;102:11011-6.

(50) Fujita T, Doihara H, Kawasaki K, et al. PTEN activity could be a predictive marker of trastuzumab efficacy in the treatment of ErbB2-overexpressing breast cancer. Br J Cancer 2006;94:247-52.

(51) Nagata Y, Lan KH, Zhou X, et al. PTEN activation contributes to tumor inhibition by trastuzumab, and loss of PTEN predicts trastuzumab resistance in patients. Cancer Cell 2004;6:117-27.

(52) Li J, Yen C, Liaw D, et al. PTEN, a putative protein tyrosine phosphatase gene mutated in human brain, breast, and prostate cancer. Science 1997;275:1943-7.

(53) Yakes FM, Chinratanalab W, Ritter CA, et al. Herceptin-induced inhibition of phosphatidylinositol-3 kinase and Akt Is required for antibody-mediated effects on p27, cyclin D1, and antitumor action. Cancer Res 2002;62:4132-41.

(54) Hollestelle A, Elstrodt F, Nagel JH, Kallemeijn WW, Schutte M. Phosphatidylinositol-3-OH kinase or RAS pathway mutations in human breast cancer cell lines. Mol Cancer Res 2007;5:195-201.

(55) Mita MM, Mita A, Rowinsky EK. Mammalian target of rapamycin: a new molecular target for breast cancer. Clin Breast Cancer 2003;4:126-37.

(56) Vignot S, Faivre S, Aguirre D, Raymond E. mTOR-targeted therapy of cancer with rapamycin derivatives. Ann Oncol 2005;16:525-37.

(57) Wullschleger S, Loewith R, Hall MN. TOR signaling in growth and metabolism. Cell 2006;124:471-84.

(58) Sarbassov DD, Guertin DA, Ali SM, Sabatini DM. Phosphorylation and regulation of Akt/PKB by the rictor-mTOR complex. Science 2005;307:1098-101.

(59) Hay N. The Akt-mTOR tango and its relevance to cancer. Cancer Cell 2005;8:179-83.

(60) Chan S. Targeting the mammalian target of rapamycin (mTOR): a new approach to treating cancer. Br J Cancer 2004;91:1420-4.

(61) Johnston SRD, Head J, Pancholi S, et al. Integration of Signal Transduction Inhibitors with Endocrine Therapy: An Approach to Overcoming Hormone Resistance in Breast Cancer. Clin Cancer Res 2003;9:524S-532.

(62) Ellis MJ, Coop A, Singh B, et al. Letrozole is more effective neoadjuvant endocrine therapy than tamoxifen for ErbB-1- and/or ErbB-2-positive, estrogen receptor-positive primary breast cancer: evidence from a phase III randomized trial. Journal of Clinical Oncology 2001;19:3808-16.

(63) Mauriac L, Keshaviah A, Debled M, et al. Predictors of early relapse in postmenopausal women with hormone receptor-positive breast cancer in the BIG 1-98 trial. Annals of Oncology 2007;18:859-67.

(64) Piccart-Gebhart MJ. Anthracyclines and the tailoring of treatment for early breast cancer. New Engl J Med 2006;354:2177-9.

(65) Slamon D, Eiermann W, Robert N, et al. Phase III randomized trial comparing doxorubicin and cyclophosphamide followed by docetaxel (AC (R) T) with doxorubicin and cyclophosphamide followed by docetaxel and trastuzumab (AC (R) TH) with docetaxel, carboplatin and trastuzumab (TCH) in HER2 positive early breast cancer patients: BCIRG 006 study. Breast Cancer Res Treat 2005;94:S5.

(66) Henney A, Superti-Furga G. A network solution. Nature 2008;455:730-1.

(67) Belardinelli L, Shryock JC, Fraser H. Inhibition of the late sodium current as a potential cardioprotective principle: effects of the late sodium current inhibitor ranolazine. Heart 2006;92 Suppl 4:iv6-iv14.:iv6-iv14.

(68) Noble D. Systems biology and the heart. Biosystems 2006;83:75-80.

(69) Noble D, Noble PJ. Late sodium current in the pathophysiology of cardiovascular disease: consequences of sodium-calcium overload. Heart 2006;92 Suppl 4:iv1-iv5.:iv1-iv5.

(70) Cho CR, Labow M, Reinhardt M, van Oostrum J, Peitsch MC. The application of systems biology to drug discovery. Curr Opin Chem Biol 2006;10:294-302.

(71) Berns K, Horlings HM, Hennessy BT, et al. A functional genetic approach identifies the PI3K pathway as a major determinant of trastuzumab resistance in breast cancer. Cancer Cell 2007;12:395-402.

(72) Valabrega G, Montemurro F, Aglietta M. Trastuzumab: mechanism of action, resistance and future perspectives in HER2-overexpressing breast cancer. Ann Oncol 2007;18:977-84.

(73) Hanahan D, Weinberg RA. The hallmarks of cancer. Cell 2000;100:57-70.

(74) Sobin LH, Wittekind CH. UICC: TNM classification of malignant tumors. 6th ed. New York: Wiley-Liss; 2002.

(75) Elston CW, Ellis IO. Pathological prognostic factors in breast cancer. I. The value of histological grade in breast cancer: experience from a large study with long-term follow-up. Histopathology 1991;19:403-10.

(76) Reis-Filho JS, Milanezi F, Steele D, et al. Metaplastic breast carcinomas are basal-like tumours. Histopathology 2006;49:10-21.

(77) Reis-Filho JS, Tutt AN. Triple negative tumours: a critical review. Histopathology 2008;52:108-18.

(78) Gusterson B. Do 'basal-like' breast cancers really exist? Nat Rev Can 2009.

(79) Perou CM, Sorlie T, Eisen MB, et al. Molecular portraits of human breast tumours. Nature 2000;406:747-52.

(80) Tan DS, Reis-Filho JS. Comparative genomic hybridisation arrays: high-throughput tools to determine targeted therapy in breast cancer. Pathobiology 2008;75:63-74.

(81) Turner NC, Reis-Filho JS. Basal-like breast cancer and the BRCA1 phenotype. Oncogene 2006;25:5846-53.

(82) Carey LA, Dees EC, Sawyer L, et al. The triple negative paradox: primary tumor chemosensitivity of breast cancer subtypes. Clin Cancer Res 2007;13:2329-34.

(83) Rouzier R, Perou CM, Symmans WF, et al. Breast cancer molecular subtypes respond differently to preoperative chemotherapy. Clin Cancer Res 2005;11:5678-85.

(84) Faratian D, Bartlett J. Predictive markers in breast cancer--the future. Histopathology 2008;52:91-8.

(85) Wood LD, Parsons DW, Jones S, et al. The genomic landscapes of human breast and colorectal cancers. Science 2007;318:1108-13.

(86) Bild AH, Yao G, Chang JT, et al. Oncogenic pathway signatures in human cancers as a guide to targeted therapies. Nature 2006;%19;439:353-7.

(87) Effects of chemotherapy and hormonal therapy for early breast cancer on recurrence and 15-year survival: an overview of the randomised trials. Lancet 2005;365:1687-717.

(88) Smith I, Procter M, Gelber RD, et al. 2-year follow-up of trastuzumab after adjuvant chemotherapy in HER2-positive breast cancer: a randomised controlled trial. Lancet 2007;369:29-36.

(89) Faratian D, Moodie SL, Harrison DJ, Goryanin I. Dynamic computational modeling in the search for better breast cancer drug therapy. Pharmacogenomics 2007;8:1757-61.

(90) O'Reilly KE, Rojo F, She QB, et al. mTOR inhibition induces upstream receptor tyrosine kinase signaling and activates Akt. Cancer Res 2006;66:1500-8.

(91) Kola I, Landis J. Can the pharmaceutical industry reduce attrition rates? Nat Rev Drug Discov 2004;3:711-5.

(92) Faratian D, Moodie SL, Harrison DJ, Goryanin I. Dynamic computational modeling in the search for better breast cancer drug therapy. Pharmacogenomics 2007;8:1757-61.

(93) Fearon ER, Vogelstein B. A genetic model for colorectal tumorigenesis. Cell 1990;61:759-67.

(94) Sherr CJ. Cancer cell cycles. Science 1996;274:1672-7.

(95) Kholodenko BN. Cell-signalling dynamics in time and space. Nat Rev Mol Cell Biol 2006;7:165-76.

(96) Kholodenko BN, Kolch W. Giving space to cell signaling. Cell 2008;133:566-7.

(97) Cohen AA, Geva-Zatorsky N, Eden E, et al. Dynamic proteomics of individual cancer cells in response to a drug. Science 2008;322:1511-6.

(98) Carlson JM, Doyle J. Highly optimized tolerance: robustness and design in complex systems. Phys Rev Lett 2000;84:2529-32.

(99) Kitano H. Biological robustness. Nat Rev Genet 2004;5:826-37.

(100) Hucka M, Finney A, Sauro HM, et al. The systems biology markup language (SBML): a medium for representation and exchange of biochemical network models. Bioinformatics 2003;19:524-31.

(101) Sauro HM, Bergmann FT. Standards and ontologies in computational systems biology. Essays Biochem 2008;45:211-22.:211-22.

(102) Fuss H, Dubitzky W, Downes CS, Kurth MJ. Mathematical models of cell cycle regulation. Brief Bioinform 2005;6:163-77.

(103) Hatakeyama M, Kimura S, Naka T, et al. A computational model on the modulation of mitogen-activated protein kinase (MAPK) and Akt pathways in heregulin-induced ErbB signalling. Biochem J 2003;373:451-63.

(104) Hendriks BS, Cook J, Burke JM, et al. Computational modelling of ErbB family phosphorylation dynamics in response to transforming growth factor alpha and heregulin indicates spatial compartmentation of phosphatase activity. Syst Biol (Stevenage) 2006;153:22-33.

(105) Kholodenko BN, Demin OV, Moehren G, Hoek JB. Quantification of short term signaling by the epidermal growth factor receptor. J Biol Chem 1999;274:30169-81.

(106) Markevich NI, Hoek JB, Kholodenko BN. Signaling switches and bistability arising from multisite phosphorylation in protein kinase cascades. J Cell Biol 2004;164:353-9.

(107) Shankaran H, Wiley HS, Resat H. Modeling the effects of HER/ErbB1-3 coexpression on receptor dimerization and biological response. Biophys J 2006;90:3993-4009.

(108) Steuer R. Computational approaches to the topology, stability and dynamics of metabolic networks. Phytochemistry 2007;68:2139-51.

(109) Schoeberl B, Eichler-Jonsson C, Gilles ED, Muller G. Computational modeling of the dynamics of the MAP kinase cascade activated by surface and internalized EGF receptors. Nat Biotechnol 2002;20:370-5.

(110) Janes KA, Albeck JG, Gaudet S, et al. A systems model of signaling identifies a molecular basis set for cytokine-induced apoptosis. Science 2005;310:1646-53.

(111) Demin O, Goryanin I. Kinetic modelling in systems biology. 2008. Chapman and Hall / CRC.

(112) Barabasi AL, Oltvai ZN. Network biology: understanding the cell's functional organization. Nat Rev Genet 2004;5:101-13.

(113) Clyde RG, Bown JL, Hupp TR, Zhelev N, Crawford JW. The role of modelling in identifying drug targets for diseases of the cell cycle. J R Soc Interface 2006;3:617-27.

(114) Brewer D, Barenco M, Callard R, Hubank M, Stark J. Fitting ordinary differential equations to short time course data. Philos Transact A Math Phys Eng Sci 2008;366:519-44.

(115) Sorribas A, Savageau MA. A comparison of variant theories of intact biochemical systems. I. Enzyme-enzyme interactions and biochemical systems theory. Math Biosci 1989;94:161-93.

(116) Cascante M, Boros LG, Comin-Anduix B, et al. Metabolic control analysis in drug discovery and disease. Nat Biotechnol 2002;20:243-9.

(117) Savageau MA, Voit EO. Power-law approach to modeling biological systems. 1. Theory. Journal of Fermentation Technology 60, 519-544. 2008.

(118) Voit EO. Models-of-data and models-of-processes in the post-genomic era. Math Biosci 2002;180:263-74.:263-74.

(119) Bosl WJ. Systems biology by the rules: hybrid intelligent systems for pathway modeling and discovery. BMC Syst Biol 2007;1:13.:13.

(120) Kirby J, Heath PR, Shaw PJ, Hamdy FC. Gene expression assays. Adv Clin Chem 2007;44:247-92.:247-92.

(121) Kennett JY, Watson SK, Saprunoff H, Heryet C, Lam WL. Technical demonstration of whole genome array comparative genomic hybridization. J Vis Exp 2008;870.

(122) Edwards RA. Laser capture microdissection of mammalian tissue. J Vis Exp 2007;309.

(123) Camp RL, Chung GG, Rimm DL. Automated subcellular localization and quantification of protein expression in tissue microarrays. Nat Med 2002;8:1323-7.

(124) Pan S, Aebersold R, Chen R, et al. Mass Spectrometry Based Targeted Protein Quantification: Methods and Applications. J Proteome Res 2008.

(125) Tibes R, Qiu Y, Lu Y, et al. Reverse phase protein array: validation of a novel proteomic technology and utility for analysis of primary leukemia specimens and hematopoietic stem cells. Mol Cancer Ther 2006;5:2512-21.

(126) Kedrin D, Gligorijevic B, Wyckoff J, et al. Intravital imaging of metastatic behavior through a mammary imaging window. Nat Methods 2008;5:1019-21.

(127) Edward M. Melanoma cell-derived factors stimulate glycosaminoglycan synthesis by fibroblasts cultured as monolayers and within contracted collagen lattices. Br J Dermatol 2001;144:465-70.

(128) Dixon JM. The scientific value of preoperative studies and how they can be used. Breast Cancer Res Treat 2004;87 Suppl 1:S19-26.:S19-S26.

(129) Dowsett M, Smith IE, Ebbs SR, et al. Proliferation and apoptosis as markers of benefit in neoadjuvant endocrine therapy of breast cancer. Clin Cancer Res 2006;12:1024s-30s.

(130) Dowsett M, Smith IE, Ebbs SR, et al. Prognostic value of Ki67 expression after short-term presurgical endocrine therapy for primary breast cancer. J Natl Cancer Inst 2007;99:167-70.

(131) Alberts DS, Markman M, Armstrong D, et al. Intraperitoneal therapy for stage III ovarian cancer: a therapy whose time has come! J Clin Oncol 2002;20:3944-6.

(132) Nagtegaal ID, Gaspar CG, Peltenburg LT, et al. Radiation induces different changes in expression profiles of normal rectal tissue compared with rectal carcinoma. Virchows Arch 2005;446:127-35.

(133) Dowsett M, Allred C, Knox J, et al. Relationship between quantitative estrogen and progesterone receptor expression and human epidermal growth factor receptor 2 (HER-2) status with recurrence in the Arimidex, Tamoxifen, Alone or in Combination trial. J Clin Oncol 2008;26:1059-65.

(134) Miller WR, White S, Dixon JM, et al. Proliferation, steroid receptors and clinical/pathological response in breast cancer treated with letrozole. Br J Cancer 2006;94:1051-6.

(135) Tovey SM, Witton CJ, Bartlett JM, et al. Outcome and human epidermal growth factor receptor (HER) 1-4 status in invasive breast carcinomas with proliferation indices evaluated by bromodeoxyuridine labelling. Breast Cancer Res 2004;6:R246-R251.

(136) Arpino G, Weiss H, Lee AV, et al. Estrogen receptor-positive, progesterone receptor-negative breast cancer: association with growth factor receptor expression and tamoxifen resistance. J Natl Cancer Inst 2005;97:1254-61.

(137) Arpino G, Green SJ, Allred DC, et al. HER-2 amplification, HER-1 expression, and tamoxifen response in estrogen receptor-positive metastatic breast cancer: a southwest oncology group study. Clin Cancer Res 2004;10:5670-6.

(138) Grabau DA, Thorpe SM, Knoop A, et al. Immunohistochemical assessment of oestrogen and progesterone receptors: correlations with the DCC method and clinical outcome in primary breast cancer patients. Breast 2000;9:208-17.

(139) Kirkegaard T, Edwards J, Tovey S, et al. Observer variation in immunohistochemical analysis of protein expression, time for a change? Histopathology 2006;48:787-94.

(140) Adams EJ, Green JA, Clark AH, Youngson JH. Comparison of different scoring systems for immunohistochemical staining. J Clin Pathol 1999;52:75-7.

(141) van Diest PJ, Weger DR, Lindholm J. Reproducibility of subjective immunoscoring of steroid receptors in breast cancer. Anal Quant Cytol Histol 1996;18:351-4.

(142) Psyrri A, Yu Z, Weinberger PM, et al. Quantitative determination of nuclear and cytoplasmic epidermal growth factor receptor expression in oropharyngeal squamous cell cancer by using automated quantitative analysis. Clin Cancer Res 2005;11:5856-62.

(143) Zafirellis K, Agrogiannis G, Zachaki A, et al. Prognostic significance of VEGF expression evaluated by quantitative immunohistochemical analysis in colorectal cancer. J Surg Res 2008;147:99-107.

(144) Aziz DC. Quantitation of estrogen and progesterone receptors by immunocytochemical and image analyses. Am J Clin Pathol 1992;98:105-11.

(145) Esteban JM, Battifora H, Warsi Z, Bailey A, Bacus S. Quantification of estrogen receptors on paraffin-embedded tumors by image analysis. Mod Pathol 1991;4:53-7.

(146) Esteban JM, Kandalaft PL, Mehta P, et al. Improvement of the quantification of estrogen and progesterone receptors in paraffin-embedded tumors by image analysis. Am J Clin Pathol 1993;99:32-8.

(147) Fritz P, Hones J, Lutz D, et al. Quantitative immunohistochemistry: standardization and possible application in research and surgical pathology. Acta Histochem Suppl 1989;37:213-9.:213-9.

(148) Turbin DA, Leung S, Cheang MC, et al. Automated quantitative analysis of estrogen receptor expression in breast carcinoma does not differ from expert pathologist scoring: a tissue microarray study of 3,484 cases. Breast Cancer Res Treat 2008;110:417-26.

(149) Carrasco JL, Jover L. Estimating the generalized concordance correlation coefficient through variance components. Biometrics 2003;59:849-58.

(150) Cicchetti DV, Sparrow SA. Developing criteria for establishing interrater reliability of specific items: applications to assessment of adaptive behavior. Am J Ment Defic 1981;86:127-37.

(151) Molenberghs G, Burzykowski T, Alonso A, Buyse M. A perspective on surrogate endpoints in controlled clinical trials. Stat Methods Med Res 2004;13:177-206.

(152) Kirkegaard T, Edwards J, Tovey S, et al. Observer variation in immunohistochemical analysis of protein expression, time for a change? Histopathology 2006;48:787-94.

(153) Graham AD, Faratian D, Rae F, Thomas JS. Tissue microarray technology in the routine assessment of HER-2 status in invasive breast cancer: a prospective study of the use of immunohistochemistry and fluorescence in situ hybridization. Histopathology 2008;52:847-55.

(154) Kyndi M, Sorensen FB, Knudsen H, et al. Tissue microarrays compared with whole sections and biochemical analyses. A subgroup analysis of DBCG 82 b&c. Acta Oncol 2008;47:591-9.

(155) Marinelli RJ, Montgomery K, Liu CL, et al. The Stanford Tissue Microarray Database. Nucleic Acids Res 2008;36:D871-D877.

(156) Soderberg O, Leuchowius KJ, Gullberg M, et al. Characterizing proteins and their interactions in cells and tissues using the in situ proximity ligation assay. Methods 2008;45:227-32.

(157) Piccart-Gebhart MJ, Procter M, Leyland-Jones B, et al. Trastuzumab after adjuvant chemotherapy in HER2-positive breast cancer. N Engl J Med 2005;353:1659-72.

(158) Romond EH, Perez EA, Bryant J, et al. Trastuzumab plus adjuvant chemotherapy for operable HER2-positive breast cancer. N Engl J Med 2005;353:1673-84.

(159) Scaltriti M, Rojo F, Ocana A, et al. Expression of p95HER2, a truncated form of the HER2 receptor, and response to anti-HER2 therapies in breast cancer. J Natl Cancer Inst 2007;99:628-38.

(160) Egan JE, Hall AB, Yatsulat BA, Bar-Sagi D. The bimodal regulation of epidermal growth factor signaling by human Sprouty proteins. Proceedings of the National Academy of Sciences of the United States of America 2002;99:6041-6.

(161) Hacohen N, Sutherland D, Krasnow MA, et al. sprouty encodes a novel antagonist of FGF signaling that patterns apical branching of the Drosophila airways. Cell 1998;92:253-63.

(162) Hall AB, Jura N, DaSilva J, et al. hSpry2 is targeted to the ubiquitin-dependent proteasome pathway by c-Cbl. Current Biology 2003;13:308-14.

(163) Leeksma OC, Van Achterberg TAE, Tsumura Y, et al. Human sprouty 4, a new ras antagonist on 5q31, interacts with the dual specificity kinase TESK1. European Journal of Biochemistry 2002;269:2546-56.

(164) Mason JM, Morrison DJ, Bassit B, et al. Tyrosine Phosphorylation of Sprouty Proteins Regulates Their Ability to Inhibit Growth Factor

Signaling: A Dual Feedback Loop. Molecular Biology of the Cell 2004;15:2176-88.

(165) Sasaki A, Taketomi T, Wakioka T, et al. Identification of a Dominant Negative Mutant of Sprouty that Potentiates Fibroblast Growth Factor-but Not Epidermal Growth Factor-induced ERK Activation. Journal of Biological Chemistry 2001;276:36804-8.

(166) Wong ESM, Fong CW, Lim J, et al. Sprouty2 attenuates epidermal growth factor receptor ubiquitylation and endocytosis, and consequently enhances Ras/ERK signalling. EMBO Journal 2002;21:4796-808.

(167) Lo TL, Yusoff P, Fong CW, et al. The ras/mitogen-activated protein kinase pathway inhibitor and likely tumor suppressor proteins, sprouty 1 and sprouty 2 are deregulated in breast cancer. Cancer Res 2004;64:6127-36.

(168) McKie AB, Douglas DA, Olijslagers S, et al. Epigenetic inactivation of the human sprouty2 (hSPRY2) homologue in prostate cancer. Oncogene 2005;24:2166-74.

(169) Wang J, Thompson B, Ren C, Ittmann M, Kwabi-Addo B. Sprouty4, a suppressor of tumor cell motility, is down regulated by DNA methylation in human prostate cancer. Prostate 2006;66:613-24.

(170) Fritzsche S, Kenzelmann M, Hoffmann MJ, et al. Concomitant down-regulation of SPRY1 and SPRY2 in prostate carcinoma. Endocr Relat Cancer 2006;13:839-49.

(171) Rhodes DR, Yu J, Shanker K, et al. ONCOMINE: a cancer microarray database and integrated data-mining platform. Neoplasia 2004;6:1-6.

(172) Richardson AL, Wang ZC, De Nicolo A, et al. X chromosomal abnormalities in basal-like human breast cancer. Cancer Cell 2006;9:121-32.

(173) Ma XJ, Wang Z, Ryan PD, et al. A two-gene expression ratio predicts clinical outcome in breast cancer patients treated with tamoxifen. Cancer Cell 2004;5:607-16.

(174) Hess KR, Anderson K, Symmans WF, et al. Pharmacogenomic predictor of sensitivity to preoperative chemotherapy with paclitaxel and fluorouracil, doxorubicin, and cyclophosphamide in breast cancer. J Clin Oncol 2006;24:4236-44.

(175) Fong CW, Chua MS, McKie AB, et al. Sprouty 2, an inhibitor of mitogen-activated protein kinase signaling, is down-regulated in hepatocellular carcinoma. Cancer Res 2006;66:2048-58.

(176) Wong ES, Lim J, Low BC, Chen Q, Guy GR. Evidence for direct interaction between Sprouty and Cbl. J Biol Chem 2001;276:5866-75.

(177) Kononen J, Bubendorf L, Kallioniemi A, et al. Tissue microarrays for high-throughput molecular profiling of tumor specimens. Nat Med 1998;4:844-7.

(178) Giltnane JM, Molinaro A, Cheng H, et al. Comparison of quantitative immunofluorescence with conventional methods for HER2/neu testing with respect to response to trastuzumab therapy in metastatic breast cancer. Arch Pathol Lab Med 2008;132:1635-47.

(179) Camp RL, Dolled-Filhart M, Rimm DL. X-tile: a new bio-informatics tool for biomarker assessment and outcome-based cut-point optimization. Clin Cancer Res 2004;10:7252-9.

(180) Altman DG, Lausen B, Sauerbrei W, Schumacher M. Dangers of using "optimal" cutpoints in the evaluation of prognostic factors. J Natl Cancer Inst 1994;86:829-35.

(181) Guy GR, Fong CW, Leong HF, et al. Tyrosine phosphorylation of Sprouty2 enhances its interaction with c-Cbl and is crucial for its function. Journal of Biological Chemistry 2003;278:33456-64.

(182) Kramer S, Hiromi Y, Okabe M, et al. Sprouty: A common antagonist of FGF and EGF signaling pathways in Drosophila. Development 1999;126:2515-25.

(183) Rubin C, Medvedovsky H, Zwang Y, et al. Sprouty fine-tunes EGF signaling through interlinked positive and negative feedback loops. Current Biology 2003;13:297-307.

(184) Edwin F, Singh R, Endersby R, Baker SJ, Patel TB. The tumor suppressor PTEN is necessary for human Sprouty 2-mediated inhibition of cell proliferation. J Biol Chem 2006;281:4816-22.

(185) Tsumura Y, Toshima J, Leeksma OC, Ohashi K, Mizuno K. Sprouty-4 negatively regulates cell spreading by inhibiting the kinase activity of testicular protein kinase. Biochem J 2005;387:627-37.

(186) Hennessy BT, Smith DL, Ram PT, Lu Y, Mills GB. Exploiting the PI3K/AKT pathway for cancer drug discovery. Nat Rev Drug Discov 2005;4:988-1004.

(187) Nagata Y, Lan KH, Zhou X, et al. PTEN activation contributes to tumor inhibition by trastuzumab, and loss of PTEN predicts trastuzumab resistance in patients. Cancer Cell 2004;6:117-27.

(188) Levi F, Lucchini F, Negri E, Boyle P, La Vecchia C. Cancer mortality in Europe, 1995-1999, and an overview of trends since 1960. Int J Cancer 2004;110:155-69.

(189) Cannistra SA. Cancer of the ovary. N Engl J Med 2004;351:2519-29.

(190) Payne SJ, Bowen RL, Jones JL, Wells CA. Predictive markers in breast cancer--the present. Histopathology 2008;52:82-90.

(191) Kobel M, Kalloger SE, Carrick J, et al. A limited panel of immunomarkers can reliably distinguish between clear cell and high-grade serous carcinoma of the ovary. Am J Surg Pathol 2009;33:14-21.

(192) Crijns AP, Fehrmann RS, de Jong S, et al. Survival-Related Profile, Pathways, and Transcription Factors in Ovarian Cancer. PLoS Med 2009;6:e24.

(193) Vogelstein B, Kinzler KW. Cancer genes and the pathways they control. Nat Med 2004;10:789-99.

(194) McCubrey JA, Steelman LS, Abrams SL, et al. Roles of the RAF/MEK/ERK and PI3K/PTEN/AKT pathways in malignant transformation and drug resistance. Adv Enzyme Regul 2006;46:249-79. Epub;%2006 Jul 18.:249-79.

(195) Graham AD, Williams AR, Salter DM. TTF-1 expression in primary ovarian epithelial neoplasia. Histopathology 2006;48:764-5.

(196) Kononen J, Bubendorf L, Kallioniemi A, et al. Tissue microarrays for high-throughput molecular profiling of tumor specimens. Nat Med 1998;4:844-7.

(197) Camp RL, Chung GG, Rimm DL. Automated subcellular localization and quantification of protein expression in tissue microarrays. Nat Med 2002;8:1323-7.

(198) Eisen MB, Spellman PT, Brown PO, Botstein D. Cluster analysis and display of genome-wide expression patterns. Proc Natl Acad Sci U S A 1998;95:14863-8.

(199) Israeli O, Goldring-Aviram A, Rienstein S, et al. In silico chromosomal clustering of genes displaying altered expression patterns in ovarian cancer. Cancer Genet Cytogenet 2005;160:35-42.

(200) Lawrenson K, Gayther SA. Ovarian Cancer: A Clinical Challenge That Needs Some Basic Answers. PLoS Med 2009;6:e25.

(201) Willner J, Wurz K, Allison KH, et al. Alternate molecular genetic pathways in ovarian carcinomas of common histological types. Hum Pathol 2007;38:607-13.

(202) Herod JJ, Eliopoulos AG, Warwick J, et al. The prognostic significance of Bcl-2 and p53 expression in ovarian carcinoma. Cancer Res 1996;56:2178-84.

(203) Hall J, Paul J, Brown R. Critical evaluation of p53 as a prognostic marker in ovarian cancer. Expert Rev Mol Med 2004;6:1-20.

(204) Baekelandt M, Kristensen GB, Nesland JM, Trope CG, Holm R. Clinical significance of apoptosis-related factors p53, Mdm2, and Bcl-2 in advanced ovarian cancer. J Clin Oncol 1999;17:2061.

(205) Fink D, Aebi S, Howell SB. The role of DNA mismatch repair in drug resistance. Clin Cancer Res 1998;4:1-6.

(206) Smith S, Su D, Rigault de la Longrais IA, et al. ERCC1 genotype and phenotype in epithelial ovarian cancer identify patients likely to benefit from paclitaxel treatment in addition to platinum-based therapy. J Clin Oncol 2007;%20;25:5172-9.

(207) Quinn JE, Carser JE, James CR, Kennedy RD, Harkin DP. BRCA1 and implications for response to chemotherapy in ovarian cancer. Gynecol Oncol 2009.

(208) Ouchi T. BRCA1 phosphorylation: biological consequences. Cancer Biol Ther 2006;5:470-5.

(209) Rogakou EP, Pilch DR, Orr AH, Ivanova VS, Bonner WM. DNA double-stranded breaks induce histone H2AX phosphorylation on serine 139. J Biol Chem 1998;273:5858-68.

(210) Shieh SY, Ikeda M, Taya Y, Prives C. DNA damage-induced phosphorylation of p53 alleviates inhibition by MDM2. Cell 1997;91:325-34.

(211) Fraser M, Bai T, Tsang BK. Akt promotes cisplatin resistance in human ovarian cancer cells through inhibition of p53 phosphorylation and nuclear function. Int J Cancer 2008;122:534-46.

(212) Marinov M, Ziogas A, Pardo OE, et al. AKT/mTOR Pathway Activation and BCL-2 Family Proteins Modulate the Sensitivity of Human Small Cell Lung Cancer Cells to RAD001. Clin Cancer Res 2009;15:1277-87.

(213) Cuatrecasas M, Villanueva A, Matias-Guiu X, Prat J. K-ras mutations in mucinous ovarian tumors: a clinicopathologic and molecular study of 95 cases. Cancer 1997;79:1581-6.

(214) Enomoto T, Weghorst CM, Inoue M, Tanizawa O, Rice JM. K-ras activation occurs frequently in mucinous adenocarcinomas and rarely in other common epithelial tumors of the human ovary. Am J Pathol 1991;139:777-85.

(215) Ichikawa Y, Nishida M, Suzuki H, et al. Mutation of K-ras protooncogene is associated with histological subtypes in human mucinous ovarian tumors. Cancer Res 1994;54:33-5.

(216) Gamallo C, Palacios J, Moreno G, et al. beta-catenin expression pattern in stage I and II ovarian carcinomas : relationship with beta-catenin gene

mutations, clinicopathological features, and clinical outcome. Am J Pathol 1999;155:527-36.

(217) Langdon SP, Smyth JF. Hormone therapy for epithelial ovarian cancer. Curr Opin Oncol 2008;20:548-53.

(218) Walker G, MacLeod K, Williams AR, et al. Estrogen-regulated gene expression predicts response to endocrine therapy in patients with ovarian cancer. Gynecol Oncol 2007;106:461-8.

(219) Smyth JF, Gourley C, Walker G, et al. Antiestrogen therapy is active in selected ovarian cancer cases: the use of letrozole in estrogen receptor-positive patients. Clin Cancer Res 2007;13:3617-22.

(220) Bafico A, Liu G, Goldin L, Harris V, Aaronson SA. An autocrine mechanism for constitutive Wnt pathway activation in human cancer cells. Cancer Cell 2004;6:497-506.

(221) Roberts D, Schick J, Conway S, et al. Identification of genes associated with platinum drug sensitivity and resistance in human ovarian cancer cells. Br J Cancer 2005;92:1149-58.

(222) Sorokin A, Paliy K, Selkov A, et al. The Pathway Editor: A tool for managing complex biological networks. IBM Journal of Research and Development.Systems Biology. 50, 561-575. 2006.

(223) Goryanin I, Hodgman TC, Selkov E. Mathematical simulation and analysis of cellular metabolism and regulation. Bioinformatics 1999;15:749-58.

(224) Spurrier B, Ramalingam S, Nishizuka S. Reverse-phase protein lysate microarrays for cell signaling analysis. Nat Protoc 2008;3:1796-808.

(225) Board RE, Thelwell NJ, Ravetto PF, et al. Multiplexed assays for detection of mutations in PIK3CA. Clin Chem 2008;54:757-60.

(226) Miyake T, Yoshino K, Enomoto T, et al. PIK3CA gene mutations and amplifications in uterine cancers, identified by methods that avoid confounding by PIK3CA pseudogene sequences. Cancer Lett 2008;261:120-6.

(227) Birtwistle MR, Hatakeyama M, Yumoto N, et al. Ligand-dependent responses of the ErbB signaling network: experimental and modeling analyses. Mol Syst Biol 2007;3:144. Epub;%2007 Nov 13.:144.

(228) Moehren G, Markevich N, Demin O, et al. Temperature dependence of the epidermal growth factor receptor signaling network can be accounted for by a kinetic model. Biochemistry 2002;41:306-20.

(229) Leslie NR, Downes CP. PTEN function: how normal cells control it and tumour cells lose it. Biochem J 2004;382:1-11.

(230) Carson JD, Van Aller G, Lehr R, et al. Effects of oncogenic p110alpha subunit mutations on the lipid kinase activity of phosphoinositide 3-kinase. Biochem J 2008;409:519-24.

(231) Goldbeter A, Koshland DE, Jr. An amplified sensitivity arising from covalent modification in biological systems. Proc Natl Acad Sci U S A 1981;78:6840-4.

(232) Stadtman ER, Chock PB. Superiority of interconvertible enzyme cascades in metabolic regulation: analysis of monocyclic systems. Proc Natl Acad Sci U S A 1977;74:2761-5.

(233) Gomez-Uribe C, Verghese GC, Mirny LA. Operating regimes of signaling cycles: statics, dynamics, and noise filtering. PLoS Comput Biol 2007;3:e246.

(234) Schmid AC, Byrne RD, Vilar R, Woscholski R. Bisperoxovanadium compounds are potent PTEN inhibitors. FEBS Lett 2004;566:35-8.

(235) Posner BI, Faure R, Burgess JW, et al. Peroxovanadium compounds. A new class of potent phosphotyrosine phosphatase inhibitors which are insulin mimetics. J Biol Chem 1994;269:4596-604.

(236) Shayesteh L, Lu Y, Kuo WL, et al. PIK3CA is implicated as an oncogene in ovarian cancer. Nat Genet 1999;21:99-102.

(237) Levine DA, Bogomolniy F, Yee CJ, et al. Frequent mutation of the PIK3CA gene in ovarian and breast cancers. Clin Cancer Res 2005;11:2875-8.

(238) Stemke-Hale K, Gonzalez-Angulo AM, Lluch A, et al. An integrative genomic and proteomic analysis of PIK3CA, PTEN, and AKT mutations in breast cancer. Cancer Res 2008;68:6084-91.

(239) Eichhorn PJ, Gili M, Scaltriti M, et al. Phosphatidylinositol 3-kinase hyperactivation results in lapatinib resistance that is reversed by the mTOR/phosphatidylinositol 3-kinase inhibitor NVP-BEZ235. Cancer Res 2008;68:9221-30.

(240) Hartwell L, Mankoff D, Paulovich A, Ramsey S, Swisher E. Cancer biomarkers: a systems approach. Nat Biotechnol 2006;24:905-8.

(241) Jia S, Liu Z, Zhang S, et al. Essential roles of PI(3)K-p110beta in cell growth, metabolism and tumorigenesis. Nature 2008;454:776-9.

(242) Agus DB, Gordon MS, Taylor C, et al. Phase I clinical study of pertuzumab, a novel HER dimerization inhibitor, in patients with advanced cancer. J Clin Oncol 2005;23:2534-43.

(243) Mullen P, Cameron DA, Hasmann M, Smyth JF, Langdon SP. Sensitivity to pertuzumab (2C4) in ovarian cancer models: cross-talk with estrogen receptor signaling. Mol Cancer Ther 2007;6:93-100.

(244) Chen WW, Schoeberl B, Jasper PJ, et al. Input-output behavior of ErbB signaling pathways as revealed by a mass action model trained against dynamic data. Mol Syst Biol 2009;5:239. Epub;%2009 Jan;%20.:239.

(245) Zhang Y, Rundell A. Comparative study of parameter sensitivity analyses of the TCR-activated Erk-MAPK signalling pathway. Syst Biol (Stevenage) 2006;153:201-11.

(246) Gutenkunst RN, Waterfall JJ, Casey FP, et al. Universally sloppy parameter sensitivities in systems biology models. PLoS Comput Biol 2007;3:1871-8.

(247) Koh G, Teong HF, Clement MV, Hsu D, Thiagarajan PS. A decompositional approach to parameter estimation in pathway modeling: a case study of the Akt and MAPK pathways and their crosstalk. Bioinformatics 2006;22:e271-e280.

(248) Adams CW, Allison DE, Flagella K, et al. Humanization of a recombinant monoclonal antibody to produce a therapeutic HER dimerization inhibitor, pertuzumab. Cancer Immunol Immunother 2006;55:717-27.

(249) Schwacke JH, Voit EO. Computation and analysis of time-dependent sensitivities in Generalized Mass Action systems. J Theor Biol 2005;236:21-38.

(250) Franklin MC, Carey KD, Vajdos FF, et al. Insights into ErbB signaling from the structure of the ErbB2-pertuzumab complex. Cancer Cell 2004;5:317-28.

(251) Maccario H, Perera NM, Davidson L, Downes CP, Leslie NR. PTEN is destabilized by phosphorylation on Thr366. Biochem J 2007;405:439-44.

(252) Vlahos CJ, Matter WF, Hui KY, Brown RF. A specific inhibitor of phosphatidylinositol 3-kinase, 2-(4-morpholinyl)-8-phenyl-4H-1-benzopyran-4-one (LY294002). J Biol Chem 1994;269:5241-8.

(253) Moelling K, Schad K, Bosse M, Zimmermann S, Schweneker M. Regulation of Raf-Akt Cross-talk. J Biol Chem 2002;277:31099-106.

(254) Litvinov RI, Bennett JS, Weisel JW, Shuman H. Multi-step fibrinogen binding to the integrin (alpha)IIb(beta)3 detected using force spectroscopy. Biophys J 2005;89:2824-34.

(255) Gericke A, Munson M, Ross AH. Regulation of the PTEN phosphatase. Gene 2006;374:1-9. Epub;%2006 Mar 14.:1-9.

(256) Birle D, Bottini N, Williams S, et al. Negative feedback regulation of the tumor suppressor PTEN by phosphoinositide-induced serine phosphorylation. J Immunol 2002;169:286-91.

(257) McConnachie G, Pass I, Walker SM, Downes CP. Interfacial kinetic analysis of the tumour suppressor phosphatase, PTEN: evidence for activation by anionic phospholipids. Biochem J 2003;371:947-55.

(258) Loew LM. Where does all the PIP2 come from? J Physiol 2007;582:945-51.

Appendix A: Patient characteristics of trastuzumab-treated cohort.

A.1 Patient characteristics of trastuzumab-treated cohort.

Cohort variable	*Number*	*Percentage*	**Log-rank p-value**
Age, years			0.46
<50	49	40.1	
>50	73	59.9	
NK	0	0	
Prognostic Index			0.22
<3.4	2	1.6	
3.4-5.4	47	38.5	
>5.4	62	50.8	
NK	11	9.0	
Grade			0.80
1	1	0.8	
2	19	15.6	
3	99	81.1	
NK	2	1.6	
Tumour Stage			0.024
1	35	28.7	
2	64	52.5	
3	12	9.8	
4	3	2.5	
NK	8	6.6	
Node stage at diagnosis			0.20
Negative	26	21.3	
Positive	87	71.3	
NK	9	7.4	
ER status			0.038
>3	72	59.0	
≤3	41	33.6	
NK	9	7.3	
HER2 status			0.38
Positive	90	73.7	
Negative	32	26.3	
NK	0	0	
Chemotherapy			<0.0001
Anthracycline-containing	66	54.1	
Taxane-containing	53	43.4	
NK	3	2.5	

Appendix B: Modeling methods and description of mathematical model.

B.1: Modeling methods

The parameter set of the model contains 82 kinetic parameters of enzymes and receptors with 15 initial concentrations of proteins/metabolites. A direct attempt to use a model parameter set obtained from existing models (103) to describe our experimental data did not yield satisfactory results, which was not unexpected since different experimental models can yield different model parameters (103;105;244;245), as seen in other models of MAPK signalling ((103;105;244-247) and Table S2 in Appendix C – mathematical model, ODEs). Also, determination of the model parameters of signalling networks are subject to uncertainty and non-identifiability of kinetic parameters of the enzymes involved in signalling (244-246). We therefore carried out parameter fitting of the model to experimental data obtained on the human carcinoma cell line PE04.

In the fitting procedure we used kinetic experimental data on phosphorylation of HER2, AKT, ERK, and PTEN obtained in the absence and presence of pertuzumab. As an initial approximation of the model parameters we used the parameter set from (103). Using the DBsolve package (223) we minimized the following cost function:

$$\Delta = \sum_{i=1}^{4}\sum_{j=1}^{2}\sum_{k=1}^{6}\left[Y_{ij}^{(th)}(t_k) - Y_{ij}^{(\exp)}(t_k)\right]^2, \quad (1)$$

where $Y_{ij}^{(\exp)}(t_k)$ and $Y_{ij}^{(th)}(t_k)$ - experimental and theoretical data on concentrations of pHER2, pERK, pAKT, pERK (i=1…4), obtained in the absence and presence of pertuzumab (j=1,2) at time points t_k = 1, 2, 5 10, 20, 60 minutes (k=1,…6) after heregulin-β stimulation. $Y_{ij}^{(\exp)}(t_k)$ and $Y_{ij}^{(th)}(t_k)$ were normalised to their maximal values.

To identify all parameters we used a semi-automatic technique which involved model decomposition, sensitivity analysis, and minimization of cost function (223). According to the model decomposition method (247) we used sensitivity analysis (see below) to determine main groups of reactions and their kinetic parameters

contributing significantly to $Y_{ij}^{(\exp)}(t_k)$. The results of sensitivity analysis (see Fig. S5-S9 in Appendix D - Figures) showed that the main contribution to pHER2 kinetics are made by the reactions of the binding of HER3 with heregulin-β and HER2/HER3 heterodimerisation followed by autophosphorylation of tyrosine residues (see reactions $V_{1,51}$, $V_{2,53}$, V_3, V_4 in main text Figure 1). Therefore, our first stage of optimization was the parameters of the reactions included in this subsystem. Most of the parameters were found to be close to the ones from (103;105) (see Table S2 in Appendix C – mathematical model, ODEs). To estimate the affinity of heregulin-β to HER2 we took into account the dose-dependence of pAKT to heregulin-β (see comparison simulation results with experimental data in Figure S13 in Appendix D - Figures).

The main contribution to pERK kinetics were, as expected, made by the RAS/RAF/MEK/ERK branch of the network. The second stage of parameterization procedure identified kinetic parameters involved in this subsystem. The third stage used pAKT and pPTEN timecourse data to identify parameters of PI3K/PTEN/AKT branch. We then identified parameters of the crosstalk between RAS/RAF/MEK/ERK and PI3K/PTEN/AKT branches (kinetic parameters of PP2A phosphatase and feedback inhibition of RAF by active AKT), using the experimental data obtained in the absence and presence of RTK inhibitor, pertuzumab. To estimate kinetic parameters of the binding of pertuzumab with HER2 we also considered experimental data on the dissociation constant of pertuzumab (248).

We next carried out local time-dependent sensitivity analysis (249) by calculating sensitivity of the observable variables $Y_i^{(th)}(t)$ (such as pHER2, pAKT, pERK, and pPTEN) to variation of the parameter p_j, given by:

$$S_{ij}(t,\boldsymbol{P},\boldsymbol{I}) = \frac{\partial \ln Y_i^{(th)}(t)}{\partial \ln p_j}, \qquad (2)$$

where t – time after HRG simulation, P – set of model parameters involving the set of kinetic parameters $K=k_1...k_n$ and initial concentrations $X_o=x_1...x_m$. Fig. S5-S9 (Appendix B – methods) represents the values of sensitivity $S_{ij}(t,\boldsymbol{P},\boldsymbol{I})$ at t=5 minutes for parameters contributing significantly in the observable variables.

B.2 Development of a kinetic model for simulation of RTK-inhibitor therapy

We adjusted and further developed the model of ERK/AKT signalling pathways proposed by Hatakeyama *et al* (103) in order to model heregulin-□ and the RTK-dimerisation inhibitor effects of pertuzumab on the human ovarian carcinoma cell line PE04. We introduced the following modifications to the model in order to obtain a set of kinetic parameters:

Ligand/receptor and receptor/receptor interaction

We generalized the model (103) to describe HER3/HER2 heterodimerisation (reactions V_2 and V_{53} in Fig.1). We omitted HER3/HER4, HER4/HER4, and HER2/HER4 complexes because there was very little detectable HER4 in PE04 cell lines (Appendix D: Fig. S16).

To describe the effect of pertuzumab on signal transduction in the ERK/AKT pathways we introduced the binding of pertuzumab to HER2 (reactions V_{49} and V_{50}). We introduced a two-step mechanism of heregulin/pertuzumab binding with receptors as well as heterodimerisation of HER3/HER2 (see Fig. S1, S2) in order to reach good agreement between the model and experimental kinetics of the HER3/HER2 dimerisation in the presence of the HER2 inhibitor. In contrast to a one step mechanism (action mass reaction rate), two-step (or multi-step) binding of the ligand to receptor proceeds through the reversible formation of ligand/receptor complexes followed by formation of tight ligand/receptor complexes (247;250).

We normalised receptor and pertuzumab concentrations to the cytosolic volume of the cell, which is necessary for conforming concentrations in different compartments. The reactions occur in the receptor compartment (cell surface) and further downstream signalling processes in the intracellular compartment (cytoplasmic volume). The coefficient is V_m/V_c , where V_m= average volume of incubation

medium per cell and V_c = cytoplasmic volume (227). In our experiments there are 10^5 cell/ml, therefore $V_m=10^{-5}$ ml, assuming $V_c=3\ 10^{-9}$ ml, $V_m/V_c=3000$.

The following approximations were made in the model. We did not consider the growth of cell population, gene regulation, or receptor synthesis in the model. We do not include additional biosynthesis of PI in response to its consumption (251) and propose the pool of the lipid second messenger PI to be constant during signal transduction. These assumptions have been made because of the relatively slow rate of these processes in comparison with signal transduction.

To model the effects caused by the loss of PTEN activity we added in the model the reaction of PTEN inhibition by bpV(pic) (reaction 57). Also we included the reaction of inhibition of PI3K by LY294002 (reaction 58).

Cross-talk between AKT and ERK branches

Since PP2A is a common phosphatase which deactivates both MEK and AKT, it can be responsible for cross-talk between ERK and AKT signalling (103). In the original model (103) the sharing of the common phosphatase PP2A was modelled by a quasi-steady-state Michaelis-Menten approach by introduction of fraction coefficients corresponding to the two branches. However Michaelis-Menten approach is not valid at the concentration of the substrates (phosphorylated MEK or AKT), being comparable with the concentration of the enzyme catalysing the reaction. To describe directly cross-regulation of MEK and AKT activation by PP2A phosphatase sharing we replaced the Michaelis-Menten approximation of PP2A reaction (103) with a mass action model of PP2A interaction with active forms of AKT and MEK (see Fig. S3). This modification permitted us to describe explicitly the competitive deactivation of MEK and AKT branches by common PP2A phosphatase.

Similarly we replaced the Michaelis-Menten approximation with mass action based model for another key enzyme, PI3K (reactions V_{31}, V_{55}, V_{56} in Figure S1b). This

modification was made on base of experimental data on non-Michaelis-Menten kinetics of PI3K catalysis (252).

The model also takes into account the cross-talk between AKT and ERK branches due to RAF inactivation by AKT (103;194;253): active AKT phosphorylates S259 on Raf and inhibits its activity (reaction V_{12}).

The results of the modelling are represented in Fig. S4 and the results of sensitivity analysis are given in Fig. S5-S9.

Detailed kinetic model of PTEN regulation

We developed a separate kinetic model of PTEN catalytic cycle and incorporated it into the whole model. The model takes into account the following kinetic and regulatory properties of PTEN: competition between lipid and protein phosphatase activity of PTEN (254), autodephosphorylation activity of PTEN (229;255), balance and interchange between PTEN and pPTEN [9], experimental data on kinetic parameters of PTEN (256).

The developed catalytic cycle of PTEN is shown in Fig. S10. We took into account that only the dephosphorylated form of PTEN possesses lipid phosphatase activity (254). We used mass action approximation of rate equation of lipid phosphatase activity on the base of experimental data on non-Michaelis-Menten kinetics of PTEN (257).

The kinetic model of PTEN includes eight ODEs (S1.40)-(S1.47). The reactions V_{32-34} describe the lipid phosphatase activity of PTEN, reaction V_{35} corresponds to phosphorylation of PTEN by CK2 and GSK3. As phosphatase being responsible for dephosphorylation of pPTEN is unknown (229), we considered autodephosphorylation mechanism of pPTEN dephosphorylation (reaction V_{36-38}) due to its weak protein phosphatase activity (229). To analyse the function of the proposed cycle of PTEN/pPTEN exchange we studied this model separately. Firstly,

we simulated dynamic balance of PTEN/pPTEN in the absence of PIP3. In the result the steady state concentrations of PTEN and pPTEN were determined in the system. In our model the kinetic parameters of PTEN protein phosphatase activity and CK2 (GSK3) kinase were set in such a way that PTEN would be mainly in dephosphorylated form.

We then studied effect of the substrate PIP3 on the PTEN/pPTEN balance. The presence of PIP3 leads to the competition between PIP3 and CK3 (GSK3) for PTEN that causes the decrease in free PTEN concentration due to formation of substrate-enzyme complex PTEN·PIP3. It results in an elevation of pPTEN concentration due to a slowdown in autodephosphorylation of pPTEN.

This model permitted us to describe a dynamic balance of PTEN/pPTEN in resting cell and reproduce experimental data on increasing of pPTEN concentration during AKT activation in PE04 ovarian carcinoma cells (see Figure S4d) and other cells (258). Figure S4d shows the experimental and theoretical kinetics of pPTEN in the absence/presence of pertuzumab. The comparison of the two kinetics in Figure S4d shows that pertuzumab moderates pPTEN rise. According the model prediction this effect is due to that PTEN consumption in lipid phosphatase reaction is lower at signal inhibition than without inhibition. So, PTEN mainly participates in autodephosphorylation reaction in this case and enhances dephosphorylation of pPTEN.

Thus the model predicts the kinetics of pPTEN may indicate the decrease of PTEN lipid activity (in the case of PTEN inhibition) or activation of PTEN/PI3K cycle due to PI3K activation. According to the model the loss of PTEN lipid phosphatase activity causes the decrease of pPTEN level as well as PI3K activation leads to the increasing of pPTEN concentration compared to normal PTEN/PI3K cycle function.

B.3 Mechanism of resistance to RTK inhibitors

Here, we analysed how sensitivity of the cancer signalling depends on PTEN/PI3K cycle. Such types of cycles comprising two interconvertible enzymes, kinase and phosphatase were extensively analysed previously(231;232).

We found that integrative parameter γ= PTEN/PI3K* is responsible for sensitivity, where PTEN and PI3K* are the enzyme activities calculated as the ratio V_{max}/K_m, where $V_{max}=k_{cat}e$ – maximum velocity, k_{cat} – catalytic constant, e – enzyme concentration, $K_m=(k_{-1}+k_{cat})/k_1= K_d+ k_{cat}/k_1$ – Michaelis constant, K_d – dissociation constant, $\gamma_0 =10^5$ (resulted from fitting to experimental Fig. 2a). The γ could be changed as a result of the enzyme inhibition, variations in enzyme expression level (e), and mutations causing changes in catalytic constant(k_{cat}) and/or affinity (K_d).

We compared the responses of the system to heregulin stimulation in the presence and absence of pertuzumab (see Fig. 2a and Fig. S6a) in the range of γ.

At the values of the parameter γ near γ_0 (see Fig. 2b) the system discriminates input signals, i.e. output signal (pAKT) is proportional to the input signal (pHER2). In this regime the PTEN/PI3K cycle functions as a discriminator of the receptor signals. PTEN/ PI3K cycle switches to amplification regime when γ decreases 5-10 times, i.e. the system amplifies all input signals pHER2 up to maximal output signal pAKT. In this regime the system becomes insensitive to the external signal. We propose that this amplification regime corresponds to resistance in RTK signal inhibition. Our theoretical results predict (Fig. S10d) that combination of two inhibitors (RTK and PIK3 inhibitors) could prevent the drug resistance caused by the loss of PTEN activity as it would lead to an increase γ back to normal γ_0 . We found that the PTEN/ PI3K cycle could exhibit a signal suppression at the high value of γ (ten times higher than γ_0). Such higher values of γ can be reached in the system, for example, by inhibition of PI3K.

To demonstrate the suppression regime we used experimental data on inhibition of PI3K by LY294002 (see Fig. S9). Fig. S10c shows the predicted kinetics of pAKT signal induced by HRG in the absence and presence of PI3K inhibitor. PI3K inhibition causes weakening of the pAKT signal to zero level, i.e. the PTEN/ PI3K cycle inhibits the signal transduction from RTK receptors.

Appendix C: Mathematical model ordinary differential equations.

C.1 System of ordinary differential equations

$$\frac{d[\mathrm{E3}]}{dt} = -V_1 \tag{S1.1}$$

$$\frac{d[\mathrm{E3H}]}{dt} = V_1 - V_2 - V_{51} \tag{S1.2}$$

$$\frac{d[\mathrm{HRG}]}{dt} = -V_1 \tag{S1.3}$$

$$\frac{d[\mathrm{E3H_c}]}{dt} = V_{51} - V_{52} \tag{S1.4}$$

$$\frac{d[\mathrm{E2}]}{dt} = -V_2 - V_{49} - V_{52} \tag{S1.5}$$

$$\frac{d[\mathrm{E23H}]}{dt} = V_2 - V_3 + V_4 + V_{52} - V_{53} \tag{S1.6}$$

$$\frac{d[\mathrm{E23H_c}]}{dt} = V_{53} - V_{54} \tag{S1.7}$$

$$\frac{d[\mathrm{pE23H}]}{dt} = V_3 - V_4 - V_5 + V_8 - V_{27} + V_{29} - V_{48} + V_{54} \tag{S1.8}$$

$$\frac{d[\mathrm{Shc}]}{dt} = -V_5 + V_{10} \tag{S1.9}$$

$$\frac{d[\mathrm{pE23H\text{-}Shc}]}{dt} = V_5 - V_6 \tag{S1.10}$$

$$\frac{d[\mathrm{pE23H\text{-}pShc}]}{dt} = V_6 - V_7 \tag{S1.11}$$

$$\frac{d[\mathrm{GS}]}{dt} = -V_7 + V_9 \tag{S1.12}$$

$$\frac{d[\mathrm{Shc\text{-}GS}]}{dt} = V_8 - V_9 \tag{S1.13}$$

$$\frac{d[\mathrm{pShc}]}{dt} = V_9 - V_{10} \tag{S1.14}$$

$$\frac{d[\mathrm{pE23H\text{-}pShc\text{-}GS}]}{dt} = V_7 - V_8 \tag{S1.15}$$

$$\frac{d[\mathrm{ppAkt\text{-}PIP3}]}{dt} = V_{44} - V_{45} \tag{S1.16}$$

$$\frac{d[\mathrm{Ras\text{-}GDP}]}{dt} = -V_{11} + V_{12} \tag{S1.17}$$

$$\frac{d[\mathrm{Ras\text{-}GTP}]}{dt} = V_{11} - V_{12} \tag{S1.18}$$

$$\frac{d[\mathrm{Raf}]}{dt} = -V_{13} + V_{14} \tag{S1.19}$$

$$\frac{d[\mathrm{Raf^*}]}{dt} = V_{13} - V_{14} \tag{S1.20}$$

$$\frac{d[\text{MEK}]}{dt} = -V_{15} + V_{18} \quad \text{(S1.21)}$$

$$\frac{d[\text{pMEK}]}{dt} = V_{15} - V_{16} - V_{19} + V_{22} \quad \text{(S1.22)}$$

$$\frac{d[\text{PP2A}]}{dt} = -V_{16} + V_{18} - V_{20} + V_{22} - V_{41} + V_{43} - V_{45} + V_{47} \quad \text{(S1.23)}$$

$$\frac{d[\text{MEKP-PP2A}]}{dt} = V_{16} - V_{17} + V_{21} - V_{22} \quad \text{(S1.24)}$$

$$\frac{d[\text{MEK-PP2A}]}{dt} = V_{17} - V_{18} \quad \text{(S1.25)}$$

$$\frac{d[\text{pAkt-PIP3-PP2A}]}{dt} = V_{41} - V_{42} + V_{46} - V_{47} \quad \text{(S1.26)}$$

$$\frac{d[\text{ppMEKPP-PP2A}]}{dt} = V_{20} - V_{21} \quad \text{(S1.27)}$$

$$\frac{d[\text{ppMEKPP-PP2A}]}{dt} = V_{20} - V_{21} \quad \text{(S1.28)}$$

$$\frac{d[\text{ppMEK}]}{dt} = V_{19} - V_{20} \quad \text{(S1.29)}$$

$$\frac{d[\text{ERK}]}{dt} = -V_{23} + V_{24} \quad \text{(S1.30)}$$

$$\frac{d[\text{pERKP}]}{dt} = V_{23} - V_{24} - V_{25} + V_{26} \quad \text{(S1.31)}$$

$$\frac{d[\text{ppERK}]}{dt} = V_{25} - V_{26} \quad \text{(S1.32)}$$

$$\frac{d[\text{ppAkt-PIP3-PP2A}]}{dt} = V_{45} - V_{46} \quad \text{(S1.33)}$$

$$\frac{d[\text{Akt-PIP3}]}{dt} = V_{39} - V_{40} + V_{43} \quad \text{(S1.34)}$$

$$\frac{d[\text{PI3K}]}{dt} = -V_{27} + V_{30} - V_{58} \quad \text{(S1.35)}$$

$$\frac{d[\text{pE23H-PI3K}]}{dt} = V_{27} - V_{28} \quad \text{(S1.36)}$$

$$\frac{d[\text{pE23H-PI3K*}]}{dt} = V_{28} - V_{29} \quad \text{(S1.37)}$$

$$\frac{d[\text{PI3K*}]}{dt} = V_{29} - V_{30} - V_{31} + V_{56} \quad \text{(S1.38)}$$

$$\frac{d[\text{PI}]}{dt} = -V_{31} + V_{34} \quad \text{(S1.39)}$$

$$\frac{d[\text{PTEN}]}{dt} = -V_{32} + V_{34} - V_{35} - V_{36} + 2V_{38} - V_{57} \quad \text{(S1.40)}$$

$$\frac{d[\text{PIP3}]}{dt} = -V_{32} - V_{39} + V_{56} \quad \text{(S1.41)}$$

$$\frac{d[\text{PTEN-PIP3}]}{dt} = V_{32} - V_{33} \quad \text{(S1.42)}$$

$$\frac{d[\text{PTEN-PI}]}{dt} = V_{33} - V_{34} \quad \text{(S1.43)}$$

$$\frac{d[\text{pPTEN}]}{dt} = V_{35} - V_{36} \quad \text{(S1.44)}$$

$$\frac{d[\text{pPTENP-PTEN}]}{dt} = V_{36} - V_{37} \quad \text{(S1.45)}$$

$$\frac{d[\text{PTEN-PTEN}]}{dt} = V_{37} - V_{38} \quad \text{(S1.46)}$$

$$\frac{d[\text{PI3K*-PI}]}{dt} = V_{31} - V_{55} \quad \text{(S1.47)}$$

$$\frac{d[\text{PI3K*-PIP3}]}{dt} = V_{55} - V_{56} \quad \text{(S1.48)}$$

$$\frac{d[\text{Akt}]}{dt} = -V_{39} \quad \text{(S1.49)}$$

$$\frac{d[\text{pAkt-PIP3}]}{dt} = V_{40} - V_{41} - V_{44} + V_{47} \quad \text{(S1.50)}$$

$$\frac{d[\text{Akt-PIP3-PP2A}]}{dt} = V_{42} - V_{43} \quad \text{(S1.51)}$$

$$\frac{d[2C4]}{dt} = -V_{49} \quad \text{(S1.52)}$$

$$\frac{d[\text{E2-2C4}]}{dt} = V_{49} - V_{50} \quad \text{(S1.53)}$$

$$\frac{d[\text{E2-2C4}_c]}{dt} = V_{50} \quad \text{(S1.54)}$$

$$\frac{d[\text{PTEN-bpV}]}{dt} = V_{57} \quad \text{(S1.55)}$$

$$\frac{d[\text{PI3K-LY}]}{dt} = V_{58} \quad \text{(S1.56)}$$

where reaction rates V_i are determined by the following equations:

$$V_1 = k_1 \cdot ([E3] \cdot [HRG] - K_{d,1} \cdot [E3H]) \quad \text{(S1.57)}$$

$$V_2 = k_2 \cdot ([E3H] \cdot [E2] - K_{d,2} \cdot [E23H]) \quad \text{(S1.58)}$$

$$V_3 = k_3 \cdot ([E23H] - K_{d,3} \cdot [E23HP]) \quad \text{(S1.59)}$$

$$V_4 = V_{max,4} \cdot [pE23H] / (K_{m,4} + [pE23H]) \quad \text{(S1.60)}$$

$$V_5 = k_5 \cdot ([pE23H] \cdot [Shc] - K_{d,5} \cdot [pE23H\text{-}Shc]) \quad (S1.61)$$

$$V_6 = k_6 \cdot [pE23H\text{-}Shc] - k_{-6} \cdot [pE23H\text{-}pShc] \quad (S1.62)$$

$$V_7 = k_7 \cdot ([pE23H\text{-}pShc] \cdot [GS] - K_{d,7} \cdot [pE23H\text{-}pShc\text{-}GS]) \quad (S1.63)$$

$$V_8 = k_8 \cdot ([pE23H\text{-}Shc\text{-}GS] - K_{d,8} \cdot [pE23HP] \cdot [Shc\text{-}GS]) \quad (S1.64)$$

$$V_9 = k_9 \cdot [Shc\text{-}GS] - k_{-9} \cdot [pShc] \cdot [GS] \quad (S1.65)$$

$$V_{10} = V_{max,10} \cdot [pShc] / (K_{m,10} + [pShc]) \quad (S1.66)$$

$$V_{11} = k_{11} \cdot [Ras\text{-}GDP] \cdot [Shc\text{-}GS] / (K_{m,11} + [Ras\text{-}GDP]) \quad (S1.67)$$

$$V_{12} = V_{12} \cdot [Ras\text{-}GTP] / (K_{m,12} + [Ras\text{-}GTP]) \quad (S1.68)$$

$$V_{13} = k_{13} \cdot [Raf] \cdot [Ras\text{-}GTP] / (K_{m,13} + [Raf]) \quad (S1.69)$$

$$V_{14} = k_{14} \cdot [Raf^*] \cdot ([ppAkt\text{-}PIP3] + [E_{Raf}]) / ([Raf^*] + K_{m,14}) \quad (S1.70)$$

$$V_{15} = k_{15} \cdot [MEK] \cdot [Raf^*] / (K_{m,15} + [MEK]) \quad (S1.71)$$

$$V_{16} = k_{16} \cdot [pMEK] \cdot [PP2A] \quad (S1.72)$$

$$V_{17} = k_{cat,16} \cdot [pMEK\text{-}PP2A] \quad (S1.73)$$

$$V_{18} = k_{18} \cdot [MEK\text{-}PP2A] \quad (S1.74)$$

$$V_{19} = k_{15} \cdot [pMEK] \cdot [Raf^*] / (K_{m,15} + [pMEK]) \quad (S1.75)$$

$$V_{20} = k_{16} \cdot ([PP2A] \cdot [ppMEK] - K_{d,16} \cdot [ppMEK\text{-}PP2A]) \quad (S1.76)$$

$$V_{21} = k_{cat,16} \cdot [ppMEK\text{-}PP2A] \quad (S1.77)$$

$$V_{22} = k_{22} \cdot [pMEK\text{-}PP2A] \quad (S1.78)$$

$$V_{23} = k_{23} \cdot [ERK] \cdot [ppMEK] / (K_{m,23} + [ERK]) \quad (S1.79)$$

$$V_{24} = V_{max,24} \cdot [pERK] / (K_{m,24} + [pERK]) \quad (S1.80)$$

$$V_{25} = k_{23} \cdot [ppMEK] \cdot [pERK] / (K_{m,23} + [pERK]) \quad (S1.81)$$

$$V_{26} = V_{max,24} \cdot [ppERK]/(K_{m,24} + [ppERK]) \quad (S1.82)$$

$$V_{27} = k_{27} \cdot ([pE23H] \cdot [PI3K] - K_{d,27} \cdot [pE23H\text{-}PI3K]) \quad (S1.83)$$

$$V_{28} = k_{28} \cdot [pE23H\text{-}PI3K] - k_{-28} \cdot [pE23H\text{-}PI3K^*] \quad (S1.84)$$

$$V_{29} = k_{29} \cdot [pE23H\text{-}PI3K^*] - k_{-29} \cdot [pE23H \cdot PI3K^*] \quad (S1.85)$$

$$V_{30} = k_{30} \cdot [PI3K^*] \quad (S1.86)$$

$$V_{31} = k_{31} \cdot ([PI] \cdot [PI3K^*] - K_{d,31} \cdot [PI3K^*\text{-}PI]) \quad (S1.87)$$

$$V_{32} = k_{32} \cdot ([PIP3] \cdot [PTEN] - K_{d,32} \cdot [PTEN\text{-}PIP3]) \quad (S1.88)$$

$$V_{33} = k_{33} \cdot [PTEN\text{-}PIP3] \quad (S1.89)$$

$$V_{34} = k_{34} \cdot [PTEN\text{-}PI] \quad (S1.90)$$

$$V_{35} = V_{max,35} \cdot [PTEN]/(K_{m,35} + [PTEN]) \quad (S1.91)$$

$$V_{36} = k_{36} \cdot ([PTEN] \cdot [pPTEN] - K_{d,36} \cdot [pTENP\text{-}PTEN]) \quad (S1.92)$$

$$V_{37} = k_{cat,37} \cdot [pPTENP\text{-}PTEN] \quad (S1.93)$$

$$V_{38} = k_{38} \cdot [PTEN\text{-}PTEN] \quad (S1.94)$$

$$V_{39} = k_{39} \cdot ([PIP3] \cdot [Akt] - K_{d,39} \cdot [Akt\text{-}PIP3]) \quad (S1.95)$$

$$V_{40} = V_{max,40} \cdot [Akt\text{-}PIP3]/(K_{m,40} + [Akt\text{-}PIP3]) \quad (S1.96)$$

$$V_{41} = k_{41} \cdot [pAkt\text{-}PIP3] \cdot [PP2A] \quad (S1.97)$$

$$V_{42} = k_{cat,42} \cdot [pAkt\text{-}PIP3\text{-}PP2A] \quad (S1.98)$$

$$V_{43} = k_{43} \cdot [Akt\text{-}PIP3\text{-}PP2A] \quad (S1.99)$$

$$V_{44} = V_{max,40} \cdot [pAkt\text{-}PIP3]/(K_{m,40} + [pAkt\text{-}PIP3]) \quad (S1.100)$$

$$V_{45} = k_{45} \cdot ([ppAkt\text{-}PIP3] \cdot [PP2A] - K_{d,45} \cdot [ppAkt\text{-}PIP3\text{-}PP2A]) \quad (S1.101)$$

$$V_{46} = k_{cat,46} \cdot [ppAkt\text{-}PIP3\text{-}PP2A] \quad (S1.102)$$

$$V_{47} = k_{47} \cdot [\text{pAkt-PIP3-PP2A}] \quad \text{(S1.103)}$$

$$V_{48} = k_{48} \cdot [\text{pE23H}] \quad \text{(S1.104)}$$

$$V_{49} = k_{49} \cdot ([\text{2C4}] \cdot [\text{E2}] - K_{d,49} \cdot [\text{E2-2C4}]) \quad \text{(S1.105)}$$

$$V_{50} = k_{50} \cdot [\text{E2-2C4}] - k_{-50} \cdot [\text{E2-2C4}_c] \quad \text{(S1.106)}$$

$$V_{51} = k_{51} \cdot [\text{E3H}] \quad \text{(S1.107)}$$

$$V_{52} = k_2 \cdot ([\text{E3H}_c] \cdot [\text{E2}] - K_{d,2} \cdot [\text{E23H}]) \quad \text{(S1.108)}$$

$$V_{53} = k_{53} \cdot [\text{E23H}] \quad \text{(S1.109)}$$

$$V_{54} = k_3 \cdot ([\text{E23H}_c] - K_{d,3} \cdot [\text{pE23H}]) \quad \text{(S1.110)}$$

$$V_{55} = k_{55} \cdot [\text{PI3K*-PI}] \quad \text{(S1.111)}$$

$$V_{56} = k_{56} \cdot [\text{PI3K*-PIP3}] \quad \text{(S1.112)}$$

$$V_{57} = k_{57} \cdot ([\text{PTEN}] \cdot [\text{bpV}] - K_{d,57} \cdot [\text{PTEN\_bpV}]) \quad \text{(S1.113)}$$

$$V_{58} = k_{58} \cdot ([\text{PI3K}] \cdot [\text{LY}] - K_{d,58} \cdot [\text{PI3K\_LY}]) \quad \text{(S1.114)}$$

C.2 Abbreviations used in the model.

Abbreviations in text, ODEs, schemes	Protein names	Abbreviations in SBML file
E2, HER2	ErbB2 receptor	E2
E3, HER3	ErbB3 receptor	E3
HRG	Heregulin	HRG
E3H	ErbB3/HRG ligand/receptor complex	E3H
$E3H_c$	ErbB3/HRG ligand/receptor complex	E3H_C
E23H	Heterodimer of ErbB3/HRG with ErbB2	E23H
$E23H_c$	Heterodimer of ErbB3/HRG with ErbB2	E23H_C
pE23H, pHER2	Phosphorylated heterodimer of ErbB3/HRG with ErbB2	E23HP
Grb2	growth factor receptor-binding protein 2	
Ras-GDP	Ras-GDP protein	RasGDP
Ras-GTP	Ras-GTP protein	RasGTP
Raf	Raf protein	Raf

Raf*	Activated Raf	Rafa
PTEN	Phosphatase and tensinhomologue deleted on chromosome ten	PTEN
pPTEN	Phosphorylated PTEN	PTENP
AKT	AKT protein	Akt
2C4	Pertuzumab	Per
MAPK	Mitogen-activated protein kinase	
MEK	MAPK/ERK kinase	
pMEK	Phosphorylated MEK	MEKP
ppMEK	Doubly phosphorylated MEK	MEKPP
ERK	extracellular signal-regulated kinase	
pERK	Phosphorylated ERK	ERKP
ppERK	Doubly phosphorylated ERK	ERKPP
MKP3	MAPK phosphatase 3	
PDK1	3-phosphoinositide-dependent kinase 1	
PI	phosphatidylinositol	PI
PIP3	phosphatidylinositol-3,4,5-trisphosphate	
PI3K	phosphatidylinositol 3'-kinase	PI3K
PI3K*	Activated PI3K	PI3Ka
PP2A	protein phosphatase 2A	PP2A
Shc	Srchomology and collagen domain protein	Shc
pShc	Phosphorylated Shc	ShcP
Sos	Son of Sevenless homologue protein	
GS	Grb2–Sos complex	GS
pE23H-Shc	Complex of pE23H with Shc	E23HP_Shc
pE23H-pShc	Complex of pE23H with pShc	E23HP_ShP
Shc-GS	Complex of Shc with GS	ShGS
pE23H-pShc-GS	Complex of pE23H-pShc with GS	E23HP_ShGS
AKT-PIP3	Complex of AKT with PIP3	AKT_PIP3
pAKT-PIP3	Complex of pAKT with PIP3	AKT_PI_P
ppAKT-PIP3	Complex of ppAKT with PIP3	AKT_PI_PP
ppAKT-PIP3-PP2A	Complex of ppAKT-PIP3 with PP2A	AKT_PI_PP_PP2A
AKT-PIP3-PP2A	Complex of AKT-PIP3 with PP2A	AKT_PIP3_PP2A
pAKT-PIP3-PP2A	Complex of pAKT-PIP3 with PP2A	AKT_PI_P_PP2A
E2-2C4	Complex of E2 with 2C4	E2_Per
E2-2C4$_c$	Complex of E2 with 2C4	E2Per
PTEN-PTEN	Complex of PTEN with PTEN	PTEN_PTEN
pPTEN-PTEN	Complex of pPTEN withPTEN	PTENP_PTEN
PTEN-PIP3	Complex of PTEN with PIP3	PTEN_PIP3
PTEN-PI	Complex of PTEN with PI	PTEN_PI
pMEKP-PP2A	Complex of pMEKP with PP2A	MEKP_PP2A
MEK-PP2A	Complex of MEK with PP2A	MEK_PP2A
ppMEKPP-PP2A	Complex of ppMEKPP with PP2A	MEKPP_PP2A
pE23H-PI3K	Complex of pE23H with PI3K	E23HP_PI3K
PI3K*-PI	Complex of PI3K* with PI	PI3Ka_PI
pE23H-PI3K*	Complex of pE23H with PI3K*	E23HP_PI3Ka

E_{Raf}	Unknown enzyme dephosphorylating Raf*	E_Raf
bpV	Bisperoxovanadium compound, bpV(pic), PTEN inhibitor	bpV
LY	LY294002, PI3K inhibityor	LY
PTEN-bpV	Enzyme-inhibitor complex of PTEN and bpV(pic)	PTEN_bpV
PI3K-LY	Enzyme-inhibitor complex of PI3K and LY294002	PI3K_LY

C.3 Kinetic parameters of the model.

k_i, k_{-i} – rate constants of forward and reverse reactions, $nM^{-1}\ min^{-1}$, $K_{d,i}$, $K_{m,i}$ – dissociation and Michaelis constants, nM.

Reaction rate	Kinetic parameters	Values in our model	Remarks	Values from (103)	Values from (105)
HER3 and HER2 binding					
V_1	k_1	0.005		0.001	0.003
	$K_{d,1}$	600; 0.2[1)]		0.6	20
V_{51}	k_{51}	0.01			
V_2	k_2	10		0.01	0.01
V_{52}	$K_{d,2}$	10±4[2)]		10	10
V_{53}	k_{53}	0.01			
V_3	k_3	1±0.2		1	1
	$K_{d,3}$	0.1±0.04		0.01	0.01
V_4	$V_{max,4}$	10±4		62	450
	$K_{m,4}$	50±30		50	50
Shc and GS binding					
V_5	k_5	0.06±0.01		0.1	0.09
	$K_{d,5}$	1		1	6
V_6	k_6	12		20	6
	k_{-6}	3		5	0.06
V_7	k_7	36		60	0.009
	$K_{d,7}$	9		9	4.3

V_8	k_8	12		2040	0.12
	$K_{d,8}$	0.1		7.8	0.002
V_9	k_9	35±4		40.8	0.1
	k_{-9}	0		0	0.2
V_{10}	$V_{max,10}$	0.0154		0.0154	1.7
	$K_{m,10}$	340		340	340
E23HP binding with PI3K and PI3K activation					
V_{27}	k_{27}	3±1		0.1	
	$K_{d,27}$	1		20	
V_{28}	k_{28}	300±30		9.85	
	k_{-28}	0		0.1	
V_{29}	k_{29}	13500		45.8	
	k_{-29}	0		0.047	
V_{30}	V_{30}	900±130		$V_{m,26}$=2620	
Ras/Raf/MEK/ERK cascade					
V_{11}	k_{11}	6±0.6		0.22	
	$K_{m,11}$	0.18		0.18	
V_{12}	$V_{max,12}$	3±0.5		0.3	
	$K_{m,12}$	0.1		0.06	
V_{13}	k_{13}	1±0.2		1.53	
	$K_{m,13}$	11.7		11.7	
V_{14}	k_{14}	0.6±0.3		$6.7\ 10^{-3}$	
	$K_{m,14}$	30±15		8	
V_{15} V_{19}	k_{15}	2.1±0.3		3.5	
	$K_{m,15}$	1±0.5		317	
V_{16}	k_{16}	0.06			
V_{17} , V_{21}	$k_{cat,16}$	0.6			
V_{18}	k_{18}	3			
V_{20}	k_{16}	0.06			
	$K_{d,16}$	1			

V_{22}	k_{22}	0.06			
V_{23} V_{25}	k_{23}	1.2±0.05		9.5	
	$K_{m,23}$	10±0.7		$1.4\ 10^5$	
V_{24} V_{26}	$V_{max,24}$	1.8±0.7		0.3	
	$K_{m,24}$	10±4		160	
PIP3 → PI					
V_{31}	k_{31}	0.03±0.006			
	$K_{d,31}$	140		K_m =40	
V_{55}	k_{55}	30		k_{27} =16.9	
V_{56}	k_{56}	30			
V_{32}	k_{32}	8000			
	$K_{d,32}$	0.01±0.004		$K_{m,28}$=9	
V_{33}	k_{33}	15±5			
V_{34}	k_{34}	3.6±1			
PTEN => pPTEN					
V_{35}	$V_{max,35}$	150±50			
	$K_{m,35}$	2			
V_{36}	k_{36}	1±0.4			
	$K_{d,36}$	2.2			
V_{37}	k_{37}	150			
V_{38}	k_{38}	150			
AKT activation pathway					
V_{39}	k_{39}	15000		507	
	$K_{d,39}$	20±6		234	
V_{40} V_{44}	$V_{max,40}$	15000±5000		$2\ 10^4$	
	$K_{m,40}$	0.1±0.035		$8\ 10^4$	
V_{41}	k_{41}	3			
V_{42}, V_{46}	k_{42}	45±20			
V_{43}	k_{43}	30			
V_{45}	k_{41}	3			

	$K_{d,41}$	0.1			
V_{47}	k_{47}	0.3			
Receptor internalization					
V_{48}	k_{48}	0.001		0.001	
2C4 binding					
V_{49}	k_{49}	0.003			
	$K_{d,49}$	$2\ 10^4$; 7[1)]	estimation, K_d=8.5 nm (248)		
V_{50}	k_{50}	0.6			
	k_{-50}	0.012			
PTEN inhibition by bpV(pic)					
k_{57}	100				
$K_{d,57}$	10		estimation IC_{50}=31 nM (234)		
PI3K inhibition by LY294002					
k_{58}	100				
$K_{d,58}$	80		Estimation, K_i=1600 nM (252)		

[1)] the value of the parameters after rescaling of HRG and 2C4 concentrations to extracellular volume.

[2)] absolute errors show the deviation of the parameter giving 5% deviation of the output signal (pHER2, pAKT, pERK) which possesses most sensitivity to this parameter. The errors are given only for the parameters having sensitivity more than 0.04 (see Fig. S5-S9).

Table S3. Initial concentrations of the metabolites in the model, nM

Metabolites	Values in our model	Remarks	Values from [1]	Values from [2]
HER3	80±3		HER4=80	EGFR=100
HER2	100±10			
HRG	100		100	
Shc	100±10		1000	150

GS	100		10	
RasGDP	120		120	
Raf	100		100	
E_{Raf}	7		7	
MEK	10±0.7		120	
ERK	10±0.3		1000	
PI3K	200±70		10	
AKT	100±3		10	
PP2A	10±2.5		11.4	
PI	300±30		800	
PTEN	50±5			

Appendix D: Supplementary figures for mathematical model.

D.1: Supplementary Figures and Legends.

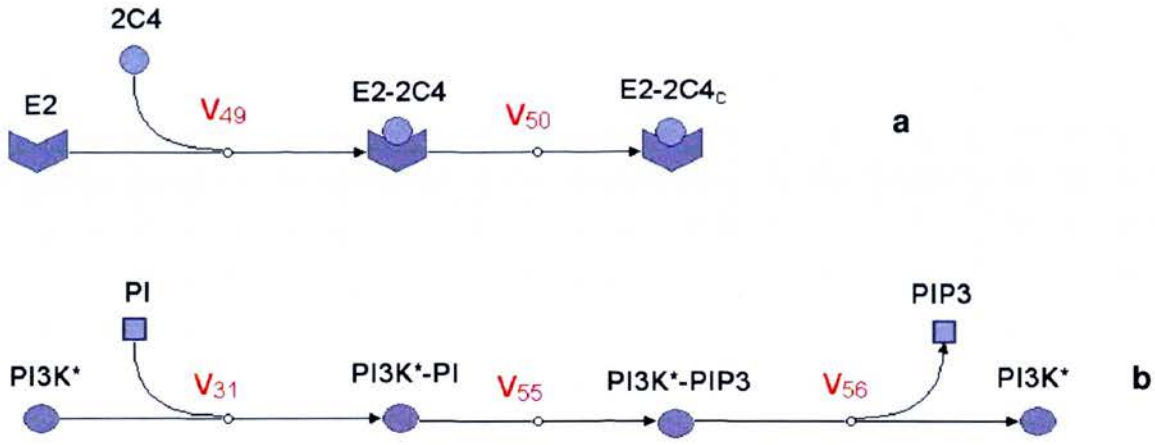

Supplementary figure S1. a - Scheme of the two-step mechanism of the binding of the receptor HER2 (E2) with ligand, pertuzumab (2C4). **b** – Detailed scheme of the reaction of PI phosphorylation catalysed by PI3K*.

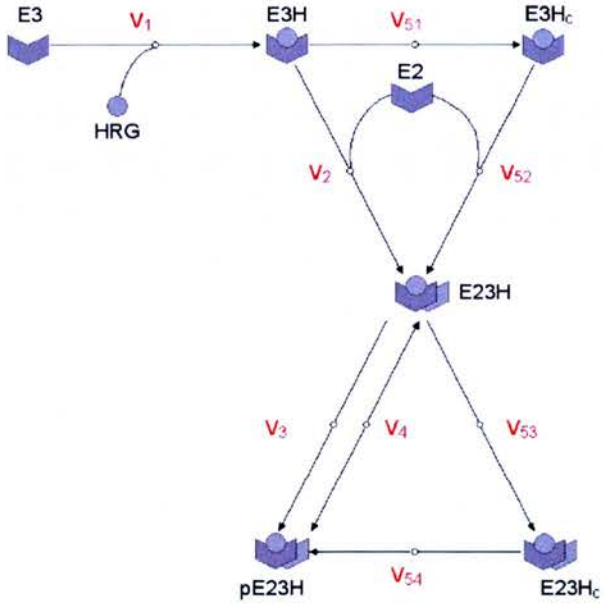

Supplementary figure S2. Detailed scheme of heterodimerisation of HER3 (E3) and HER2 (E2) receptors along with formation of the transphosphorylated complex,

pE23H. Reactions V_1, V_{51} corresponds to a two-step mechanism of the binding of HER3 (E3) receptor and heregulin (HRG) with a formation of the intermediate, E3H and the final $E3H_c$ ligand-receptor complex. Reactions V_2, V_{52}, and V_{53} describe the two-step mechanism of heterodimerisation of HER3 (E3) and HER2 (E2) receptors leading to formation of intermediate E23H and final $E23H_c$ heterodimer. Reactions V_3 and V_{54} describe transphosphorylation of E23H and $E23H_c$ heterodimers with formation of complex pE23H. V_4 – reaction of pE23H dephosphorylation.

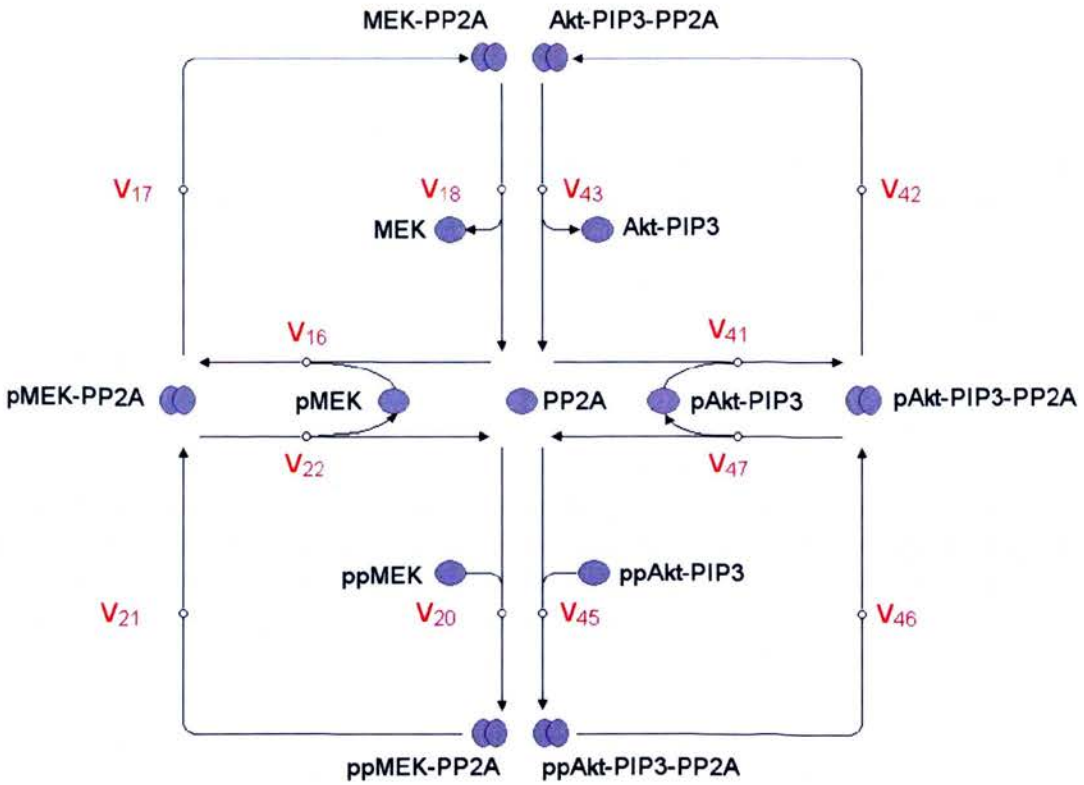

Supplementary figure S3. Detailed scheme of dephosphorylation of pMEK (reactions V_{16}, V_{17}, V_{18}) , ppMEK (reactions V_{20}, V_{21}, V_{22}), pAkt (reactions V_{41}, V_{42}, V_{43}), ppAkt (reactions V45, V46, V47) by the phosphatase PP2A.

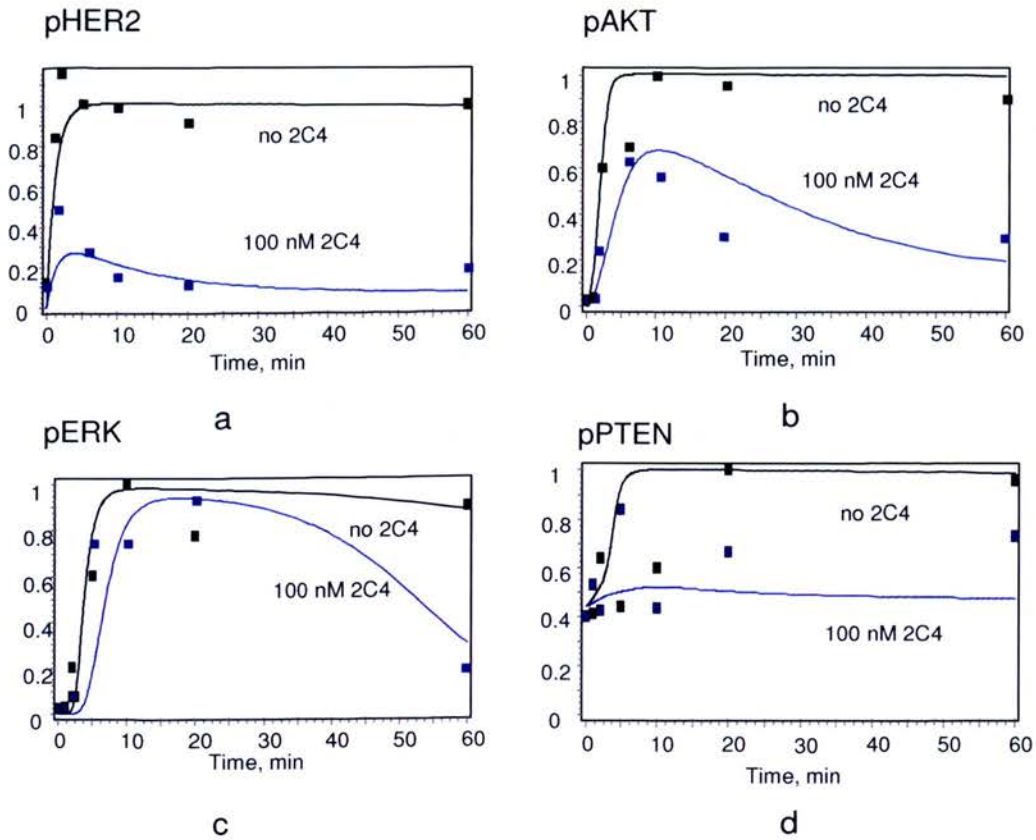

Supplementary figure S4. Time-course plots of computational simulations (bold lines) and experimental data (points) in the PE04 cell line showing the effect and heregulin-β (black) and pertuzumab (blue) on kinetics of pHER2 (a), pAKT (b), and pERK (b), pPTEN (c) and matching of experimental data with model simulations, used to parameterise the computational model.

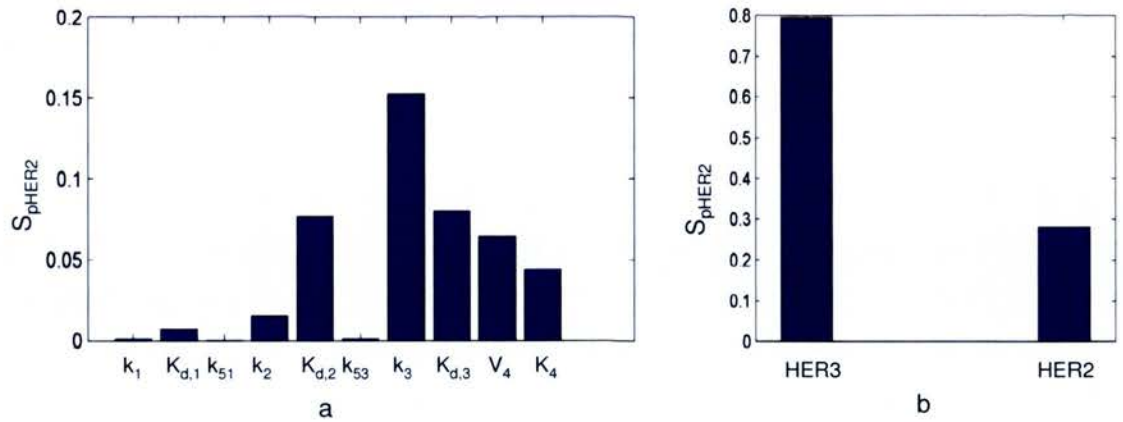

Supplementary figure S5. Sensitivity S_{pHER2} of pHER2 to kinetic parameters of the reactions (1-4, 51, 53, see Figure 6.1) (a) and initial concentrations of the enzymes (b) involved in HER3/HER2 heterodimerisation and autophosphorylation.

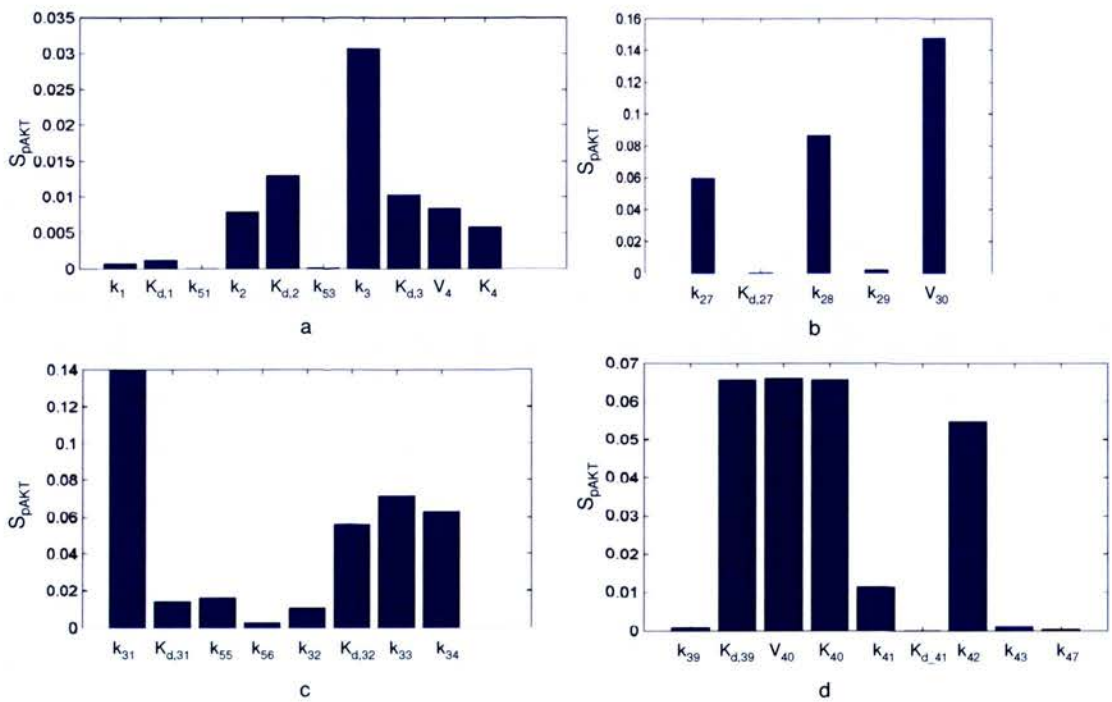

Supplementary figure S6. Sensitivity S_{pAKT} of pAKT to kinetic parameters of the reactions involved in HER3/HER2 heterodimerisation and autophosphorylation

(reactions 1-4, 51, 53) (a); PI3K activation (reactions 27-30) (b); PI3K/PTEN cycle (reactions 31-34) (c); and AKT phosphorylation (reactions 39-47) (d).

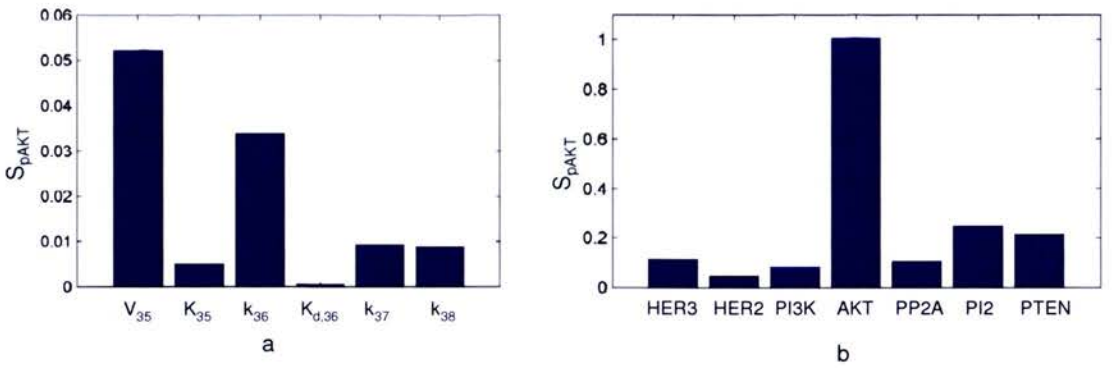

Supplementary figure S7. Sensitivity S_{pAKT} of pAKT to kinetic parameters of reactions (35-38) involved in PTEN/pPTEN cycle (a) and initial concentrations of the enzymes and metabolites (b).

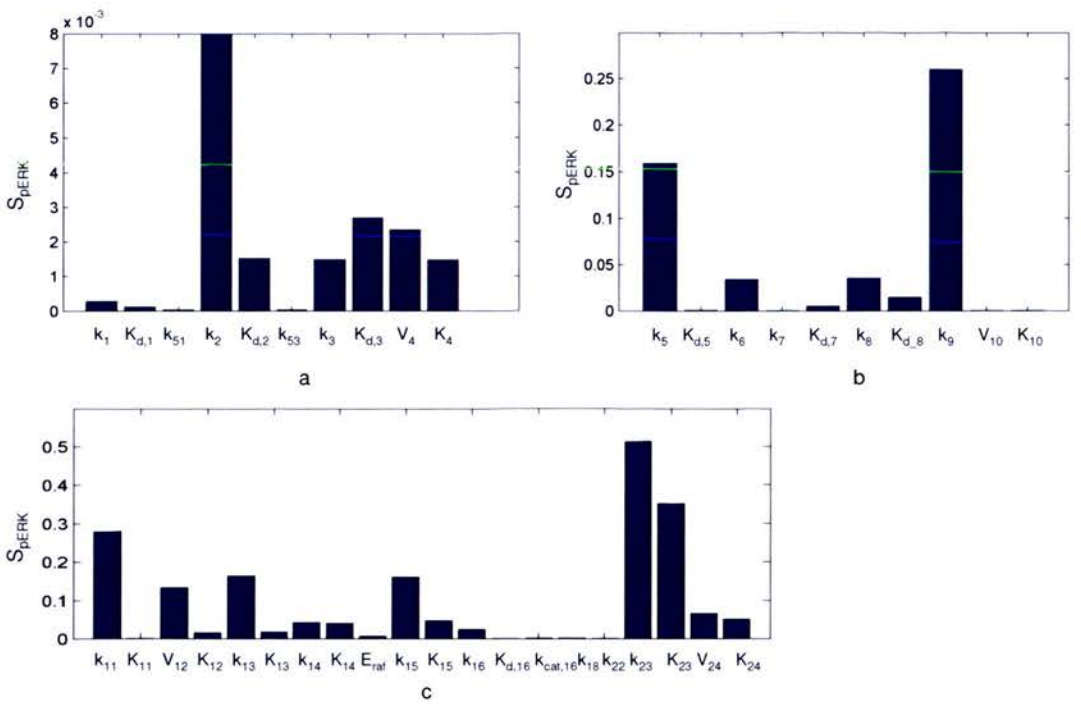

Supplementary figure S8. Sensitivity S_{pERK} of pERK to kinetic parameters of the reactions involved in HER3/HER2 heterodimerisation and autophosphorylation (reactions 1-4, 51,53) (a); the formation of Shc-GS complex (reactions 5-10) (b); and the Ras/RAF/MEK/ERK pathway (reactions 11-26) (c).

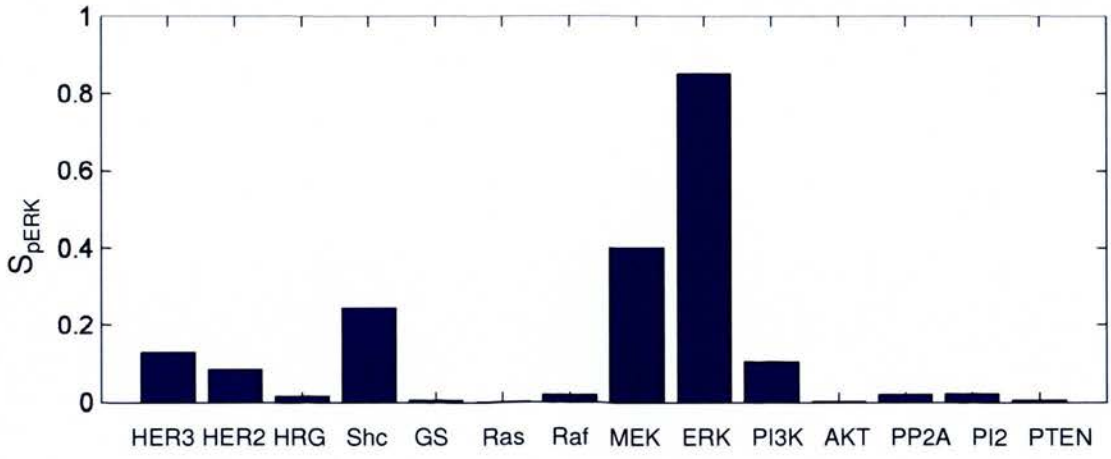

Supplementary figure S9. Sensitivity S_{pERK} of pERK to initial concentrations of the enzymes and metabolites.

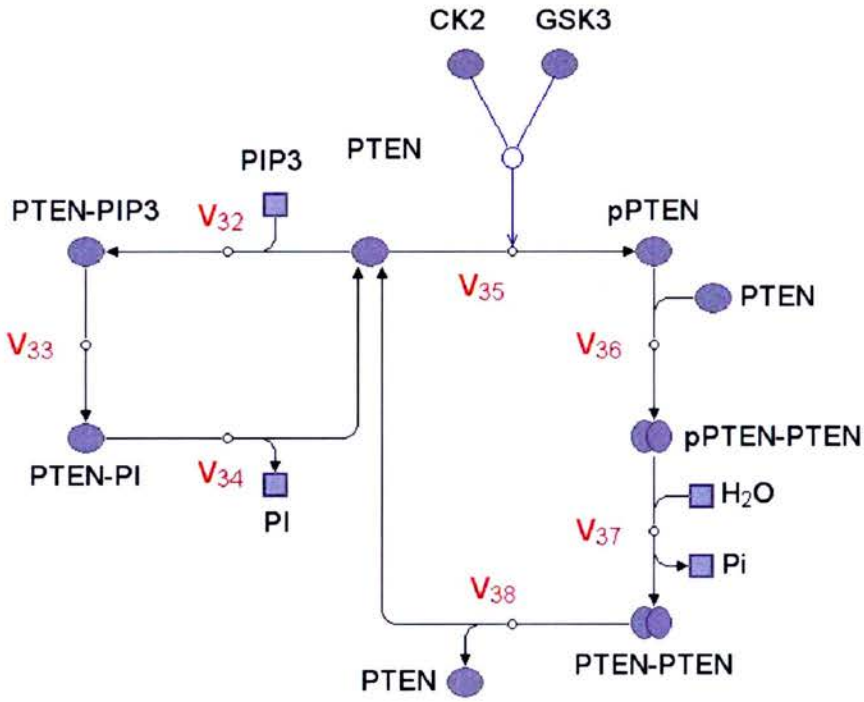

Supplementary figure S10. Catalytic cycle of PTEN with lipid phosphatase activity (reactions V_{32}, V_{33}, V_{34}) and it's autodephosphorylation activity (reactions V_{35}, V_{36}, V_{37}, V_{38}).

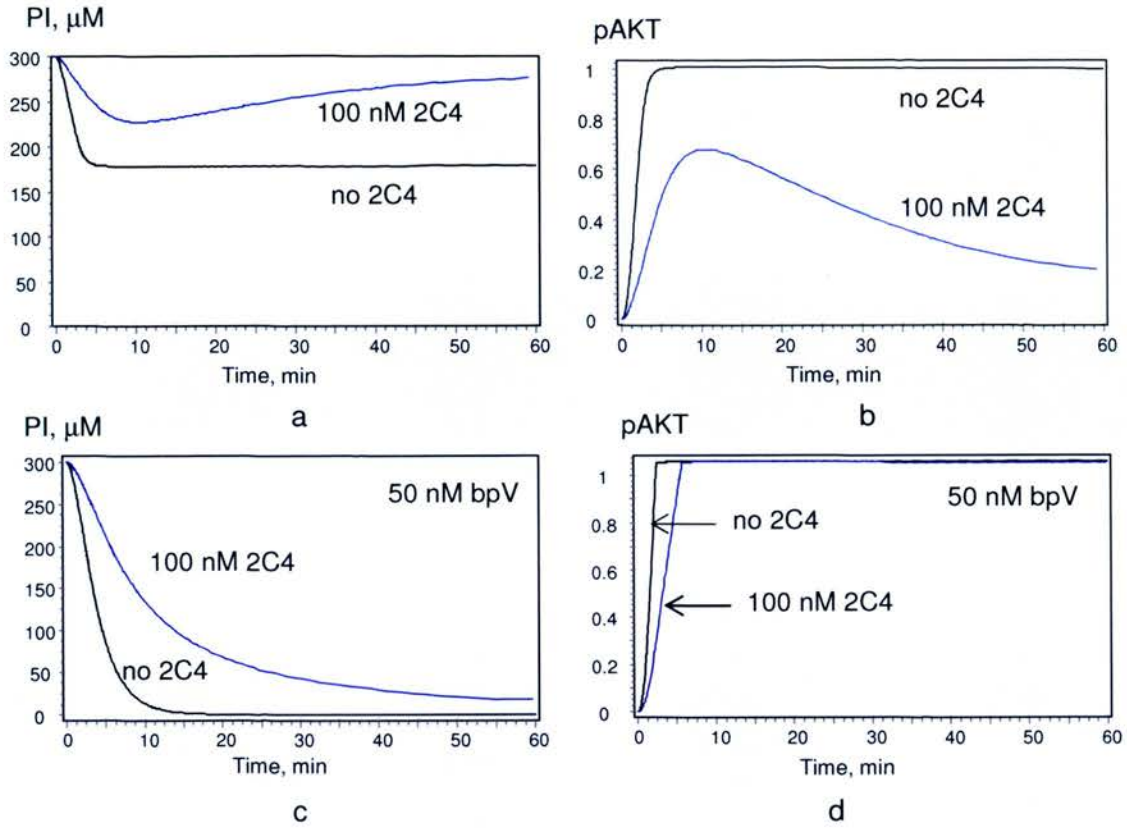

Supplementary figure S11: Theoretical results illustrating the mechanism of the resistance to pertuzumab (2C4) due to the loss of PTEN activity. Computational kinetics of PI consumption (a, c) in the PTEN/PI3K cycle and pAKT signal (b, d) at different levels of PTEN activity in the absence of 2C4 (black lines) and presence of 100 nM of 2C4. (a, b) - inhibition effect of 2C4; (c,d) - resistance to 2C4 due to PTEN inhibition by bpV. Concentration of pAKT is given in relative units.

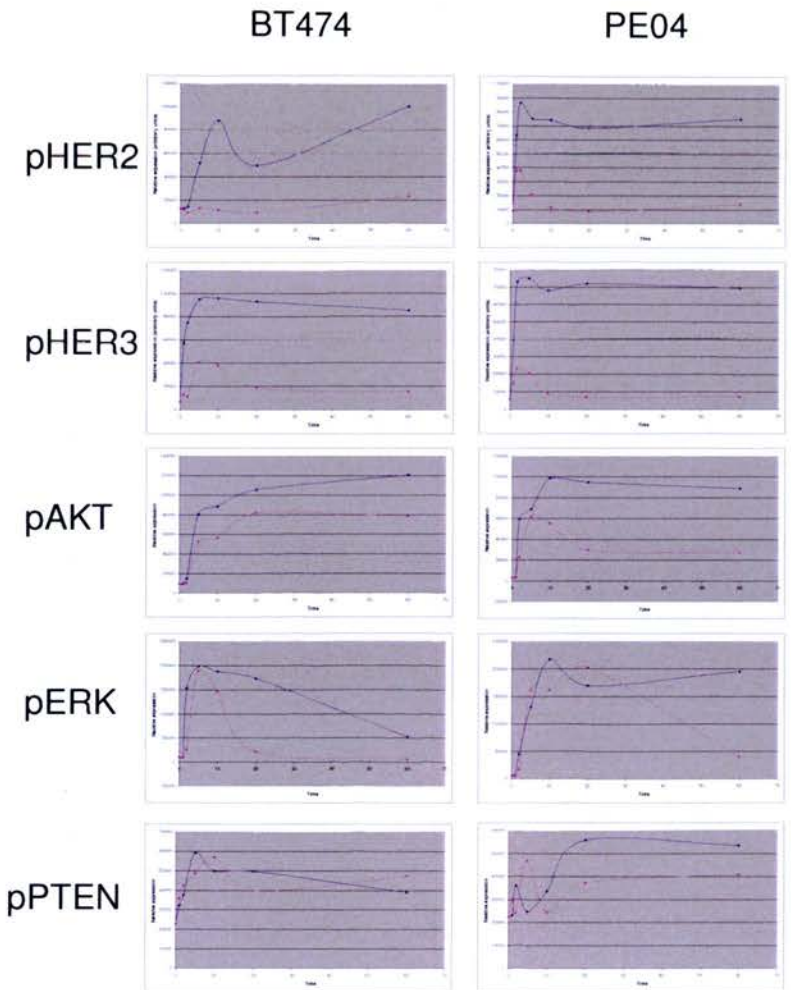

Supplementary figure S12: Time course experiments profiling the phosphorylation of PI3K and MAPK signalling molecules for computational model validation. Figures are representative of qualitative changes in activation state generated from three experimental replicates and different detection methods (western blotting and RPPA). Blue line = heregulin stimulation, magenta line = heregulin stimulation plus pertuzumab.

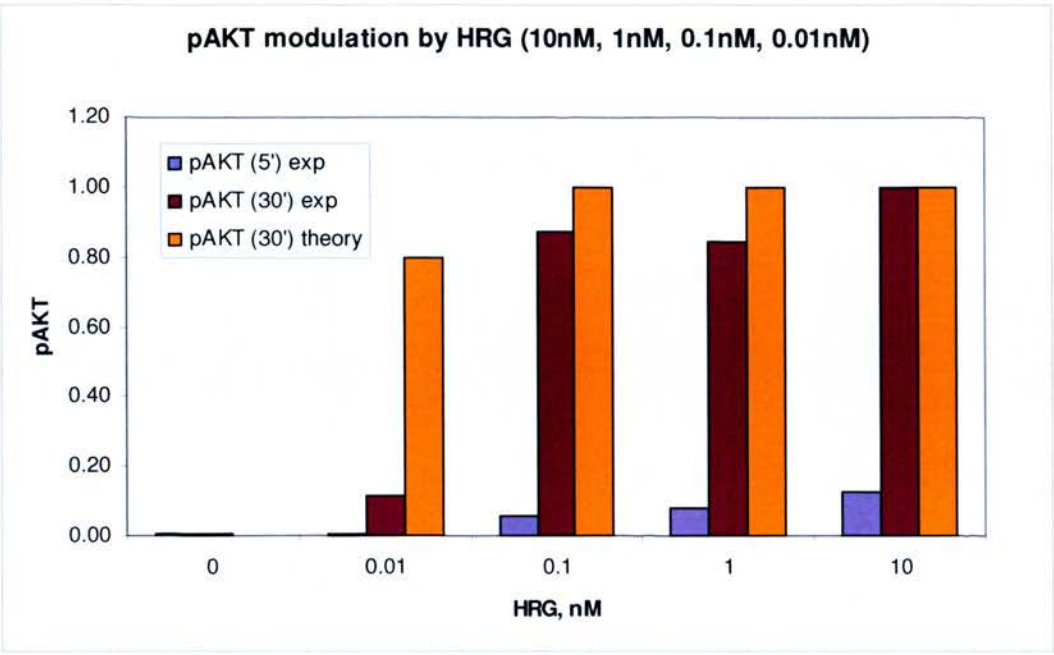

Supplementary figure S13: Experimental and theoretical dose-response of pAKT to heregulin-β at 5 and 30 minutes.

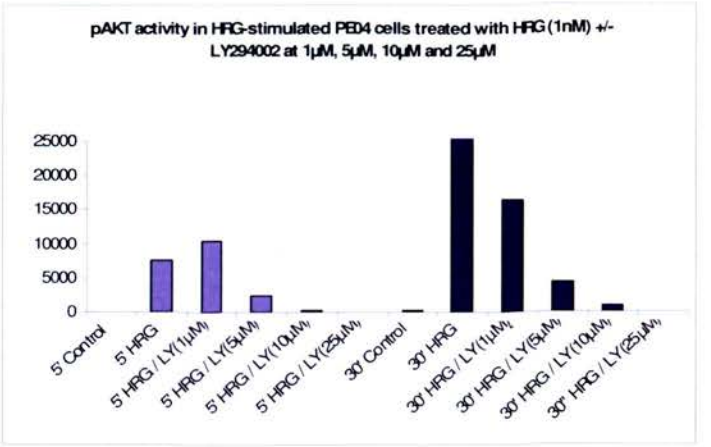
pAKT activity in HRG-stimulated PE04 cells treated with HRG (1nM) +/- LY294002 at 1μM, 5μM, 10μM and 25μM
25000
20000
15000
10000
5000
0
5' Control
5' HRG
5' HRG / LY(1μM)
5' HRG / LY(5μM)
5' HRG / LY(10μM)
5' HRG / LY(25μM)
30' Control
30' HRG
30' HRG / LY(1μM)
30' HRG / LY(5μM)
30' HRG / LY(10μM)
30' HRG / LY(25μM)

a

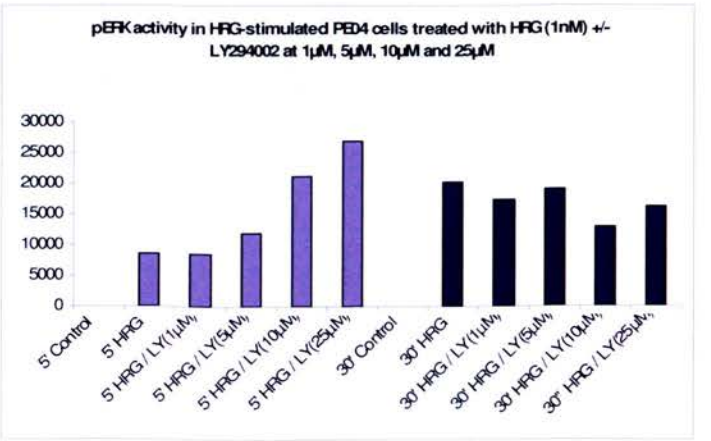
pERK activity in HRG-stimulated PE04 cells treated with HRG (1nM) +/- LY294002 at 1μM, 5μM, 10μM and 25μM
30000
25000
20000
15000
10000
5000
0
5' Control
5' HRG
5' HRG / LY(1μM)
5' HRG / LY(5μM)
5' HRG / LY(10μM)
5' HRG / LY(25μM)
30' Control
30' HRG
30' HRG / LY(1μM)
30' HRG / LY(5μM)
30' HRG / LY(10μM)
30' HRG / LY(25μM)

b

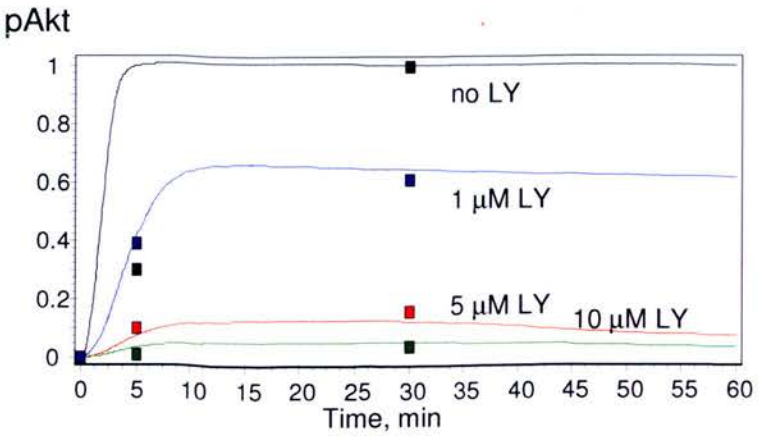
pAkt
1
0.8
0.6
0.4
0.2
0
no LY
1 μM LY
5 μM LY
10 μM LY
0
5
10
15
20
25
30
35
40
45
50
55
60
Time, min

c

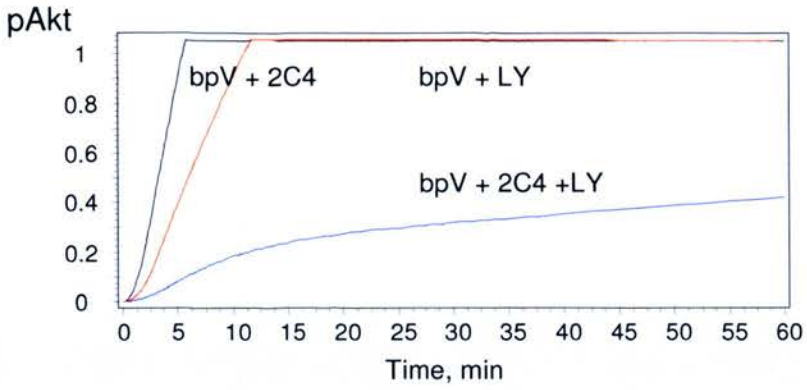

d

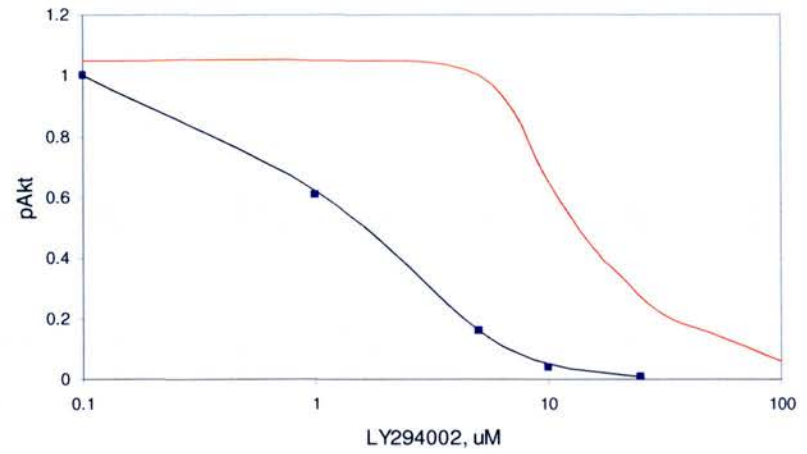

e

Supplementary figure S14: Inhibition of PI3K with LY294002 (LY) results in dose-dependent inhibition of pAKT, but not pERK, in response to heregulin (a,b). c – theoretical kinetics of pAKT at the different concentration of LY294002 (lines), points – experimental data. d – Suppression of the resistance to pertuzumab (2C4) by PI3K inhibition. pAKT kinetics in the presence of bpV and 2C4 (black line); bpV, 2C4, and LY294002 (blue line); bpV, LY294002 (red line). e – pAKT dose-dependence on LY294002 in the absence and presence of bpV (50 uM) for 30 min. Points – experimental data.

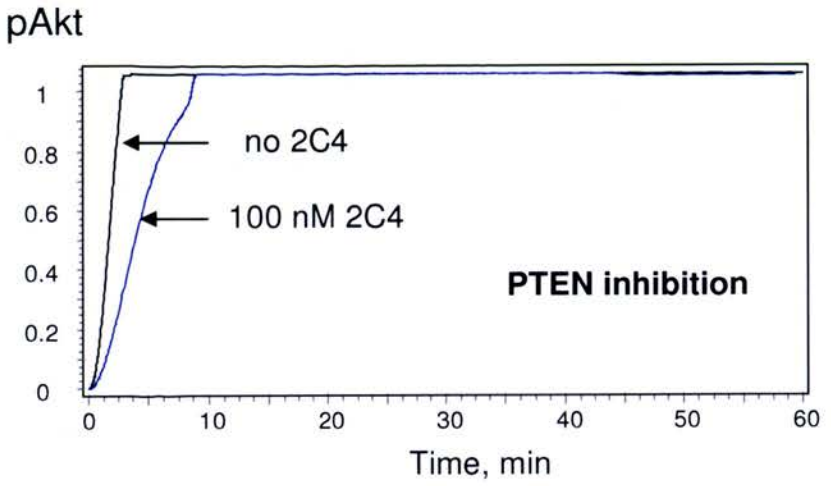

a

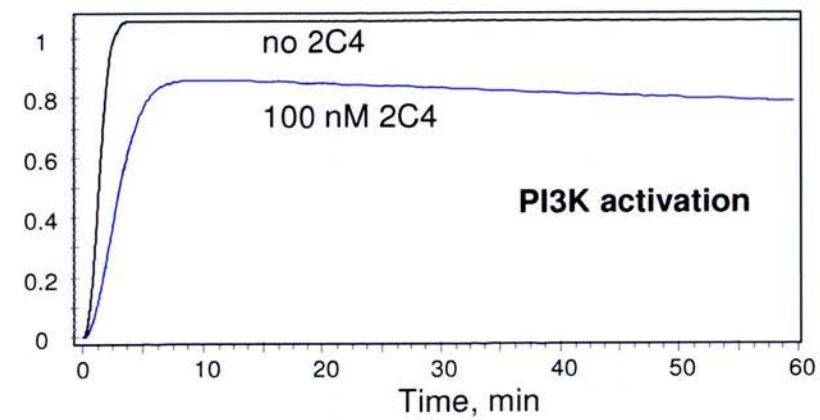

b

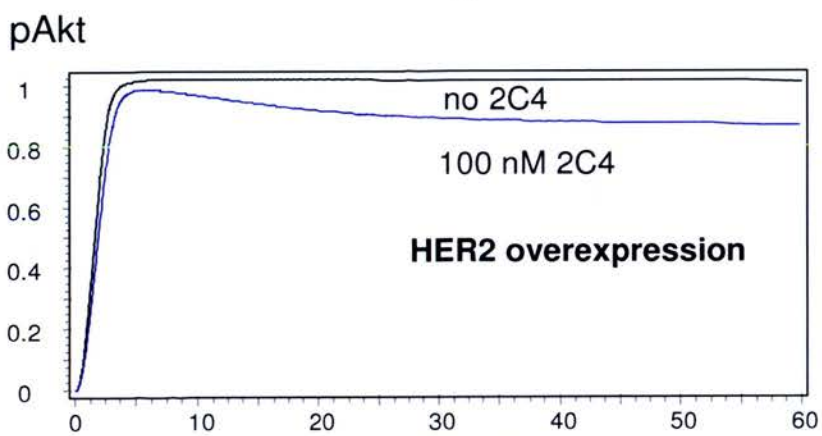

c

Supplementary figure S15: Computational analysis of MAPK-PI3K network predicts that PTEN loss (a), PIK3CA mutation (b), and HER2 overexpression (c) will abrogate inhibiton of pAKT by pertuzumab (black line, heregulin-β alone, blue line,

+ pertuzumab 100nM).

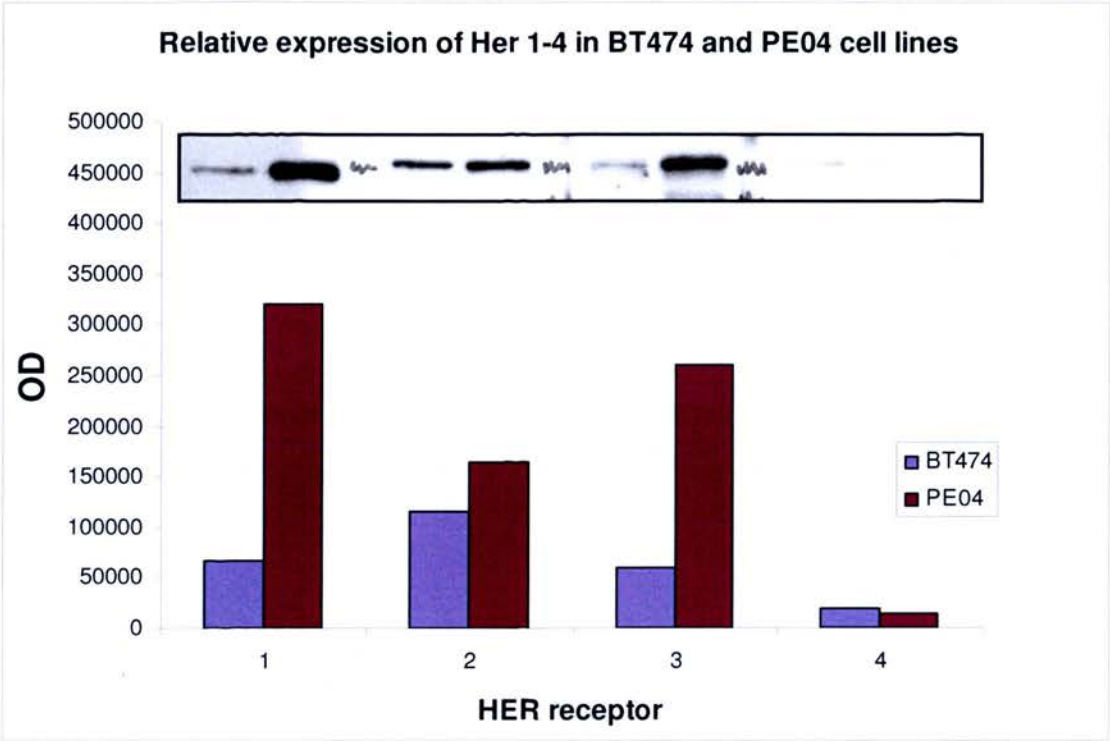

Supplementary figure S16: Relative expression of HER1–4 in BT474 and PE04 cell lines.